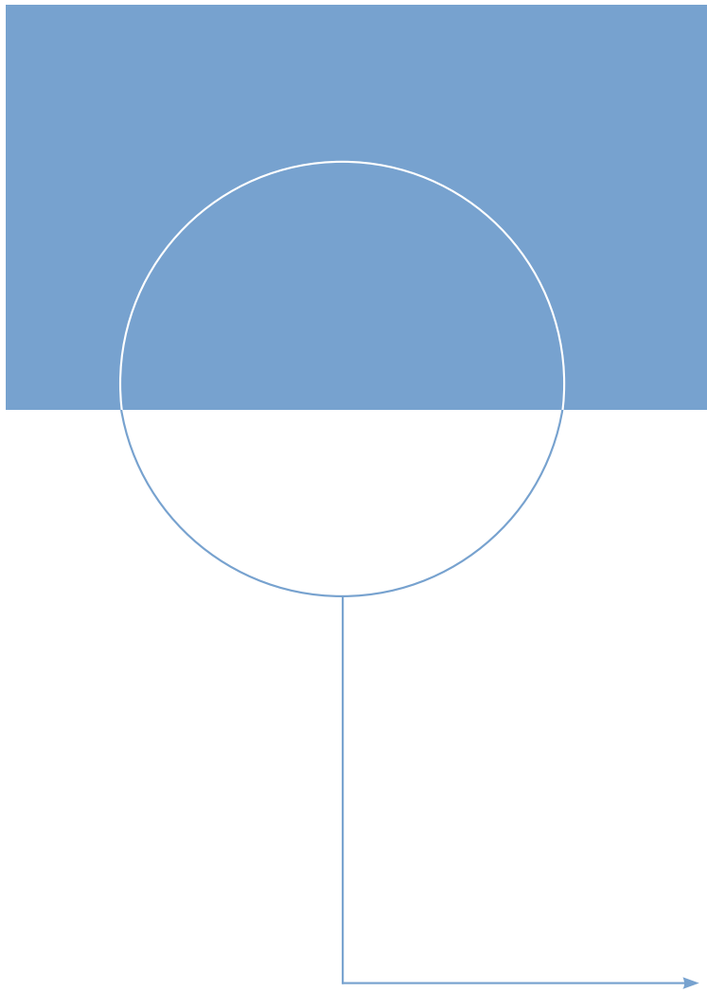

Master's thesis

2021

Liang Zhao

NTNU
Norwegian University of
Science and Technology
Faculty of Natural Sciences
Department of Chemistry

Liang Zhao

Particulate Iron Bioavailability to Phytoplankton in Antarctic and Arctic Waters: Effects of Ocean Acidification and the Organic Ligand EDTA

December 2021

NTNU
Norwegian University of
Science and Technology

NTNU
Norwegian University of
Science and Technology

NTNU

Norwegian University of
Science and Technology

Particulate Iron Bioavailability to Phytoplankton in Antarctic and Arctic Waters: Effects of Ocean Acidification and the Organic Ligand EDTA

Liang Zhao

Environmental Toxicology and Chemistry
Submission date: December 2021
Supervisor: Murat Van Ardelan
Co-supervisor: Geir Johnsen

Norwegian University of Science and Technology
Department of Chemistry

Particulate Iron Bioavailability to Phytoplankton in Antarctic and Arctic Waters: Effects of Ocean Acidification and the Organic Ligand EDTA

Liang Zhao

Environmental Toxicology and Chemistry

Submission Date: 7th December 2021

Supervisor: Murat Van Ardelan, IKJ

Co-supervisor: Geir Johnsen, IBI

NTNU
Fakultet for naturvitenskap
Institutt for kjemi

Preface

长风破浪会有时，直挂云帆济沧海。

—— 李白 （唐）

A time will come to ride the wind and cleave the waves; I'll set my cloudlike sail to cross the sea which raves.[1]

——Li Bai (Tang dynasty)

[1] Translated into English by Xu Yuanchong in Selected Poems of Li Bai (《李白诗选》).

Abstract

Particulate iron (PFe) usually is not considered as a bioavailable iron fraction to phytoplankton. In this study we tested the bioavailability of one PFe species, goethite (α-FeO(OH)), to phytoplankton community in Southern Ocean under the effect of ocean acidification (OA) (pH_T ca. 7.5) and representative concentration pathways (RCP) 8.5 condition (pCO_2 ca. 1300 µatm), and to an Arctic diatom species, *Nitzschia frigida*, under the effect of the organic ligand, EDTA (using the commercially available salt disodium ethylenediaminetetraacetate dihydrate), as a chelator, respectively.

In March 2019, a natural phytoplankton community was sampled and used for the deck incubation experiment in the Southern Ocean. The sampling site was 68.10°S, 6.00° W, which was in the region of Queen Maud Land (Norwegian: Dronning Maud Land, DML). We observed marine biogeochemical performance of the phytoplankton community under OA. Different chemical and biological parameters during the incubation were determined, including dissolved iron (DFe), total acid leachable iron (TaLFe), macronutrients including nitrate (NO_3^-), phosphate (PO_4^{3-}) and silicate, total pH (pH_T), dissolved inorganic carbon (DIC), the concentration & fugacity of carbon dioxide (fCO_2), chlorophyll a (Chla) concentration & *in vivo* fluorescence. The results show that the tested phytoplankton assemblage was more severely influenced by OA than iron bioavailability, especially under severe OA. Goethite, as one type of PFe, is insoluble under the tested OA scenarios. There could be PO_4^{3-} remineralization in all treatments but species shift to diatoms only in ambient pH treatments (mild OA), which coincides with the judgement that OA impact is predominant in comparison to iron enrichment in this experiment. We should analyze phytoplankton species to test this hypothesis. OA can result in that phytoplankton launches H_v channel-mediated H^+ efflux mechanism, carbon concentration mechanism (CCM) down-regulation of phytoplankton and the thriving of more tolerant species with more efficient CCM.

In April 2021, using an Arctic diatom species, *Nitzschia frigida*, we investigated the possibility of EDTA increasing goethite bioavailability to phytoplankton and photosynthetic performance by measuring relative electron transport rate (rETR) in the experiment performed at Trondheim Biological Station (Norwegian: Trondheim Biologiske Stasjon, TBS). The results show that elevating EDTA concentration can increase the bioavailability of goethite while decrease that of ferric chloride ($FeCl_3$). This is inconclusive according to possibly negatively biased α (the slope of a typical P/E (photosynthesis/irradiance) curve), because it results in underestimation of goethite bioavailability under the influence of EDTA.

Further research regarding the combined effect of OA and EDTA on PFe bioavailability to phytoplankton is recommended.

Key words: iron bioavailability, goethite, phytoplankton, ocean acidification, EDTA.

Acknowledgement

Firstly, I would like to thank my supervisor, Murat Van Ardelan, the most impressive and humorous professor who is a big fan of chocolate and yogurt, not only for your professional guidance in my master project, but also your passion for science, caring about my mental health and teaching me how to become an "iron lady". I am also grateful to Dr. Nicolas Sanchez, for your meticulous instruction and patience for detailed information, as well as all review points at the final stage. I was happy to work with you in the lab together. Also, thanks to my co-supervisor, Geir Johnsen, and his PhD candidate, Natalie Summers, for the instruction of microbiological culture and PHYTO-PAM analyzer at TBS.

Sincere thanks to Dr. Agneta Fransson from Norwegian Polar Institute (NPI) and Dr. Melissa Chierici from Institute of Marine Research (IMR) for them bringing expertise in ocean carbonate chemistry, fine tuning of OA treatments, CO_2 fluxes, biogeochemical processes, CO_2 instrumentation and macronutrients, which were all involved in DML incubation experiment and providing relevant data for us to complete my master project.

Thanks to PhD candidates Stephen Gustav Kohler and Maria Guadalupe Digernes for answering my questions and providing wise tips for me during the breaks from working at Gløshaugen, plus all the memorable jokes and relaxing small talks.

I would like to appreciate engineers Kyyas Seyitmuhammedov and Anica Simic for helping me understand seaFAST and ICPMS.

Thanks to my study in the program of Environmental Toxicology and Chemistry (ENVITOX), which has tempered me to be a better person. Special thanks to master students Sylvia Weging, Natalia Vylegzhanina and Sara Johnson. It is fabulous to get to know your ladies and become friends with you all. You are so emotionally important! I will remember the moments that we have shared forever.

I would also express my gratitude to my Chinese buddy in Trondheim, Huimi Chen, for helping me with the programming section on R Studio involved in my master project and acculturating me to the local life throughout the past 2.5 years.

Thanks to my former flat mate, Yi Ru, for the unforgettable two years that we spent together. The food, the talks, the hugs… they are all in my heart!

Thanks to my Erasmus friend Natalie Paluchova, my best teacher of apple strudel and apprentice of Chinese dumplings, for always being there to support me spiritually!

Thanks to my friends in China, especially Jialin Ren and Keshu Liu for the texts, video- and voice- calls during COVID tough time. Thanks to that we still can naturally maintain the friendship despite jet lag and geological distance.

I am also grateful to my IELTS teacher Ming Li. Without your help, I would not have been studying in Norway!

In the end, to my parents, thanks for your tremendous and immense support. I miss you and I love you!

Contents

List of Figures

List of Tables

List of Abbreviations

A

Ar: argon

A_T: total alkalinity

AL: actinic light (in PHYTO-PAM analyzer)

C

$CaCO_3$: calcium carbonate

CCM: carbon concentrating mechanism

Chla: chlorophyll a

Chlb: chlorophyll b

Chlc: chlorophyll c

CO_2: carbon dioxide

CO_3^{2-}: carbonate anion

$CoCl_2 \cdot 6H_2O$: cobaltous chloride hexahydrate

$CuSO_4 \cdot 5H_2O$: cupric sulfate pentahydrate

D

dF: an increase of fluorescence yield

DFe: dissolved iron

DIC: dissolved inorganic carbon

DIP: dissolved inorganic phosphate

DML: Queen Maud Land (Norwegian: Dronning Maud Land)

DMS: dimethyl sulfide, formula: $(CH_3)_2S$

DMSP: dimethyl sulphoniopropionate, formula: $(CH_3)_2S^+CH_2CH_2COO^-$)

DNA: Deoxyribonucleic acid

DOC: dissolved organic carbon

E

E: irradiance

E_k: minimum saturating irradiance

$E_{(\lambda)}$: Spectral Irradiance (unit: $W*m^{-2}$)

E_{PAR}: photosynthetically active photon flux density (unit: mol photons $m^{-2}s^{-1}$)

EDTA: disodium ethylenediaminetetraacetate dihydrate, chemical formula: $[CH_2N(CH_2CO_2H)_2]_2$

EisenEx: (Eisen (=iron) Iron Fertilisation Experiment in spring in the Antarctic Polar Frontal Zone in 2000.

EPA: Environmental Protection Agency of United States

ETR: electron transport rate

F

F_0/F_{min}: the minimum fluorescence of a dark-adapted sample (also called *dark fluorescence*, *constant fluorescence*, *initial fluorescence*, or *fluorescence minimum)*

F_m: the maximum fluorescence of a dark-adapted sample

F': F2 (in the Report of PHYTO-PAM), fluorescence in actinic light at chosen wavelength

F_m': Fmn (n = 1, 2, 3 or 4, representing the applied wavelength for excitation) values in the "Report" of PHYTO-PAM analyzer, maximum fluorescence yield in actinic light

fCO_2: the fugacity of CO_2

Fe (II): ferrous iron

Fe (III): ferric iron

$FeCl_3$: ferric chloride

$FeCl_3 \cdot 6H_2O$: ferric chloride hexahydrate

$Fe(OH)_3$: ferric hydroxides

$Fe(OH)_x^{(3-X)+}$: iron hydroxides

Fe_3O_4: magnetite

$FeO(OH) \cdot nH_2O$: amorphous iron oxyhydroxides

FR: far-red light

Ft: chlorophyll fluorescence yield

G

Gain: photomultiplier voltage of PHYTO-PAM analyzer

GF/F: Glass Microfiber filters

H

H^+: proton

HCl: hydrochloric acid

HCO_3^-: bicarbonate anion

H_2CO_3: carbonic acid

HEPA: high-efficiency particulate absorbing filter and high-efficiency particulate arrestance filter

H_2O: the chemical formula of water

HNLC: high nutrient - low chlorophyll

HNO_3: nitric acid

HR-ICP-MS: High Resolution Inductively Coupled Plasma Mass Spectrometry

H_v: plasma membrane voltage-gated H^+

I

I/I_2: the second inflection in the fast phase of a chlorophyll a induction curve

ICP-MS: Inductively Coupled Plasma Mass Spectrometry

IKJ: Department of Chemistry (Norwegian: Institutt for kjemi) at Norwegian University of Science and Technology

IMR: Institute of Marine Research

IPCC: the Intergovernmental Panel on Climate Change

L

LDPE: low-density polyethylene

LET: linear electron transport

LHC: light harvesting complex

M

ML: measuring light (in PHYTO-PAM analyzer)

$MnCl_2 \cdot 4H_2O$: manganese (II) chloride tetrahydrate

N

N_2 fixation: nitrogen fixation

Na_2CO_3: sodium carbonate

NADPH: nicotinamide adenine dinucleotide phosphate

$NaH_2PO_4 \cdot H_2O$: sodium dihydrogen phosphate monohydrate

$Na_2MoO_4 \cdot 2H_2O$: sodium molybdate dihydrate

$NaNO_3$: sodium nitrate

Na_2SeO_3: sodium selenite

$Na_2SiO_3 \cdot 9H_2O$: sodium metasilicate nonahydrate

$NH_4CH_3CO_2$: ammonium acetate

NH_4OH: ammonium hydroxide

NO_3^-: nitrate

N_2O: nitrous oxide

NPI: Norwegian Polar Institute

NPQ: non-photochemical quenching

NTNU: Norwegian University of Science and Technology (Norwegian: Norges teknisk-naturvitenskapelige universitet)

O

O_2: oxygen

OA: ocean acidification

OASIS: the scientific project of Ocean Acidification impact on the Solubility & bioavailability of particulate Iron in the coastal region of Queen Maud Land in the Southern Ocean

OH^-: hydroxide anion

P

P: photosynthesis

PAR: Photosynthetically active radiation/Photosynthetic available radiation (unit: mol quanta $m^{-2}s^{-1}$)

pCO_2: the partial pressure of carbon dioxide

PE: polyethylene

PFA: perfluoroalkoxy alkanes

PFe: particulate iron

pH_{25}: pH for each discrete treatment during carbon chemistry determination

pH_i: intracellular pH

pH_T: total pH

PHYTO-PAM: PHYTOplankton Pulse Amplitude Modulated (analyzer)

PHYTO-C: the Power-and-Control-Unit (of PHYTO-PAM analyzer)

PHYTO-MS: the Miniature Magnetic Stirrer (of PHYTO-PAM analyzer)

PO_4^{3-}: phosphate

POC: particulate organic carbon

PQ: plastoquinone

PS I: photosystem I

PS II: photosystem II

PTFE: polytetrafluoroethylene

Q

Q_A: primary (bound) quinone electron acceptor of PS II

Q_A^-: the reduced product of Q_A

Q_B: secondary (mobile) quinone electron acceptor of PS II

Q_B^-: the reduced product of Q_B

Q_B^{2-}: the reduced product of Q_B^-

R

RCP: representative concentration pathways

REDOX: reduction-oxidation

rETR: relative electron transport rate

RF: radio frequency

RFU: raw fluorescence units

RLC: rapid light curve

RNA: ribonucleic acid

RS II: reaction centre II

RuBisCo: Ribulose-1,5-bisphosphate carboxylase-oxygenase

S

SD: standard deviation

SEEDS I: The Subarctic Pacific Iron Experiment for Ecosystem Dynamics Study

SERIES: Subarctic Ecosystem Response to Iron Enrichment

SiO_4^-: silicate

SOFeX: Southern Ocean Iron Experiment in 2002

SOIREE: Southern Ocean Iron RElease Experiment in 1996

SPM: suspended particulate matter

ST: single-turnover flashes

T

TALFe: total acid leachable iron

TBS: Trondheim Biological Station (Norwegian: Trondheim Biologiske Stasjon)

U

UiO: University of Oslo (Norwegian: Universitet i Oslo)

US-SQS: the Spherical Micro Quantum Sensor (of PHYTO-PAM analyzer)

US-T: the Temperature Control Unit (of PHYTO-PAM analyzer)

Y

Y2: Quantum yield at chosen wavelength in the PHYTO-PAM report

$ZnSO_4 \cdot 7H_2O$: zinc sulfate heptahydrate

Other initials

α: the slope of a P/E curve

α – FeO(OH): goethite

Φ_{PSII}: the effective quantum yield of photosynthetic energy conversion in PSII

1. Introduction

1.1 Phytoplankton

Phytoplankton are microscopic, single-celled, and photosynthetic organisms that inhabit the surface waters of the oceans [1], with a diverse diameter range from 0.02 to 200 μm [2]. They convert dissolved inorganic carbon (DIC) into organic matter via photosynthesis, when light, nutrients, and water are available, of which the process is termed as primary production [3]. Consequently, they are confined to live in euphotic zone in the ocean, which reflects the depth where only 1% surface photosynthetic available radiation (PAR) remains [4]. Phytoplankton accounts for almost 50% of the annual primary production globally, together with other marine phototrophs [2], and as the foundation of aquatic food web [5], they are of great importance to marine biodiversity and biogeochemical cycles.

1.2 The Essence of Iron

Iron (Fe) as a micronutrient is vital for a number of cellular functions of marine phytoplankton. Its essence mainly exhibits in its structural role in pertinent enzymes involved in marine biogeochemistry, which catalyze relevant reactions and promote the build-up of biomass, including electron transport in photosynthesis [6-8] & respiration [9, 10], nitrogen fixation (N_2 fixation) [11, 12], DNA replication [13], methane oxidation [14], formation of phosphate ester [15] etc.

Due to the very diverse functions of various enzymes involved in many biochemical processes, which all require iron as cofactors, iron is essential in marine biogeochemical cycles, especially in enhancing primary production by phytoplankton and alleviating climate change via biological carbon pump involved in carbon cycle.

1.3 Iron Cycling and Speciation in Seawater

Figure 1.1 [16] schematically interprets the complicated iron cycling in seawater. Along with iron cycling, iron speciation is controlled by a series of physical, chemical, and biological processes including reduction-oxidation (REDOX) reactions, organic complexation, precipitation, and photochemistry [17, 18]. The main sources of iron in seawater generally include sediments, hydrothermal vents, atmospheric deposition, and fluvial inputs [19]. In polar regions, ice-derived iron sources including melting of sea ice, icebergs and glacial inputs may make a more significant contribution compared with ocean areas located at low and intermediate latitudinal zones. But according to previous field work [20], and model studies [21], they are still incomparable to water column or sedimentary sources of iron that persist over the winter [22]. Therefore, the main iron sources to surface water are considered from water column and sediment.

In seawater, iron exists in different physical fractionations, which are traditionally and artificially distinguished mainly as dissolved and particulate iron (DFe & PFe, respectively) fractions using membrane filtration techniques (0.2-0.45 μm, cellulose acetate or polycarbonate). iron fractions below this diameter range are defined as DFe, while those above it are PFe [16]; some iron speciation in the 10 nm – 1 μm diameter

fraction, which covers parts of both DFe and PFe, is classified as "colloidal iron" [23, 24], so they are technically still small particles. The proportion of different iron fractions varies among different regions in the ocean: In coastal waters, there is less DFe than PFe (e.g., 0.05–10μM in the North Sea [25]) and a large portion of DFe can be consisted of colloidal iron, e.g., approximately 40% of DFe < 0.2 μm occurred in the colloidal phase (10 kDa - 0.2 μm) in the high salinity zone of San Francisco Bay [26]; In some open ocean areas, DFe concentration is higher than that of PFe, e.g., the oligotrophic region of central North Pacific [27].

There are only two chemical oxidation states of iron in biological systems: Ferric iron (Fe (III)) and ferrous iron (Fe (II)). Fe (III) prevails in oxygenated seawater, but its solubility is sparse. 80%-99% DFe (III) occurs as organic complexes [28-30] by chelating with natural ligands, which are possibly produced by iron limited phytoplankton [31] or bacteria [32]. By mean of chelation, the solubility of iron is enhanced. One example of natural iron ligand produced by phytoplankton is that *synechococcus* sp., one species of cyanobacteria producing siderophores in low iron media [33, 34]. The other example regarding natural iron ligand produced by bacteria is that Fe (III) is generally transported as an Fe (III)–siderophore complex that enters the periplasmic space of gram-negative bacteria through specific outer-membrane receptors [32].

The unchelated fraction is present as hydrolyzed species $Fe(OH)_X^{(3-X)+}$ (X can be 2, 3, or 4), with the neutral species $Fe(OH)_3$ being very insoluble [35]. Via hydrolysis reactions, they can also form colloidal Fe (III), which is the major iron form in seawater. According to Johnson *et al.*, DFe has a nutrient-like profile in global scale: iron concentration is almost 0 at surface water but increases with increasing depth till ca. 1000 m and then keeps roughly constant [36]. This is because the complexation by strong iron ligands keeps the solubility of iron within the mentioned depth, which acts to diminish inter-ocean fractionation and allow nutrient-like profile to develop before scavenging removes iron [36].

Some portion of DFe (III) and colloidal iron (III) are reduced to DFe (II) via photochemical reactions (photolysis and photochemical reductive dissolution in Figure 1.1), which is regarded as more readily bioavailable to phytoplankton [37] and then to participate food web or become oxidated to Fe (III) in oxygenated seawater. Deceased plankton and larger animals can release PFe, which can be remineralized to DFe after necessary specific degradation [38]. Some larger animals, e, g., Antarctic krills take up lithogenic (deep-sea ocean sediment) particles and transfer these into the surface ocean through the egestion of faecal pellets, which contain PFe [39]. Hydrothermal circulation significantly contributes to constant DFe fraction on millennial timescale, especially in the Southern Ocean [40], yet incomparable to sediment [41].

Colloidal iron (III) is also adsorbed and becomes suspended particulate iron, of which some is ultimately exported out of the water column. Bacterial uptake and scavenging of DFe contribute to PFe fraction [38]. Some aged PFe settles down and is buried into sediments, which may resuspend and dissolve in sub-oxic bottom waters.

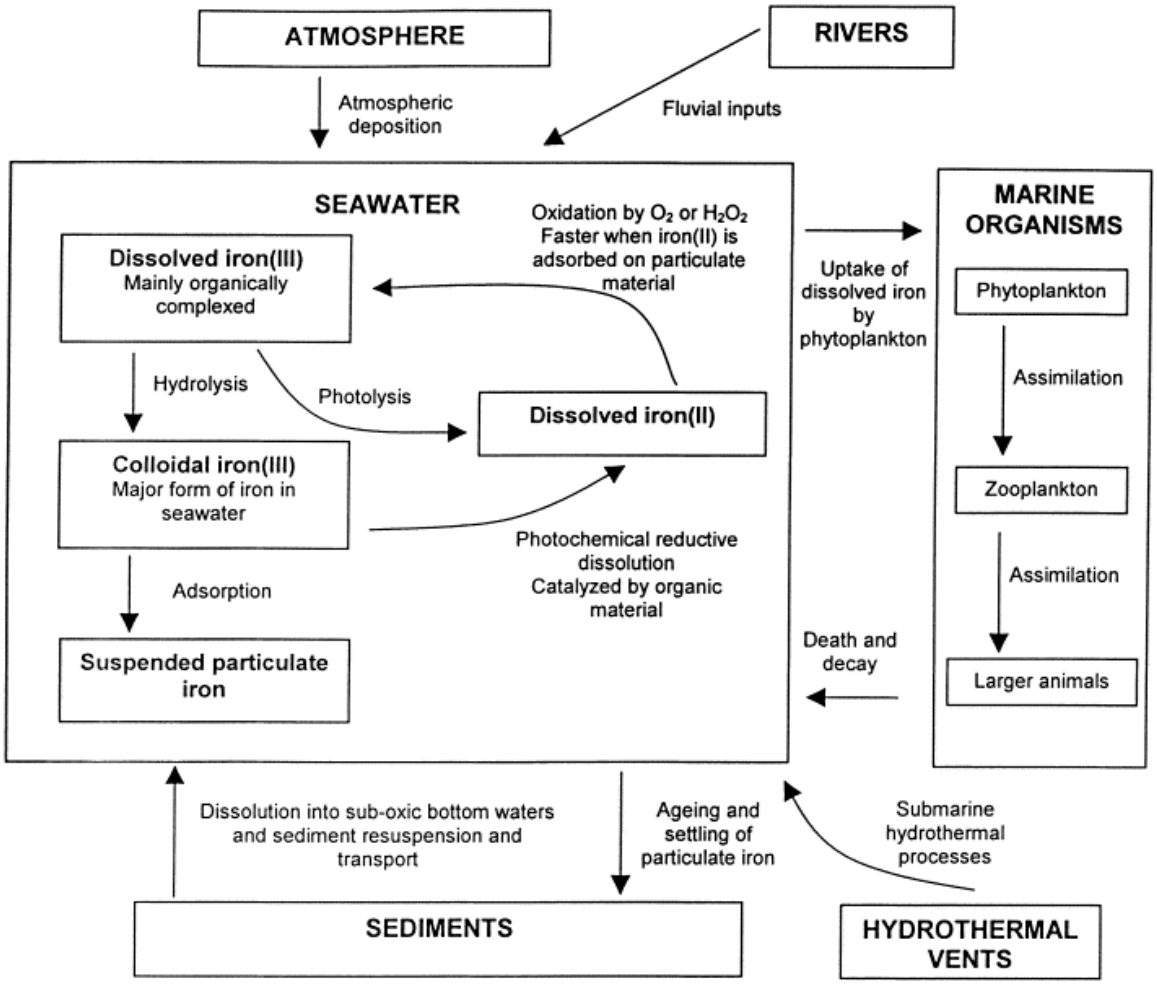

Figure 1.1. Schematic diagram of biogeochemical iron cycling in the ocean (reproduced from [16]).

1.4 Limiting Phytoplankton Growth and Primary Production, Liebig's Law & Redfield Ratio

Considering Liebig's law of the minimum [42] in the context of the ocean, when light and temperature are optimal, the nutrient in the least supply relative to the requirement by phytoplankton will limit their growth. In 1934, Alfred C. Redfield first described Redfield ratio or Redfield stoichiometry - the atomic ratio of carbon, nitrogen, and phosphorus globally found in phytoplankton and other marine organic matter [43]. This empirically developed ratio was remarkably constant to be C: N:P=106:16:1. During photosynthesis, the uptake of these 3 elements by phytoplankton in the ocean conforms to this ratio when relevant trace elements as micronutrients and light as energy source are bioavailable. When all these necessary nutrients are bioavailable and utilised, carbon dioxide (CO_2) can be efficiently synthesized as organic matter by photosynthesis of phytoplankton and sequestrated downward to deep ocean and sediment via biological carbon pump.

1.5 Iron Limitation

However, recent research in last three decades has confirmed that Fe has become the nutrient in least supply in several ocean regions, limiting primary production, carbon sequestration and carbon export.

1.5.1 Iron Hypothesis & High Nutrient – Low Chlorophyll Regions

In 1931, Gran suggested that the growth of the plankton diatoms was determined by other factors than the concentration of phosphate (PO_4^{3-}) and nitrate (NO_3^-) besides light and temperature, and postulated iron limiting phytoplankton growth in The Southern Ocean [44]. This led to John Martin to propose his "iron hypothesis" that phytoplankton growth was limited by iron in the Southern Ocean and equatorial Pacific, based on historical ice records and other evidence [45]. And his collegues proved it in equatorial Pacific in 1994 [46]. This hypothesis enlightened a series of artificial iron fertilization experiments since 1993 [44].

Along with continuous scientific investigations, three major High Nutrient – Low Chlorophyll (HNLC) zones have been named: the Southern Ocean, the equatorial Pacific Ocean, and the subarctic Pacific Ocean [47], where nitrate and phosphate concentration are high all year around whereas standing stocks of phytoplankton are always low. North Atlantic Ocean is noted as a potential HNLC zone [48]. These HNLC regions account for about one third of the world ocean [44], and they are of great interest in scientific research of marine biogeochemistry.

1.5.2 Correlation of CO_2 Concentration and Iron Supply Sources

Different data sources including ice cores [49], sediments [50] and models [51] indicate that atmospheric iron fluxes were higher in glacial times by a factor of 2-5 on a global scale, and 10-50 in the Southern Ocean. Consequently, atmospheric iron fluxes in the Southern Ocean during glaciations might have surpassed iron supplied by upwelling, which would result in more efficient biological carbon pump. In contrast, 10-box model suggests that nowadays more than 99% of iron supply to the surface in the Southern Ocean derives from upwelling instead of local atmospheric flux, and significant fortification on decreasing CO_2 concentration due to aeolian iron fertilization during glacial-interglacial time could only have happened if other processes were also at work [52]. According to different data sources, the correlation between atmospheric CO_2 concentration and iron supply sources at pre- and post- glacial and interglacial time shows that natural iron fertilization could have enhanced drawing down CO_2 concentration in the atmosphere.

1.5.3 Artificial Iron Fertilization Experiments

1.5.3.1 Overall Results of Artificial Iron Fertilization Experiments

The results from many artificial iron fertilization experiments like SOIREE[2] [53], EisenEx[3] [54] & SOFeX[4] [55] have exhibited notable increases in biomass associated with decreases in CO_2 and macronutrients (NO_3^-, PO_4^{3-} & silicate) in mixed layer [56]. However, carbon export via the formation of particulate organic carbon (POC) downward to the deep ocean was inefficient or uncertain [44]. Some iron enrichment experiments observed species shift but high grazing pressure from zooplankton as well [57]. Among all artificial iron fertilization experiments, there was observation of chlorophyll a (Chla) increase and blooms whereas patchy [44, 57] despite some remarkable blooms in SOIREE, EisenEx etc. [57].

1.5.3.2 Ecological and geophysical concerns of artificial iron fertilization

Additionally, when the potential ecological and geophysical devastating impacts of iron fertilization are concerned, especially commercial iron enrichment, their benefits seem to be negligible.

From the viewpoint of ecology, firstly, they can significantly change the composition of phytoplankton community [1] because the biomass of smaller phytoplankton increased but then were rapidly grazed with concurrent diatom blooms. Consequently, marine food web and biogeochemical circulation can be unpredictably altered in a detrimental way, which can pose a further negative impact on other marine species and industries, e.g., fisheries [58]. Besides, artificial iron enrichment can result in depletion of macronutrients [59]. As a result, it can possibly induce long-term reduction in biological productivity over a large ocean area, which could significantly threaten fisheries [60]. It is also concerned that subsequent increases in phytoplankton growth, carbon export and remineralization can cause deoxygenation in subsurface and deep ocean [44]. Moreover, commercial iron fertilization has the potential to result in harmful algal bloom, which can cause severe consequences for both marine organisms and human [61].

From the viewpoint of geophysics, there has been discussion that large-scale iron fertilization could induce high nitrous oxide (N_2O) yield to the atmosphere due to the breakdown of organic nitrogen involved [44]. Since a successful artificial iron fertilization experiment will increase not only the export of organic carbon out of surface ocean via promotion of CO_2 fixation in surface ocean, but also the remineralization in the interior ocean. As a result, one of the pathways to produce N_2O, nitrification, can be enhanced and thus more O_2 in the interior ocean is consumed, which can lead to potential deoxygenation [62]. This can reversely increase N_2O yield in its second pathway termed as low oxygen pathway, in which a highly O_2 concentration dependent fraction of the original organic nitrogen is converted to N_2O

[2] SOIREE: The Southern Ocean Iron RElease Experiment in Australasian-Pacific sector of the Southern Ocean in February 1999.
[3] EisenEx: (Eisen (=iron) Iron Fertilisation Experiment in spring in the Antarctic Polar Frontal Zone in 2000.
[4] SOFeX: Southern Ocean Iron Expriment in January 2002.

[63]. Although some of the newly produced N_2O is consumed in the interior of the ocean, most of it will be emitted eventually into the atmosphere [62]. As the radiative forcing for N_2O is nearly 300 times stronger per molecule than that for CO_2 [64], the reduced CO_2 in atmosphere stemming from iron fertilization could eventually be offset.

Some researchers also noted the production of dimethyl sulfide (DMS) was increased in some artificial iron fertilization experiments [65, 66], which is a climate-active gas that reduces the radiative flux to the surface of the earth [44]. It is produced from degradation of dimethyl sulphoniopropionate (DMSP) by certain classes of phytoplankton [44]. However, the observation of DMS increase is not clear-cut: a reduction in DMS was recorded in SERIES[5] and no change was observed in SEEDS I[6] [66].

Overall, because carbon cycle is coupled with many other elements, it seems impractical to artificially fertilize the ocean with iron in a long term and at a large-scale without perturbation to the structure of phytoplankton community and marine biogeochemical cycle. It is necessary to conduct more scientific research in order to investigate and evaluate the practicality and possible side effects.

1.6 Ocean Acidification and Its Impacts

Ocean acidification (OA) refers to a reduction in the pH of the ocean over an extended period, typically decades or longer, primarily caused by the uptake of CO_2 from the atmosphere, but it can also be caused by other chemical additions or subtractions from the ocean [67]. Pre-industrial influx of CO_2 from the atmosphere to ocean was 70 Gt C/year [68], while since the Industrial Revolution, the anthropogenic flux has been superimposing the natural flux [67]. The ocean absorbs about 30% of the CO_2 released into the atmosphere [69]. As the concentration of CO_2 in the atmosphere increases, so does it in the ocean.

From the viewpoint of aquatic chemistry, the process can be summarized as the following reaction in Figure 1.2 [69]. Firstly, atmospheric CO_2 dissolves in the ocean, forming carbonic acid (H_2CO_3) after reacting with H_2O. H_2CO_3 is a weak acid, and in the ocean quickly dissociates as bicarbonate anion (HCO_3^-) and one proton (H^+). Consequently, accumulating H^+ results in more and more acidic seawater, and causes carbonate ions (CO_3^{2-}) relatively less abundant [69] but HCO_3^- more abundant.

[5] SERIES: Subarctic Ecosystem Response to Iron Enrichment in northeast subarctic Pacific from 9th July to 4th August in 2002.
[6] SEEDS I: The Subarctic Pacific Iron Experiment for Ecosystem Dynamics Study from 18th July to 1st Aug 2001.

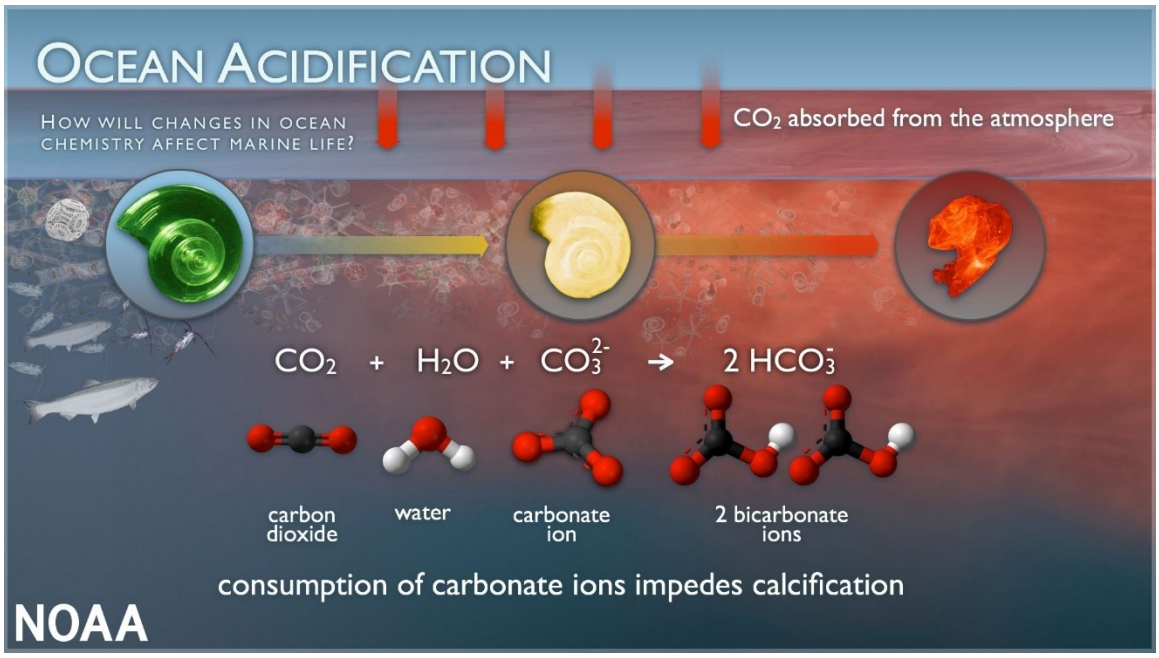

Figure 1.2. Chemical reactions of Ocean Acidification (OA) (downloaded from [69])

OA can pose a series of detrimental effects on marine organisms, biogeochemical circulation and eventually contributes to climate change.

Firstly, more abundant H^+ can dissolve calcium carbonate ($CaCO_3$), so the saturation states of aragonite ($CaCO_3$ in orthorhombic crystal form) and calcite ($CaCO_3$ in trigonal crystal form) will increasingly become lower in the upper ocean [70]. Since $CaCO_3$ is a vital building block of some $CaCO_3$-secreting organisms, such as planktonic coccolithophores and pteropods, and invertebrates such as mollusks and corals, OA makes it more difficult for these organisms to produce their shells and skeletons [71], for which the process is so-called calcification. Similarly, it can also intensify the dissolution of silica frustules of diatoms [72]. Consequently, OA reduces marine biodiversity, especially that of coralline and benthic communities, and indirectly leads to perturbation to marine food webs.

Secondly, OA may influence the speciation of some elements, despite inconclusive concerns. Taking iron for an example, magnetite (Fe_3O_4) may transform into goethite under alkaline pH conditions [73], which can be influenced by OA. Besides, iron bioavailability to phytoplankton and biological requirement of phytoplankton can also be affected by the effect of OA on iron speciation. On one hand, it has been discovered that a pH decrease by 0.3 unit should slightly increase iron solubility [74] because low pH decreases the concentration of OH^-, resulting in its compartment – natural organic ligands is more competitive for DFe and iron complexes become more available for ambient organisms [35]; on the other hand, increasing extracellular concentration of CO_2 may cause downregulation of carbon concentrating mechanism (CCM) for carbon fixation and then induces iron economy for pertinent photosynthetic and respiratory processes [75, 76]. But it has also been observed that OA changed the variation of iron compounds and thus the iron uptake rate by diatoms and coccolithophores decreased whereas Fe requirement remained unchanged [35].

Some marine primary producers may physiologically adapt to an acidified environment and cope with higher nutrient demand [77]. One example is that the diazotrophic cyanobacterium *Trichodesmium erythraeum* was found to respond strongly to elevated partial pressure of CO_2 (pCO_2) by increasing N_2 fixation [78]. The enhanced N_2 fixation rates were found to be caused by a prolongation of the N_2 fixation period [79]. They were not accompanied by larger protein pools of nitrogenases that require iron as the core cofactor [80] but may have been achieved by post-translational modification and/or higher energy availability for nitrogenase activity [78]. The demand of iron as a nutrient can thus be lowered, and other processes requiring iron e.g., electron transport in photosynthesis could be fueled.

Nevertheless, the impact of OA on iron bioavailability to phytoplankton and even marine biogeochemistry remains a gaping hole.

1.7 Marine Iron Bioavailability to Phytoplankton

As has been stated in 1.1, iron solubility in the ocean is improved via chelation with natural organic ligands, and according to their binding affinities to iron, they have been categorized into two classes: strong and weak [29]. The best documented strong chelators are siderophores [81, 82], a group of designer ligands synthesized by marine biota [82] and confined to the upper ocean [83]. Weak ligands include photoactive siderophores [83], photolysis products of high-affinity marine siderophores [83], saccharides and amino acids. They have functional groups that can form weak complexes with iron in seawater [84] and are generally observed throughout water column [29, 83]. Little has been known about the transport mechanism of iron complexed with these weak ligands, but their chemical nature is relevant to the bioavailability of iron. The complexes formed between weak ligands like saccharides and iron are more readily dissociating once reaching the surface of a cell, where they are rapidly reduced to the only bioavailable species iron – Fe (II) [85].

In recent years, it has also been discovered that PFe can be an important iron source for phytoplankton when DFe is depleted, especially iron from melting sea ice. Sugie *et al.* found that PFe associated with suspended particulate matter (SPM) in the nepheloid layer in Kuril Islands was bioavailable and provided healthy growth of phytoplankton, especially coastal diatoms [86]. Kanna *et al.* found that some of the PFe stored in sea ice was bioavailable to phytoplankton and contributed to their growth when it was released to surface seawater during the spring in ice-covered oceans [87, 88].

1.8 Objectives and Hypothesis

1.8.1 Objectives

Since the bioavailability of PFe is dependent on many different factors. Taking inorganic oxyhydroxide as an example, its bioavailability depends on its surface reactivity [89-91], which decreases with an increase in aging time and temperature and also depends on the crystal structure [89, 91] and pH. These factors can make various influence on the bioavailability of iron oxyhydroxide to marine phytoplankton. In addition, disodium ethylenediaminetetraacetate dihydrate (EDTA) as a strong iron chelator is widely used in the experiments relevant to marine iron bioavailability and

used in the form of EDTA-oxalate to eliminate extracellular-bonded iron [92, 93]. It has also been used to buffer a constant iron concentration of chemical equilibrium [94, 95]. Therefore, in this master project, we aimed to understand the bioavailability of PFe to phytoplankton under different environmental conditions. Two experiments were conducted to study the bioavailability of goethite (α-FeO(OH)): one was in the region of Queen Maud Land (DML) in the Southern Ocean in March, austral summer of 2019, culturing phytoplankton community under different pH scenarios (Part of OASIS[7]); the other was in Trondheim Biologiske Stasjon (TBS) in April 2021, culturing an Arctic Diatom species, *Nitzschia frigida*, in amended seawater from Trondheim Fjord with the addition of different concentrations of EDTA.

1.8.2 Hypotheses

DML constitutes a region where impacts of OA on the transformation, solubility and hence bioavailability of PFe by rapidly reducing pH may have effects on phytoplankton nutrient uptake and overall physiology. Enhanced influx of particulate inorganic material combined with reduced pH may in principle increase the bioavailability of PFe with crucial effects in the composition of natural plankton assemblages in the Southern Ocean. The potential changes in iron biogeochemistry due to OA and its impact on the microbial ecosystem will generate feedbacks on the global CO_2 drawdown and thus future climate change.

It is well known that EDTA is an effective chelator that is widely used to bind iron and calcium irons. Consequently, in this master project, it is anticipated that EDTA may reduce the bioavailability of DFe to the investigated species, *Nitzschia frigida*, but prepare PFe, goethite, more readily dissociating for the uptake by phytoplankton.

[7] OASIS: the scientific project Ocean Acidification impact on the Solubility & Bioavailability of Particulate Iron in the coastal region of DML

2. Methodology

2.1 Instrumental Summaries

2.1.1 SeaFast

Since the concentration of DFe of seawater samples are usually as low as nano- or even pico- molar level, for analytical purposes, it is required to preconcentrate seawater samples before determination [96]. SeaFast (Elemental Scientific Incorporated) is a high performance and fully automated software-controlled sample preconcentration and introduction system for the determination of ultra-trace metals in undiluted seawater and other high matrix samples [97]. Consequently, it lowers procedural blanks and improves detection limits [97]. It can be seamlessly integrated with Inductively Coupled Plasma Mass Spectrometry (ICP-MS) in online mode and without ICP-MS in offline mode [97]. The autosampler unit is housed in a clean mobile stand equipped with a low particulate air filter and its major component is a S400 syringe module with a perfluoroalkoxy alkanes (PFA) sample loop. In practice, acidified sample (pH ≤ 2) is firstly vacuum loaded by the autosampler probe via the syringe module into a 10 mL PFA sample coil. Subsequently, before the sample is introduced to the preconcentration column, a 6.0 ± 0.2 ammonium acetate ($NH_4CH_3CO_2$) buffer is passed through the parallel buffer clean-up column for removal of excess metals in the buffer, and then combined with MilliQ water. And as it is illustrated in Figure 2.1 [97]: the mixture of buffer and MilliQ water pushes the acidified sample onto the preconcentration column, a PFA column that is layered with an immobilized iminodiacetic acid and ethlenediaminetriacetic acid resin. It has superior selectivity to chelate trace metal ions [97] while matrix elements (group 1 and 2) are rinsed by buffer-water solution from the column at pH~6 maintained by a continuous flow of $NH_4CH_3CO_2$ buffer. After the vacuum is closed, the sample with trace elements of interest is eluted with ~ 1 M Ultrapure nitric acid (HNO_3) solution in reversed flow, concentrated to a desired volume and dispensed into a polytetrafluoroethylene (PTFE) collection tube in offline mode by 1.0 bar pressurized argon (Ar) gas.

During the process, pH is ~1 [97]. After sample elution is finished, the sampler probe is rinsed with 0.1 M Ultrapure HNO_3 and both preconcentration column and buffer clean-up column are rinsed with 1.5 M Ultrapure HNO_3. Then they are preconditioned with buffer-water mixture for next preconcentration. After all samples have been preconcentrated, they can be accordingly diluted for ICP-MS conditions and delivered for determination.

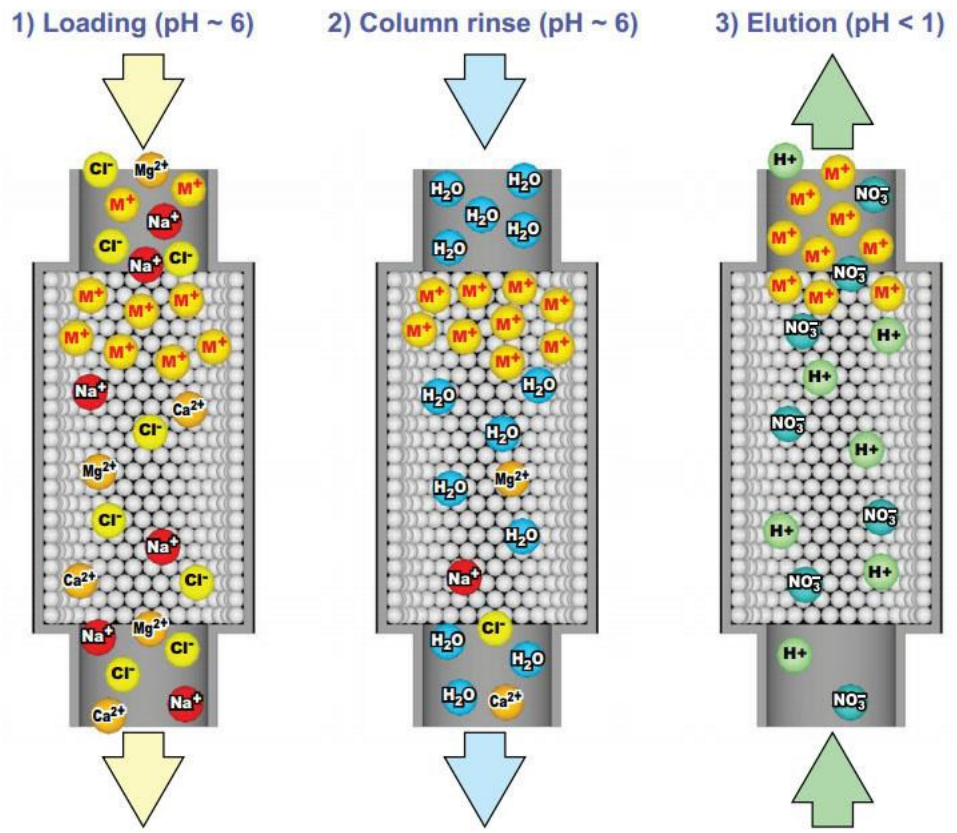

Figure 2.1. SeaFAST preconcentration column loading, rinsing and elution (reproduced from [97]).

2.1.2 HR-ICP-MS

High Resolution Inductively Coupled Plasma Mass Spectrometry (HR-ICP-MS) has been widely used in determination of iron concentration of seawater due to the following advantages: high sensitivity [96], analyzing multiple elements in one single run, low detection limit down to PPT level [98]. The main components are a sample introduction nebulizer, horizontally positioned plasma torch, interface region, mass spectrometer and detector. Detailed structure is shown in Figure 2.2 [99]. The sample in liquid form is usually pumped with a peristaltic pump into the nebulizer, in which it is converted to a fine aerosol with Ar gas [99]. Then the spray chamber separates fine aerosol droplets representing only 1-2% of the introduced sample from larger droplets. Subsequently, these fine droplets are transported into the plasma torch by a sample injector. The plasma is produced by the interaction of an intense magnetic field (produced by radio frequency (RF) passing through a copper coil) on a tangential flow of gas (normally Ar) [99]. Ar gas flows through the torch at high speed, which results in ionization of the gas when the gas is born with a source of electrons from a high-voltage spark. Consequently, a plasma discharge at very high temperature (~10,000 K) is formed at the open end of the tube to generate positively charged ions [99]. Ions are extracted from the interface region consisting of two metallic cones termed as sampler and skimmer cones and then directed into the main vacuum chamber in mass spectrometer via a series of electrostatic lenses called ion optics [99]. As they stop photons, particulates, and neutral species from reaching the detector, the ion beam is electrostatically focused onto the heart of the mass spectrometer – the mass separation device. Three of the most common types are quadrupole, magnetic sector, and time-of-flight technology. Eventually, the ion detector converts the ions into an electrical signal. Interface region, ion optics and mass separation device are at operational vacuum via mechanical pump and turbomolecular pumps as are shown in Figure 2.2 [99].

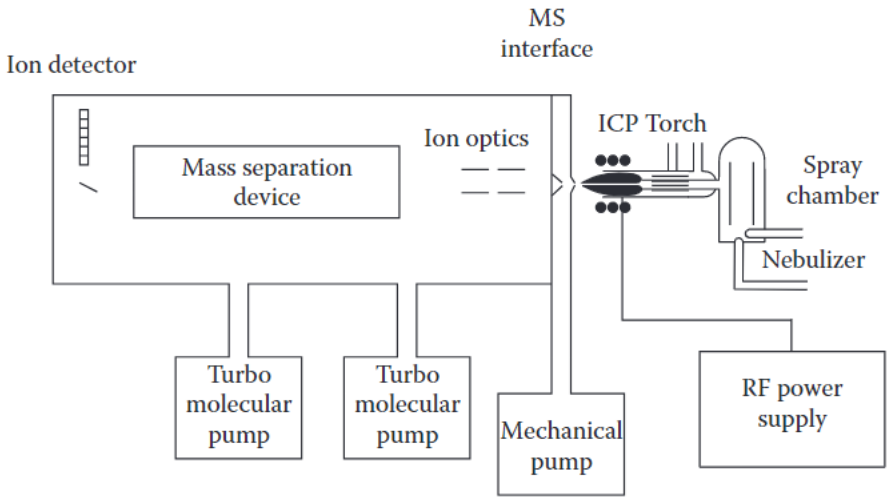

Figure 2.2. Basic instrumental components of an ICP-MS (reproduced from [99]).

2.1.3 Instruments for Determining Chlorophyll-Related Parameters

2.1.3.1 Chlorophylls, Fluorescence, and Photosynthetically Active Radiation (PAR)

Photosynthesis or primary production is a process consisting of 2 reactions: light reaction and dark reaction. In light reaction, water molecules are separated into H^+ and oxygen (O_2) and release metabolic energy; In dark reaction, CO_2 is fixed via Calvin cycle in darkness. For phytoplankton, it is the chlorophyll that harvest light and then utilize part of the energy for photosynthesis. Chlorophylls are the most widely distributed natural pigments [100] and there are also other light-absorbing pigments in photoautotrophs, such as phycocyanin, phycoerythrin, and β-carotine, which are termed accessory pigments [2]. Of the algae, Chla is the major chlorophyll and is green because it absorbs blue (maximum at 430 nm) and red wavelengths (maximally at 680 nm) of light and reflects green wavelengths [2]. In marine biology, it is used as an index for algal biomass due to its ubiquity in diverse marine photosynthetic organisms.

Fluorescence is the phenomena of certain atoms and molecules to absorb specific wavelengths of light and almost instantaneously re-emit energy in the form of longer wavelengths of light or a photon. The wavelengths of light ranging between 400 and 700 nm are generally considered the photosynthetically active component of total spectral irradiance ($E_{(\lambda)}$) and is termed Photosynthetically Active Radiation (PAR) or photosynthetically active photon flux density (E_{PAR}) [101]. For a chlorophyll molecule, it is excited after absorbing light of less than 670 nm wavelength [102]. If the energy is not utilized in charge separation, heat dissipation (non-photochemical quenching (NPQ)), or resonance energy transfer, fluorescence will occur as an electron returns to ground state [101].

2.1.3.2 10-AU Turner Fluorometer

In onboard incubation experiments, it is necessary to acquire fast real-time information about algal health and biomass. Consequently, 10-AU Turner fluorometer is widely applied specifically for Chla measurement. Using fluorescence optical module for operation, it can measure Chla concentration via quantifying the fluorescence of the extracted Chla using acidification method; or measure *in situ* or *in vitro* Chla concentration using non-acidification method. Technically, a fluorometer is composed of a light source, excitation filter, sample cell where a cuvette containing sample should be placed, emission filter, light detector, and digital readout section. The key components are shown as Figure 2.3 [103].

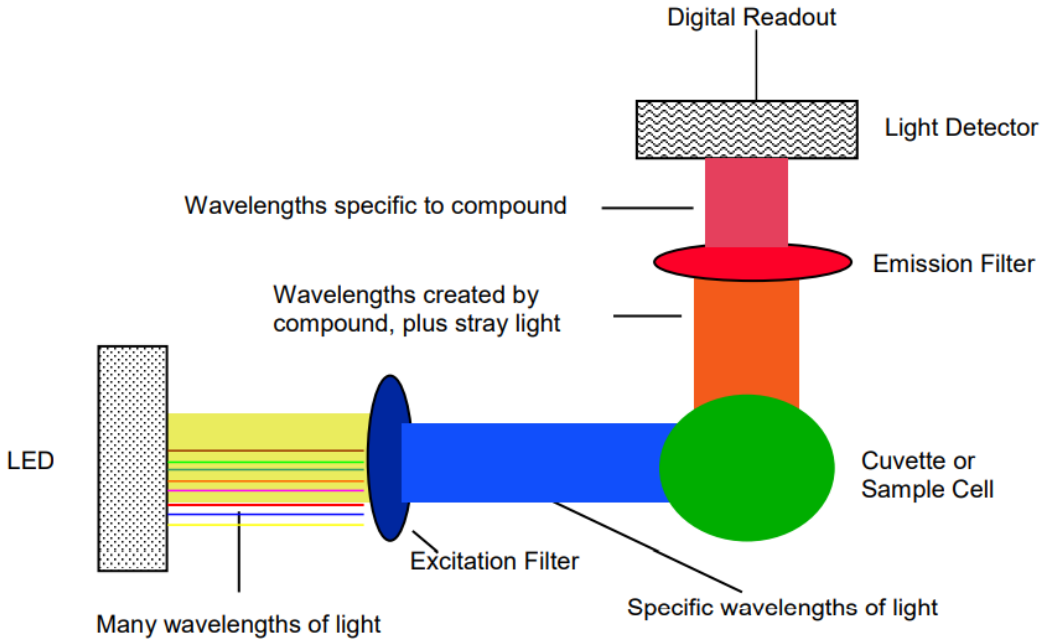

Figure 2.3. Key components of a 10-AU Turner Designs fluorometer (reproduced from [103]).

The LED emits light of different wavelengths and then the light of specific wavelengths for exciting the samples are selected by excitation filter. When the selected light passes through the sample cell, accompanied by stray light, part of the light for excitation is absorbed by the sample. As a result, the fluorophores existing in the sample fluoresce. In order to eliminate the influence of stray light (incident light and scatter light), the fluorescence is usually detected perpendicular to incident light (light source) by the detector and then concerted to digital signal by the readout system. Depending on the used mode (raw fluorescence mode or direct mode), either Chla concentration or *in vivo* fluorescence is read by the user.

2.1.3.3 Phytoplankton Pulse Amplitude Modulated (PHYTO-PAM) fluorometry

During photosynthesis, under optimal growth conditions and sub-saturating light, all absorption of light energy (photons) by pigments in the light harvesting antenna of photosystem II (PSII) are used for charge separation there, and the majority of electrons are used for linear electron transport (LET) to photosystem I (PSI) and CO_2-assimilation [104], while photosynthetic rate keeps increasing, which lead to a typical

P/E curve – the response to photosynthesis (P) in response to changes in irradiance (E).

However, when incident light is higher than saturation irradiance, photosynthetic rate levels off and even decreases because of photoinhibition at very high irradiance. At the meanwhile, the excitation energy from incident irradiance exceeds the chemical outflux in reaction centre II (RCII), and the excess excitation energy can cause photodamage to photosystems, creating a bottleneck for LET before photosystem I (PSI) [104]. Therefore, they must be safely dissipated via other processes around RSII, which could result in high electron transport rate (ETR).

Based on this, a rapid light curve (RLC) method conducted via Phytoplankton Pulse Amplitude Modulated (PHYTO-PAM) fluorometry is used to monitor the photosynthetic performance of phytoplankton in marine biogeochemistry. In practice, PHYTO-PAM analyzer (standard System I) integrated with PhytoWin 2.13 Software (3rd ed) was adopted in the experiment at TBS.

As is shown in Figure 2.4 [105], the PHYTO-PAM analyzer is a highly sensitive research instrument with multiple excitation wavelength for phytoplankton, being composed of:

1) the Power-and-Control-Unit (PHYTO-C),

2) the Optical Unit (ED-101US/MP with standard 10x10 mm quartz-cuvette) which mounts on the Stand with Base Plate (ST-101),

3) the Measuring LED-Array-Cone (PHYTO-ML), for fluorescence excitation with blue (470 nm), green (520 nm), light red (645 nm) and dark red light (665 nm); with additional red LEDs (655 nm) for actinic illumination (up to 550 µE m-2s-1); to be attached to the Optical Unit,

4) the Photomultiplier-Detector (PM-101P) with filter box and special Detector-Filter set; to be attached to the Optical Unit at right angle with respect to Measuring LED-Array-Cone,

5) the Battery Charger (MINI-PAM/L) to charge the internal battery of the Power-and-Control-Unit,

6) PC with Pentium processor and special Windows Software PhytoWin 2.13,

Below are optional components:

7) the Actinic LED-Array-Cone (PHYTO-AL) for the study of high light adapted phytoplankton,

8) the Miniature Magnetic Stirrer (PHYTO-MS),

9) the Spherical Micro Quantum Sensor (US-SQS),

10) the Temperature Control Unit (US-T).

Figure 2.4. PHYTO-PAM Standard System I Components (reproduced from [105]).

Overall, the core of the optical system PHYTO-ML & PHYTO-AL, which serve for pulse-modulated measuring light (ML), actinic light (AL). It can be applied in form of strong ms pulses, far-red light (FR) to saturate single-turnover flashes (ST) for instantaneous, quantitative closure of photosystem II (PS II) reaction centres (RCII). The light passes a short-pass dichroic filter and then enters a 10x10 mm Perspex rod that guides it to the 10x10 mm cuvette, optically mixing the various light qualities by multiple reflections [105]. PHYTO-MS continuously stirs the suspension within the cuvette to prevent the sample sink to the bottom of the cuvette. Push-in rods with mirror front surfaces are inserted perpendicular and horizontal to incident light, and the Perspex rod is perpendicular to incident light. This layout increases both the effective light intensities and the amount of fluorescence picked up by Perspex rod. The fluorescence passes a special low-background bandpass filter (650-750 nm) that is used to absorb stray light. Consequently, only the fluorescence reaches the photomultiplier or photodiode detector. The pulse-modulated fluorescence signal is selectively amplified by a pulse-preamplifier within the detector unit and then further processed by a special selective window amplifier within the main control unit PHYTO-C [105].

As is interpreted in Figure 2.5, the 4-channels excitation mode is the standard mode of operation of the PHYTO-PAM. After the start of the program, the "Channels"-window is displayed on the PC monitor screen. It demonstrates the current Chl fluorescence yields (Ft), which are measured continuously with 4 different excitation wavelengths (470 nm, 520 nm, 645 nm, and 665 nm) at default settings. Normally they are close to 0 because photomultiplier voltage (Gain) is set to a low value by default in order to avoid unintended damage. The mean values of 4 fluorescence signals are also visible.

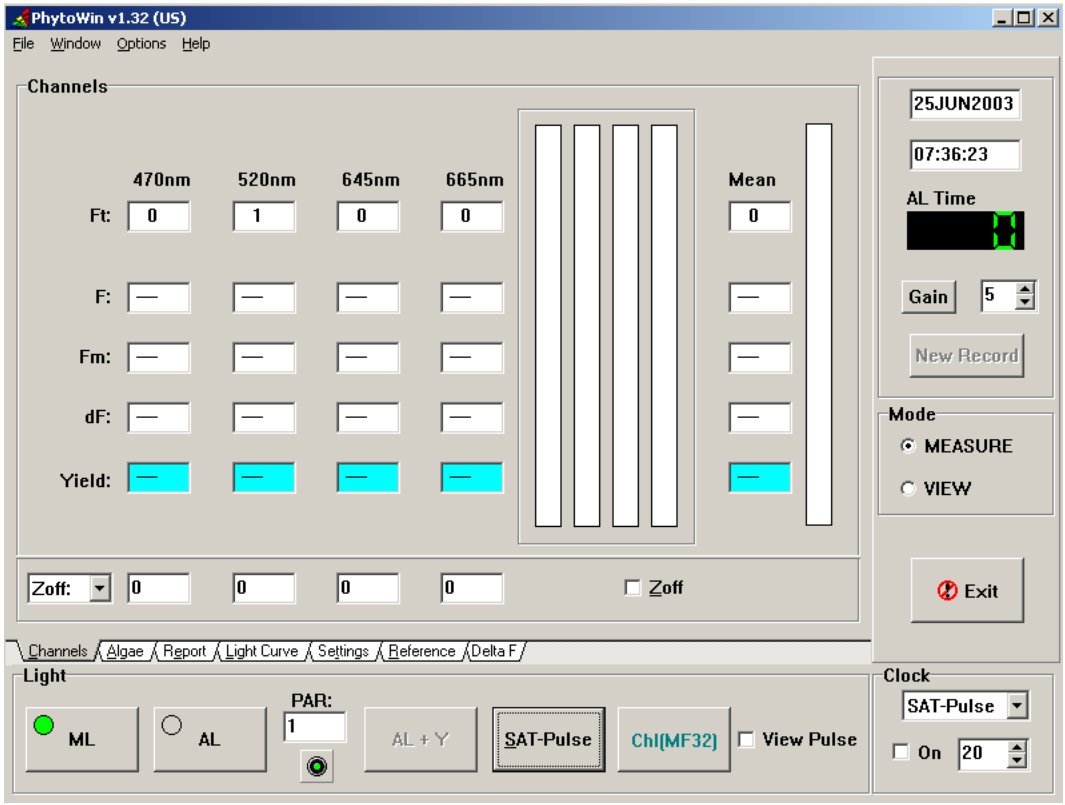

Figure 2.5. Channels-Window of PHYTO-PAM, as displayed after program start (reproduced from [105]).

ML is automatically switched on, which is indicated by the status of the ML-switch (bottom, left). To assess the minimum fluorescence of a dark-adapted sample (F_0), a width of 12µ second at low frequency is set by default (equivalent to approximately 25Hz), so its actinic irradiance is weak. Consequently, no electrons accumulate at the acceptor side of PSII and, hence, the determination of F_0 is completed.

AL is on the same array of ML, which is used for actinic illumination, but they only emit when AL-switch (bottom left, next to ML-switch) is turned on. When actinic illumination starts, there will be an automatic increase of the frequency of ML-pulses, resulting in the intensity of ML-LEDs increasing. It contributes to overall actinic intensity, which is displayed in PAR section (bottom, left, next to AL-switch). As a consequence, the signal to noise ratio is increased and the fluorescence changes during actinic illumination are assessed at high time resolution.

The measurement of the maximum fluorescence of a dark-adapted sample (F_m) is accomplished by triggering the "Sat-pulse" button (bottom, middle). In this mode, the light emitting from the LED-array source is so strong that it can cause eye damage. Thus, it must be pointed on a piece of paper. After pressing the button, the saturation pulse can cause thorough reduction of the PSII acceptor pool and thus induce an increase of fluorescence yield (dF) from F_t to F_m [105]. It is the first Fmn value (F_m') in each measurement run. Consequently, the effective quantum yield of photosynthetic energy conversion in PSII (Φ_{PSII}) can be determined, using the simple relationship [105]:

$$\Phi_{PSII} = (Fmn\text{-}F)/Fmn = dF/Fmn \text{ [105]}$$

The calculation of Φ_{PSII} is automated by the software and saved in the report. To eventually achieve a RLC, the actinic illumination is incremented in multiple steps including initial darkness measurement, of which each takes ca. 30s. And relative electron transport rate (rETR) is calculated manually using the equation below:

$$rETR = \Phi_{PSII} * PAR \text{ [106]}$$

In the Channels-mode of operation, the PHYTO-PAM is equivalent to 4 separate PAM Fluorometers using 4 different excitation wavelengths that are chosen for optimal differentiation between cyanobacteria, green algae and diatoms/dinoflagellates, which differ substantially in the absorbance spectra of their antenna pigments [105]. In cyanobacteria sample, no signal in the 470 nm Channel can be detected, because of no chlorophyll b (Chlb) in this species, while a large signal is detectable in the 645 nm Channel due to allophycocyanin absorption; A green algae sample shows a large signal with 470 nm excitation because of the existing Chlb and a low signal after the excitation by 520 nm actinic light; Due to absorption by chlorophyll c (Chlc), fucoxanthin and carotenoids, diatoms display strong signals not only with 470 nm, but also 520 nm wavelength excitation [105].

2.2 Incubation Experiment of Phytoplankton Assemblage at Queen Maud Land (DML) region

2.2.1 Experimental Water Collection

~ 400 L of seawater was collected through a peristaltic pump (Watson Marlow Varmeca, MG0723, 261-26rpm), which was connected to a PTFE tubing (10 mm ID x 12mm OD) and deployed at the depth of 20 m at Station 53 (68.10°S - 6.00° W) at Dronning Maud Land (DML) on March 12th, 2019. It was then pumped into a makeshift clean bubble equipped with a laminar flow hood (AirClean system 600 workstation) and stored in two 200 L polyethylene (PE) bags (acrylic containers) with silicon connectors. All peristaltic and PTFE tubing used were acid washed following the GEOTRACES cookbook [107]. The water was then pumped from PE bags into thirteen 20 L low-density polyethylene (LDPE) cubitainers (VWR) and sat for 32 hours at approximately open room temperature.

2.2.2 Experiment Setup

The above-mentioned 13 cubitainers were designed for 4 different treatments: Control, FeO(OH), Low pH Control & Low pH + FeO(OH), of which each had triplicates, plus one Extra Control treatment.

Goethite, α – FeO(OH), occurs in rocks and throughout the various compartments of the global ecosystem [108]. It has the diaspore structure based on hexagonal close packing of anions and is one of the most thermodynamically stable iron oxides at ambient temperature [108]. In massive crystal aggregates, goethite is dark brown or black, whereas its powder is yellow and responsible for the color of many rocks, soils, and ochre deposits [108]. It is an important pigment in industry [108]. In marine environment, it has been found that iceberg and glacial sediments from Antarctica contain aggregates of nano-goethite, and it can be transported by icebergs away from coastal regions in the Southern Ocean [109]. A portion of this nanoparticulate Fe is likely to be bioavailable either directly or indirectly (following photochemical reactions or grazing by zooplankton) [109]. Therefore, to test the bioavailability of particulate iron, 10 nM goethite was added to each cubitainer of both ambient and low pH treatments, i.e., FeO(OH) and Low pH + FeO(OH) treatments. The scheme of goethite addition is as follows:

Firstly, 100 ml of 0.252 mM FeO(OH) stock solution was prepared. 0.8 ml of this stock solution was added per cubitainer (20 L) of FeO(OH) and Low pH + FeO(OH) treatments. The final goethite concentration to be added was thus 0.8 ml*0.252mM /20000 ml = 0.00001008 mM = 10.008 nM ≈ 10 nM.

According to the 5th Assessment Report of the Intergovernmental Panel on Climate Change (IPCC) [110], pH as a climatic stressor was set as representative concentration pathways (RCP) 8.5 (pCO_2 1370 µatm) for low pH treatments and ambient pH represented the controls treatments. The adjustment of pH was carried out by a one-time addition of 7.2 mL 0.5 M hydrochloric acid (HCl, Ultrapure) and 7.2 mL 0.5 M sodium carbonate (Na_2CO_3, Trace Clean) based on the calculation by using SEACARB package in R cran and further fine tuning by Dr. Chierici M at Institute of Marine Research (IMR).

One cubitainer was intended as an Extra Control to be kept closed over the course of all experiments. All the 13 cubitainers were placed on an acrylic on-deck aquarium like, with running water from the vessel's intake (~ 5 m depth) in a configuration as is shown in Table 2.1. All treatments and their replicates are shown in Table 2.2.

Table 2.1: Ondeck configuration of all experimental cubitainers.

1	**7**	**5**	**9**	**12**	**13**
6	**2**	**8**			
4		**3**	**10**	**11**	

Table 2.2: The corresponding treatments to all the 13 cubitainers.

1	**Low pH Control**	**5**	**Low pH Control**	**9**	**Low pH Control**
2	**Control**	**6**	**Control**	**10**	**Control**
3	**Low pH + FeO(OH)**	**7**	**Low pH + FeO(OH)**	**11**	**Low pH + FeO(OH)**
4	**FeO(OH)**	**8**	**FeO(OH)**	**12**	**FeO(OH)**
13 Extra Control					

The irradiance for this community microcosm incubation experiment was adjusted through filters/screens to that of the depth where the water was collected. Based on the measurements of light intensity inside and outside the 13 cubitainers, and the absorption factor of the cubitainers themselves, the average light intensity was calculated (54.15 ± 5.21) μ mol photons m^{-2} m^{-1} (Detailed calculation available in Appendix 1.1).

2.2.3 Incubation, Measurement, and Sampling

At approximately 10pm on March 13th, 2019, the incubation started. During the first five days, intermittent water freezing problems occurred. At 6pm on March 18th, 2019, 12 of all cubitainers were moved to a temperature-controlled room (1.9 ± 0.4 °C), where the first sampling started. They were later sampled every third day for different variables within the following 7 days, i.e., on 20th, 22nd and 24th, the 2nd, 3rd and 4th sampling were implemented. Detailed information of the sampling scheme is illustrated in Table 2.3.

Table 2.3: The sampled variables and the serial numbers of corresponding cubitainers.

Incubation Day		0	5	7	9	11
Date		13/03/2019	18/03/2019	20/03/2019	22/03/2019	24/03/2019
Task	Variables sampled	Serial number of sampled cubitainers				
CO_2 Chemistry	Fugacity of CO_2 (fCO_2)	1, 5, 9 & 2/6/10	1, 6, 8, 11	1, 2, 3, 4, 5, 6, 8, 11	1 -12	1-13
	Total Alkalinity (A_T)					
	Dissolved Inorganic Carbon (DIC)					
	Total pH (pH_T)					
Macronutrients	NO_3^-, PO_4^{3-}, silicate					
Trace Elements	Total trace elements			1, 6, 8, 11	1, 6, 7, 8, 9 10, 11, 12	1, 6, 7, 8, 9 10, 11, 12, 13
	Dissolved trace elements					
Biological Parameters	Chla		1, 6, 8, 11	1, 2, 3, 4, 5, 6, 8, 11, 12	1 -12	1 -13
	in vivo fluorescence					

2.2.3.1 Carbon chemistry sampling and measurement

During the incubation, the samples relevant to carbonate chemistry were taken and measured on board. In total, four variables, total alkalinity (A_T), dissolved inorganic carbon (DIC), CO_2 fugacity (fCO_2), and total pH (pH_T), were measured. The measurement of A_T and C_T in this work were used to calculate fCO_2. Relevant instrumental manipulation and measurements were provided by IMR and Norwegian Polar Institute (NPI).

The seawater sample from each cubitainer was collected with a clean glass container in a manner designed to minimize gas exchange with the atmosphere [111], treated with saturated mercuric chloride solution (250 µL per 1000 mL sample) to prevent biological activity [112], and then the container is closed to prevent exchange of carbon dioxide or water vapor with the atmosphere [111]. The head-space air was gently removed from the small spigot on the bag, using a small hand pump (e.g., a Nalgene 6132 Repairable Hand Operated Vacuum pump) [112].

A_T was determined by potentiometric titration with 0.05 M HCl according to Haraldsson *et al.* [113], and C_T was determined by gas extraction from acidified seawater samples followed by coulometric titration with photometric detection [114, 115].

In order to acquire pH results that finally will be expressed in total pH scale (pH_T), firstly, pH was determined by using a semi-continuous system where a diode array spectrophotometer was connected to the ship's on-line supply and pH was analyzed every 7 min [116], which is similar to that used by Bellerby *et al.* [117]. And then the pH was determined by using the sulphonephtalein dye, *m*-cresol purple, as indicator [118, 119], and measured in a 1 cm flow cell thermostatic to 25 °C, and then pH results in the scale of pH_{25} were obtained. The temperature was determined in the seawater sample upstream of the flowcell.

The *in-situ* pH was calculated with the CO_2 calculation programme developed by Lewis and Wallace [120] by using the parameters A_T and pH_{25} for each discrete treatment and the *in-situ* temperature. Finally, all pH values are reported on the total pH scale (pH_T). pH_T hereby means the total pH scale introduced by Hansson in 1973 [121]. He used a medium containing sulphate ions and defined the total scale as given in the equation below:

$$pH_T = -log\left([H^+]_F + [HSO_4^-]\right) = -log[H^+]_T \text{ [121]},$$

where $[H^+]_F$ is the 'free' hydrogen ion concentration, including hydrated forms.

2.2.3.2 Macronutrients sampling and measurement

50 mL of seawater was collected from each treatment on each sampling day and spiked with 0.5 ml chloroform before storage in the dark at 4 °C. The samples were analyzed for NO_3^-, NO_2^-, PO_4^{3-}, and silicate at IMR and relevant data are provided by Dr. Chierici M. For this experiment, we mainly focus on nitrate, phosphate, and silicate.

2.2.3.3 Trace elements sampling and measurement

On each sampling day, trace element samples were only collected from one cubitainer per treatment for the determination of dissolved iron (DFe) and total acid leachable

iron (TaLFe), except Day 11, on which samples were collected from all three cubitainers of each treatment. The cubitainer was firstly well mixed by gentle shaking under a laminar flow hood (AirClean system 600 workstation) and then a sub-sample was collected for all DFe & TaLFe analysis.

For DFe sub-samples, water was filtered through Sartorius filters (0.45 + 0.2 µm pore size filtration) using acid washed Tygon tubes. The DFe fractions were defined operationally by the 0.2 µm nominal pore size. During filtration, an additional HEPA[8] air-filter cartridge (HEPA-CAP/HEPA VENT, 75 mm, Whatman) was connected to the pressure relief/ air-vent valve of the GO-FLO bottles to ensure that the air in contact with the sample during the filtration was clean. Sub-samples for TaLFe determination were collected directly into the 125 mL LDPE Nalgene bottles without filtration. All sub-samples for DFe and TaLFe were acidified to pH 1.7–1.8 with ~3 M double quartz distilled HNO_3 (Ultrapure). The acidified water samples were stored (> 1 year) until analysis.

All collected samples were preconcentrated with seaFAST and analysed by HR-ICP-MS by Syverin Lierhagen at Department of Chemistry (IKJ) at Norwegian University of Science and Technology (NTNU).

2.2.3.4 Chlorophyll a sampling and measurement

Chla determination was performed following EPA[9] Method 445.0 [122]: 500 – 1000 mL of seawater was filtered through 25 mm Whatman GF/F filters (Glass Microfiber Filters). The filters were placed in plastic vials with 5 ml of 100% methanol to extract Chla in the samples and kept at 4 °C for 24 hours. After 24 hours the samples were warmed up to room temperature in the darkness for 10-15 minutes, following a gentle inversion to remove particulates from the filter. 90% acetone solution was used to zero the instrument on the sensitivity setting that will be used for sample analysis [122]. The supernate of extracted sample was poured or pipetted into a sample cuvette, and then it was placed into the fluorometer. The fluorescence was measured and noted as R_B. Sensitivity setting used for the sample were also recorded. Next, the cuvette was removed from the fluorometer, and the sample was acidified with 2 drops of 5% HCl (1.2 M, reagent grade). Then the sample was properly mixed using a pasteur type pipet in order to aspirate and dispense chlorophylls into the cuvette. During the mixing process, the pipet tip was constantly below the surface of the liquid to avoid aerating the sample [122]. After 90 s, the fluorescence was measured again, and noted as R_A.

[8] HEPA filter: high-efficiency particulate absorbing filter and high-efficiency particulate arrestance filter.
[9] EPA: Environmental Protection Agency of United States.

Chla concentration of the samples were calculated (see the equation in Appendix 1.7) according to the readings in a Turner Designs 10 AU fluorometer and an external calibration curve (Figure 2.6 [122]) created by Solid Secondary standards raw chlorophyll (Sigma C6144), which were recorded in raw fluorescence units (RFU) on 25th Oct 2018.

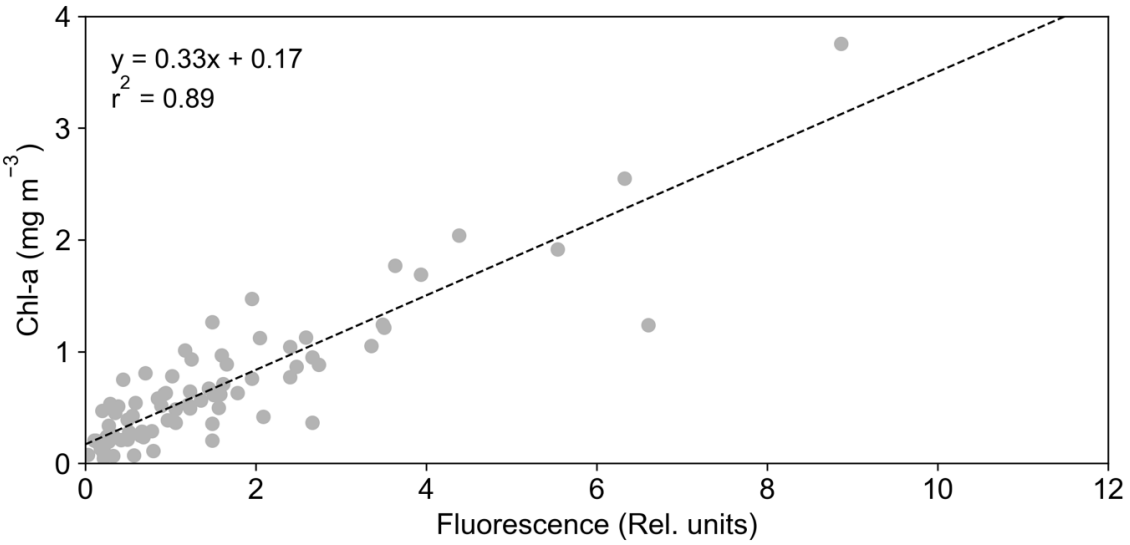

Figure 2.6. Linear regression of *in vivo* fluoerescence against fluorescence (reproduced from [122])

2.3 Incubation of Arctic Diatom *Nitzschia frigida*

2.3.1 Pre-experiment Cleaning

Meticulous cleaning of all plasticware used in this experiment laid the foundation for the quality control. The cleaning procedure is a miniature of GEOTRACES cookbook [107] and Achterberg EP *et al.* [16], which was completed as follows: All plasticware was immersed in concentrated methanol, 3M HCl (analytical grade), 1 M HCl (analytical grade) and 0.1 M HCl (analytical grade) for at least 1-2 hours. In between all plasticware should be rinsed at least 3 times with Milli-Q water, before being transferred to next cleaning. Subsequently, they were transferred to a clean lab and immersed into 0.1 M HNO_3 (UltraPure) for at least 1-2 hours. Under a clean air flow hood, they were rinsed with MQ water for 5 times until no traces of acid, sealed and stored in double plastic bags inside large plastic boxes until further use.

All pipettes intended for this experiment were cleaned under a clean air flow hood in a clean lab: Firstly, a pipette tip was mounted to a pipette and then it was plunged in 0.1 M HNO_3 (Ultra-pure). Afterwards, it was quickly rinsed with MQ water for 3 times or more until there were no traces of acid.

2.3.2 Synthesis of Culture Medium

The culture medium adopted in this experiment was based on Aquil. It is a chemically synthesised medium that was designed for lab-scale trace element study of phytoplankton. The original recipe was published by Morel *et al.* [123] in 1979. The

recipe represented here is slighted modified, combining the developed Aquil by Neil M. Price *et al.* in 1988 [124] with IMR ½ medium recipe provided by Luka Supraha from University of Oslo (UiO), based on Eppley *et al.* 1967 [125] and Edvardsen *et al.* 1990 [126].

2.3.2.1 Preparation of Chelex-100 slurry

Biotechnology Grade Chelex 100 resin is analytical grade resin which is certified to contain less than 100 micro-organisms per grams of resin [127]. It is styrene divinylbenzene copolymers containing paired iminodiacetate ions which act as chelating groups in binding polyvalent metal ions [127]. Due to its carboxylic acid groups, chelex chelating resin is classed with weakly acidic cation exchange resins [127]. It is different from ordinary exchangers because of its high selectivity for metal ions and its much higher bond strength [127]. Chelex chelating resin is efficiently regenerated in dilute acid and operates in basic, neutral, and weakly acidic solutions of pH 4 or higher [127].

In this experiment, Chelex 100 resin was used as a cleaning reagent to remove trace elements, especially iron. If their initial concentration of trace elements is known, the weight of needed Chelex 100 resin can be calculated based on several equations as follows:

$$\text{Equivalence} = \frac{\text{Total weight of trace elements (g)}}{\frac{\text{Average molecular weight of trace elements (g/mol)}}{\text{average valence of trace elements (eq/mol)}}}$$
$$= \frac{\text{Total volume of solution (L)} \times \text{Initial concentration of trace elements (ppm)}}{\frac{\sum \text{MW}}{\text{n}}} \text{(meq)}$$

$$\text{The needed weight of Chelex 100 resin} = \frac{\text{Equivalence (meq)}}{\text{Wet capacity of Chelex resin (meq/ml)}} \times \text{Density of Chelex resin (g/ml)}$$

(Equations are reproduced from Bio-rad Chelex 100 and 20 Intruction manual [127].)

The wet capacity and density of Chelex resin is 0.40 meq/ml and 0.65 g/ml, respectively [127].

Prior to use, the Chelex must be purified based on a simplified protocol according to *Price, et al.* [124]. Firstly, the Chelex resin was soaked in methanol for 3-4 h at room temperature (w/v; 40 g to 200 mL) and then rinsed with 750 mL MilliQ water. A plastic filter funnel was used for all rinsing steps. And then it was soaked in 1 M HCl and softly shaken for 30 minutes on a shaker at room temperature, which was followed by 1 L MilliQ water rinsing. Afterwards, it was soaked in 3 M ammonium hydroxide (NH_4OH), was shaken softly by a shaker for 3-5 hours at room temperature and then rinsed with 1 L MilliQ water. The next step was to soak the Chelex resin in 0.1 M HCl for 10 min and rinse it with 2 L MilliQ water. It was subsequently rinsed with and suspended in appropriate medium solution (Aquil nutrients), and slowly titrated to pH 8.3 with 1M NH_4OH. It was rinsed again with medium and packed as slurry with an acid-cleaned 50 ml vial. The first 500 ml was discarded before use.

2.3.2.2 Preparation of the stock solutions

All the stock solutions were prepared based on *Price et al.* [124] and IMR ½ medium [125]. In order to provide test phytoplankton with optimal living conditions, the higher concentration of each individual nutrient was chosen between these 2 recipes. Overall, the concentrations of $NaH_2PO_4 \cdot H_2O$ and $Na_2SiO_3 \cdot 9H_2O$ corresponds to those in IMR ½ medium.

- **Section 1**: Preparation of macronutrient stock solutions

To prepare the macronutrient stock solution of NO_3^-, PO_4^{3-} and silicate, 2.1016 g $NaNO_3$, 0.3448 g $NaH_2PO_4 \cdot H_2O$, 9.3774 g $Na_2SiO_3 \cdot 9H_2O$ were weighed and placed into three 125 ml acid-cleaned bottles, respectively. They were dissolved with MilliQ water and fixed at the volume of 100 ml. They were homogenized by vigorous shaking and then filter-sterilized by a VWR 0.2 µm cellulose acetate sterile syringe filter mounted to an acid-cleaned syringe. Afterwards, 1 ml of Chelex slurry was added to per liter of macronutrient stock solution and was shaken overnight. Chelex resin was then removed by a filter column. The trace element-free macronutrient stocks were then placed in double bags, labelled, and stored in a large plastic box until use.

- **Section 2**: Preparation of trace element mixture stock solution

To prepare the stock solution of trace element mixture (without iron), 6 trace element chemicals were weighed according to Table 2.4. After being weighed, they were placed to one 125 ml acid-cleaned LDPE Nalgene bottle. The mixture was then dissolved with MQ water and filled up to 100 ml. The bottle was then vigorously shaken to homogenise the mixture, which was followed by filter-sterilisation of a VWR 0.2 µm cellulose acetate sterile syringe filter mounted to an acid-cleaned syringe. The stock of trace element mixture was then sealed in double bags, labelled, and stored in the large plastic box mentioned above till use.

Table 2.4: Chemical weights for trace element mixture stock solution.

Chemicals	**Weight (g)**
$ZnSO_4 \cdot 7H_2O$	0.02292
$MnCl_2 \cdot 4H_2O$	0.02395
$CoCl_2 \cdot 6H_2O$	0.01197
$CuSO_4 \cdot 5H_2O$	0.00489
$Na_2MoO_4 \cdot 2H_2O$	0.02420
Na_2SeO_3	0.00173

- **Section 3**: Preparation of vitamin stock solution

To prepare the vitamin stock solution, 0.055 g cyanocobalamin (Vitamin B12), 0.005 g biotin (Vitamin H) and 0.01 g Thiamine HCl (Vitamin B1) were weighed, dissolved in 3 acid-cleaned 50 ml vials and brought up to 50 ml. 0.1 ml of Vitamin B12 solution and 1 ml Vitamin H were added to Vitamin B1 solution, which composed the stock solution of vitamin mixtures. It was subsequently sterilized by a VWR 0.2 µm cellulose acetate sterile syringe filter mounted to an acid-cleaned syringe. The stock of vitamin mixture was then sealed in double bags, labelled, and stored in the large plastic box mentioned above till use.

- **Section 4**: Preparation of iron stocks

To prepare DFe stock solution, firstly, 5ml of 0.1 M HNO_3 (Ultrapure) was diluted in a 50ml acid-cleaned vial with a little MQ water. And then 0.06118g $FeCl_3 \cdot 6H_2O$ was weighed and dissolved in the acid, and the volume was raised up to 50ml. The preparation of PFe stock solution is similar to that of dissolved iron stock solution, but the chemical was changed to 0.02024 g of goethite.

In this experiment, only DFe stock was filter-sterilized with a VWR 0.2 µm cellulose acetate sterile syringe filter, which was mounted to an acid-cleaned syringe. PFe stock was neither filter-sterilized, nor sterilized by microwave, because of the large particle size of goethite and its thermal instability. We have tested before completing the preparation of PFe stock that microwave sterilization may destroy the structure of goethite.

- **Section 5**: Preparation of the main body of culture medium.

As for the experiment at TBS, 2L of seawater were filter-sterilized with a Sartorius Sartobran cartridge filter (0.2 µm), which was accelerated by a portable pump. And then 1 ml of macronutrient stock solution, 0.1 ml of trace element mixture stock, and 0.5 ml of vitamin mixture stock were added to per litre of the filtered seawater.

2.3.2.3 Composing Experiment Treatments

To test the bioavailability of goethite under the influence of EDTA, 4 different treatments of culture medium were prepared on April 10th, 2021, which were characterized by different molarity of EDTA and iron species: 200ml of the main bulk of culture medium mentioned in 2.3.2.3 Composing Experiment Treatments was respectively distributed to 4 acid-cleaned 250ml plastic bottles. Into two of them, 200µl of EDTA stock was added; and for the other two, 600µl of EDTA was added. In the two EDTA treatments of low concentration (200µl), 20µl of $FeCl_3 \cdot 6H_2O$ and goethite were respectively added, which was also applied to the two EDTA treatments of high concentration. All 4 treatments were prepared as triplicates, distributed into 12 acid-cleaned 50ml culture bottles, and then placed in a temperature-controlled culture room (4 °C).

1 ml of original culture of *Nitzschia frigida* was inoculated to each culture bottle under a sterile fume hood and then placed back to the cooling room.

2.3.3 Photosynthetic Analysis Using PHYTO-PAM Analyzer

On April 14th, a few ml of culture was taken with a suction glass pipette after gentle shaking from the culture bottle and transferred into a 50 ml beaker that was placed in an ice bath beforehand. This assembly was then taken from the temperature-controlled culture room to an observatory lab for PHYTO-PAM analysis. The process was repeated 3 times for each replicate. After all the 12 times of analysis had finished, the remaining culture for analysis was decreased with soap. All used beakers and pipettes were rinsed with tap water and naturally dried. Detailed conduction of PHYTO-PAM is available in Appendix 2.2.

3. Results

3.1 Results of Incubation Experiment of Phytoplankton Assemblage at Queen Maud Land (DML) region in the Southern Ocean

Before interpreting the results, we would clarify that firstly samples of trace elements on Day 0 were unfortunately lost and we did not collect samples of Chla and *in vivo* fluorescence before Day 5. Therefore, we can only present concentration of these 3 parameters from Day 5 onward. Results of macronutrients, Redfield ratio, and carbon chemistry are presented from Day 0 in the following subchapters, but for them we did not collect samples between Day 0 and 5 because there was usually a "lag phase" [128] during the growth of phytoplankton and it can be more obvious for polar phytoplankton species [129]. Moreover, because DFe concentration of Low pH Control treatment on Day 7 and TaLFe concentration of Control treatment on Day 7 are exceedingly higher than the concentrations on the sampling days before and after (Day 5 and 9), and they have no replicates to be compared, we believe that they are outliers and their corresponding samples for analysis were contaminated. Consequently, even if both the figures of DFe (Figure 3.1) and TaLFe (Figure 3.2) have their outliers on the corresponding plots, we focus on interpreting and discussing the variation trend of DFe and TaLFe without them (i.e., the corresponding plot lines do not pass the outliers and they are not discussed in subchapter 4.1).

3.1.1 Dissolved Iron (DFe)

Figure 3.1 illustrates how DFe concentration was changing during the incubation in all 4 treatments. There is no clearly discernible trend over time for each single treatment. However, by Day 5, the two ambient pH treatments exhibited similar trends, which also applies to the two low pH treatments.

DFe concentration of low pH treatments was generally lower than that of ambient pH treatments and was slowly decreasing from ca. 0.30 nM on Day 5 to 0.23 nM on Day 9, quite approaching to each other. And then they were increasing from Day 9 to Day 11. DFe concentration of Low pH Control treatment was increasing faster than that of Low pH + FeO(OH) treatment from Day 9 to Day 11 and ended as the highest among all treatments on Day 11, whereas DFe concentration of Low pH + FeO(OH) treatment was the lowest on Day 11.

DFe concentration of ambient pH treatments was generally decreasing from ca. 0.70 nM (FeO(OH) treatment) & 0.85 nM (Control treatment) on Day 5, respectively, to both ca. 0.49 nM on Day 11, with a rebound from Day 7 to Day 9. DFe concentration of Control treatment was lower than that of FeO(OH) from Day 6 to Day 11.

DFe concentration of Extra Control treatment was lower than that of all treatments on Day 11.

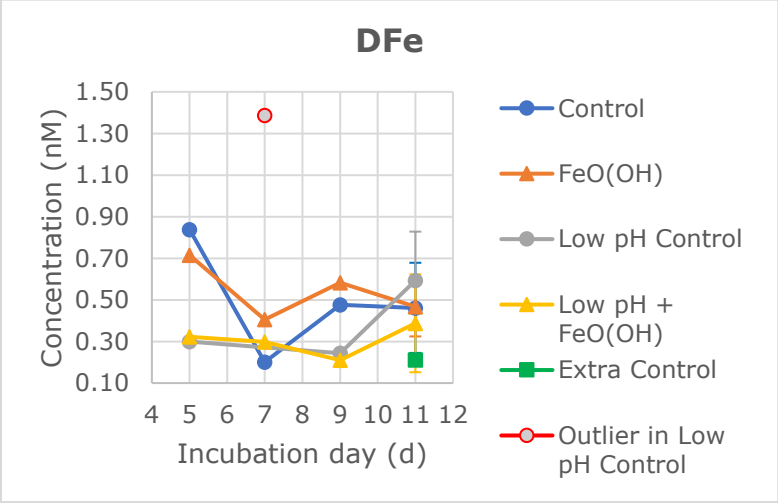

Figure 3.1. Dissolved iron (DFe) concentration during the incubation.

3.1.2 Total Acid Leachable Iron (TaLFe)

In Figure 3.2 only a rough decreasing trend of TaLFe concentration of all 4 treatments can be seen. They all decreased to 0 nM except Low pH + FeO(OH) treatment because it lacks data in Day 11.

TaLFe concentration of ambient pH treatments were quite similar during the incubation. Both of them were decreasing from ca. 1.00 nM (FeO(OH) treatment) and ca. 1.25 nM (Control treatment) on Day 5 to 0 on Day 9.

TaLFe concentration of Low pH + FeO(OH) treatment was the highest over the course of the incubation from Day 5 (ca. 1.50 nM) to Day 9 among all treatments, whereas TaLFe concentration of Low pH Control was lower than that of the two ambient pH treatments before ca. Day 6.5, but higher afterwards.

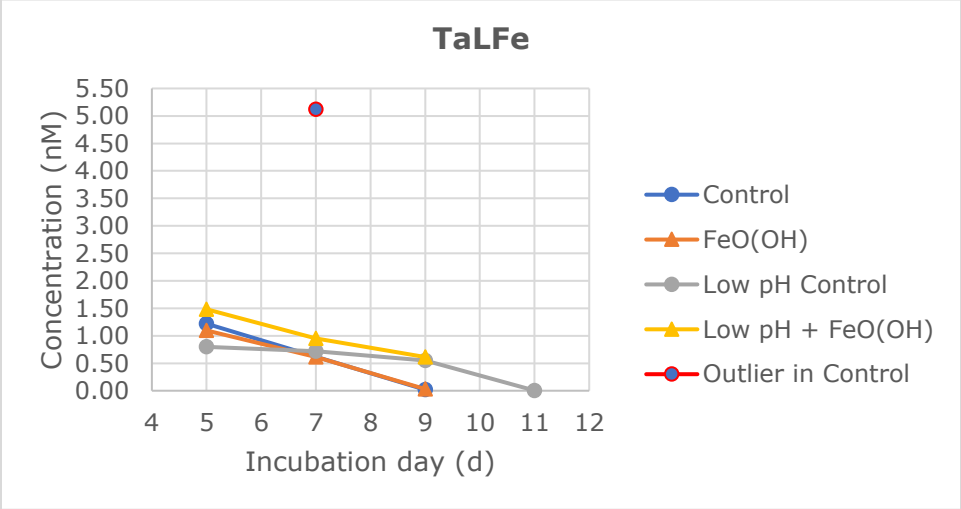

Figure 3.2. Total acid leachable iron (TaLFe) concentration during the incubation.

3.1.3 Macronutrients

According to Figure 3.3, Figure 3.4 & Figure 3.5, all macronutrients showed almost the same tendency: Firstly, they were decreasing during the incubation except PO_4^{3-}, which after Day 7 levelled off in low pH treatments but slightly increased in ambient pH treatments. Besides, the concentration profiles of two FeO(OH) treatments were more or less overlapped with their corresponding control, except of that of PO_4^{3-} of Low pH + FeO(OH) treatment from Day 0 to Day 9.

3.1.3.1 Nitrate (NO_3^-)

According to the variation of NO_3^- concentration in Figure 3.3, NO_3^- concentration of ambient pH treatments decreased more sharply compared with that of low pH treatments, reducing from 24 µmol/L to ca. 14 µmol/L. In contrast, NO_3^- concentration of low pH treatments ended with final concentration around 18 µmol/L, which is ca. 28.5 % excess relative to that of ambient pH treatments on the last day. Comparing the two ambient pH treatment, NO_3^- concentration of FeO(OH) treatment decreased faster from Day 9 to Day 11, so in the end it was ca. 1 µmol/L lower than that of Control treatment on Day 11.

NO_3^- concentration of Extra Control treatment (15 µmol/L) was between ambient and low pH treatments but approached to Control treatment on Day 11.

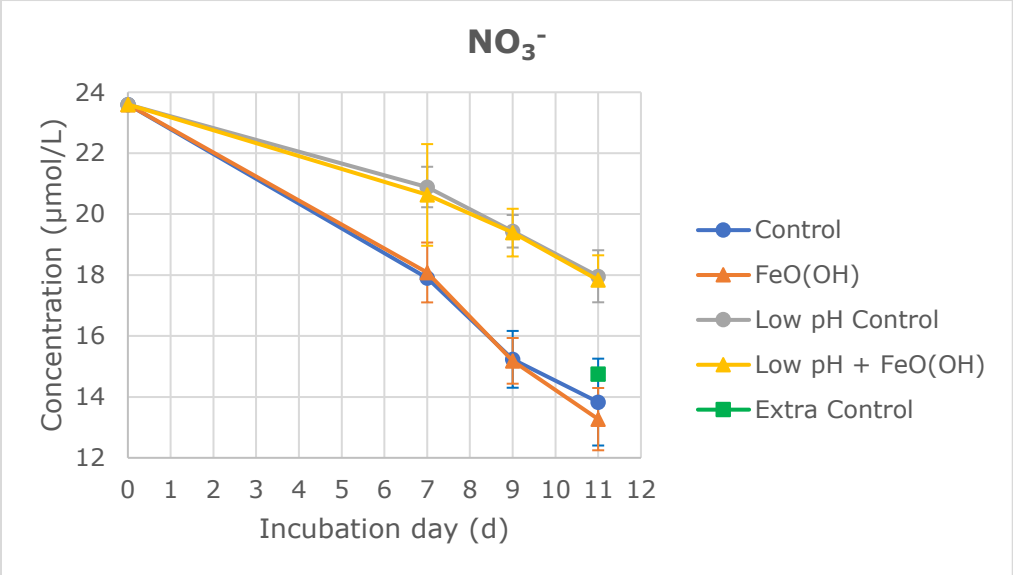

Figure 3.3. Nitrate (NO_3^-) concentration during the incubation.

3.1.3.2 Phosphate (PO_4^{3-})

It is shown in Figure 3.4 that PO_4^{3-} concentration in all treatments were decreasing from Day 0 to Day 7 with the same initial value. From Day 7 to Day 11, PO_4^{3-} concentration of ambient pH treatments were slightly increasing. In contrast, PO_4^{3-} concentration of Low pH + FeO(OH) treatment levelled off during the period, while that of Low pH Control was still decreasing from Day 7 to Day 9 and became stable from Day 9 to Day 11.

PO_4^{3-} concentration of Control treatment decreased from ca. 1.80 µmol/L on Day 0 to 1.42 µmol/L on Day 7, and then gradually climbed up to 1.48 µmol/L on Day 11. PO_4^{3-} concentration of FeO(OH) treatment is overlapped with that of Control treatment from Day 7 to Day 11, which started and ended with the concentration that is only 0.01 µmol/L higher than that of Control treatment on Day 7 and Day 11.

PO_4^{3-} concentration of Low pH Control treatment on Day 0 was also ca. 1.80 µmol/L, the same as that of Low pH + FeO(OH) treatment. In comparison to PO_4^{3-} concentration of Low pH + FeO(OH) treatment, that of Low pH Control treatment was decreasing less sharply till 1.52 µmol/L Day 9, despite high standard deviation (SD) of the value on Day 7. Subsequently it kept stable until the end of incubation. The concentration of Low pH + FeO(OH) treatment generally had no change from Day 7 to Day 11, during which it was steady at ca. 1.53 µmol/L.

PO_4^{3-} concentration of Extra Control treatment on Day 11 (1.45 µmol/L) was lower than all treatments, but more approximate to that of Control treatment.

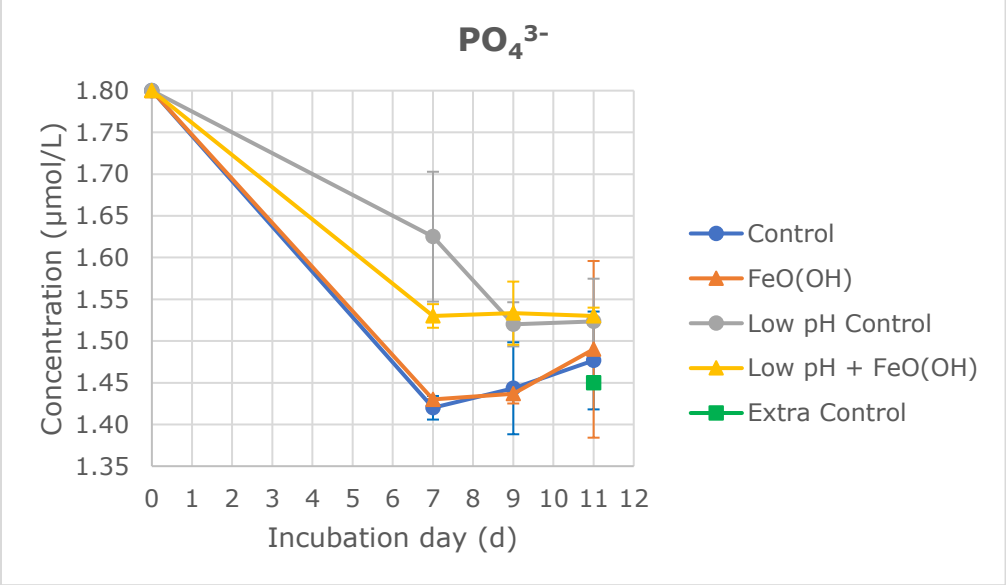

Figure 3.4. Phosphate (PO_4^{3-}) concentration during the incubation.

3.1.3.3 Silicate

Silicate concentration is vividly exhibited in Figure 3.5. Comparing with PO_4^{3-} concentration, silicate concentration was generally decreasing in all treatments, but the decreasing speed from Day 7 to Day 11 was slower than that from Day 0 to Day 7. And they all decreased with identical initial value. Besides, the difference of silicate concentration between ambient pH treatments and low pH treatments are smaller in comparison to that of NO_3^- & PO_4^{3-} concentration between their ambient pH treatments and low pH treatments.

Silicate concentration of Control treatment decreased from ca. 52 µmol/L on Day 0 until ca. 43 µmol/L on Day 7, and then slowly decreased to ca. 41 µmol/L on Day 11. In contrast, silicate concentration of FeO(OH) treatment was slightly higher than that of Control from Day 7 to Day 11: it was stable at the value of slightly higher than 43 µmol/L from Day 7 to Day 9 and decreased to ca. 41 µmol/L on Day 11.

Silicate concentration of Low pH Control treatment on Day 0 was equal to that of Control treatment (ca. 52 µmol/L), but in contrast was decreasing less sharply till nearly 45 µmol/L on Day 7. And then it slowly decreased to ca. 44 µmol/L on Day 9 in the end, without data available for Day 11. Silicate concentration of Low pH + FeO(OH) treatment was slightly lower than that of Low pH Control treatment from Day 0 to Day 9 and decreasing from ca. 52 µmol/L to ca. 44 µmol/L during the incubation.

Silicate concentration of Extra Control treatment on Day 11 (43 µmol/L) was lower than that of Low pH + FeO(OH) treatment but higher than that of ambient pH treatments.

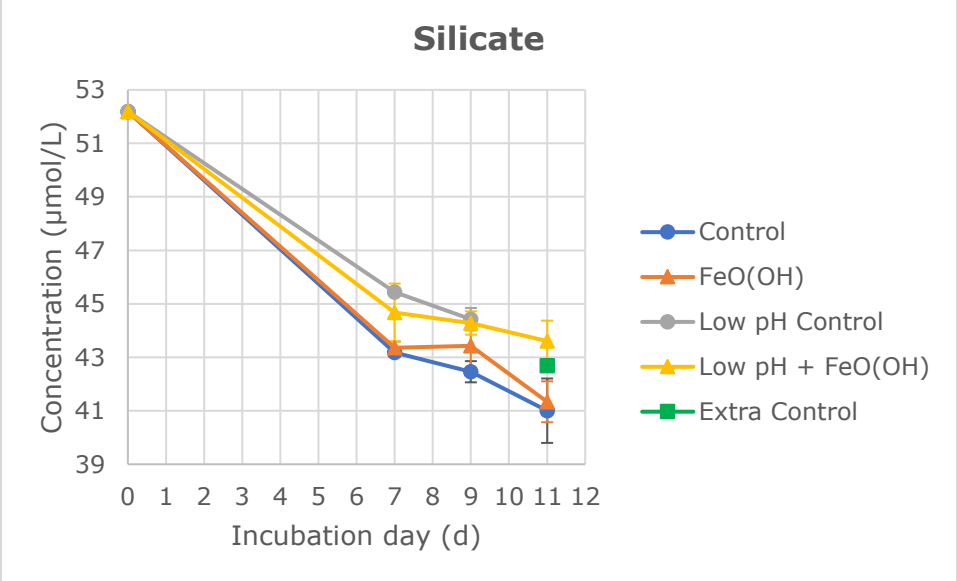

Figure 3.5. Silicate concentration during the incubation.

3.1.3.4 Redfield ratio of N/P

Redfield ratio of N/P (it is simply referred to as N/P ratio in all the following text) is shown in Figure 3.6. All treatments had identical initial N/P ratio, 13.1, on Day 0 because they had the same initial NO_3^- & PO_4^{3-} concentration, and respectively marched on a considerably slow decline, expect Low pH + FeO(OH) treatment.

N/P ratio of Low pH Control treatment decreased from 13.1 on Day 0 to 12.8 on Day 9 while that of ambient pH treatments slid to 12.6 on Day 7. Subsequently, N/P ratio of Low pH Control treatment dropped from 12.8 on Day 9 to 11.8 on Day 11 while that of ambient treatments collapsed to 9.4 (Control treatment) and 8.9 (FeO(OH) treatment) on Day 11, respectively.

On the contrary, N/P ratio of Low pH + FeO(OH) treatment was climbing up from 13.1 on Day 0 to 13.5 on Day 7, and was the highest among all treatments during the period. Then it rapidly decreased to 11.7 on Day 11. Its values on Day 9 and 11 are almost equal to those of Low pH Control, only very slightly lower.

N/P ratio of Extra Control treatment on Day 11 was 10.2, which was between ambient and low pH treatments.

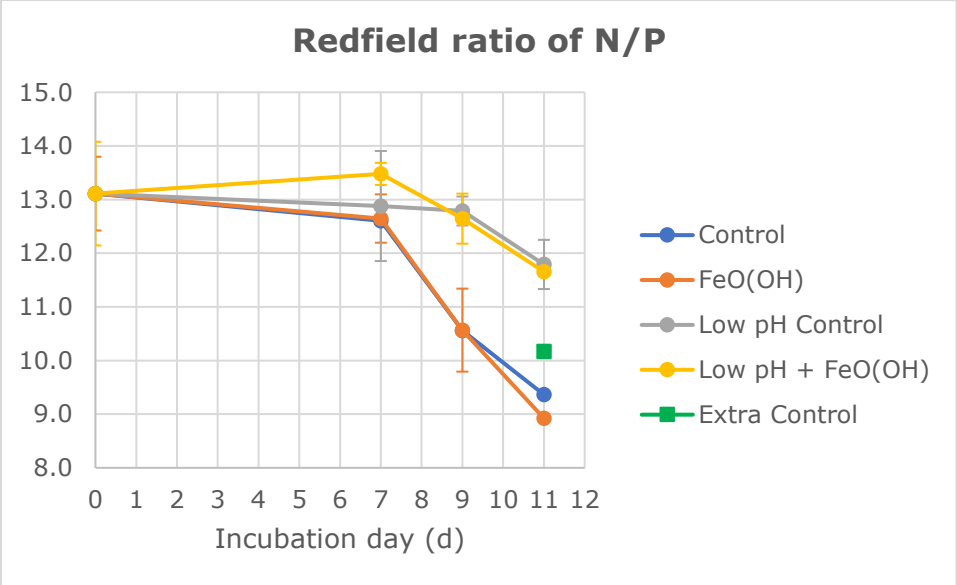

Figure 3.6. Redfield ratio of N/P during the incubation.

3.1.4 Results of Biological Parameters

3.1.4.1 Chlorophyll a (Chla)

In Figure 3.7, Chla concentration of ambient pH treatments was considerably higher than that of low pH treatments, and Chla concentration of the two FeO(OH) treatments was higher than that of their respective control treatments. Chla concentration of all treatments was decreasing from Day 5 to Day 7 and then increased at a drastically faster pace until the end of the experiment, except Control treatment, of which Chla concentration was constantly increasing. SD shows that there is no obvious difference among the replicates on each sampling day.

Chla concentration of Control treatment initially was slowly climbing up from slightly below 4 mg/L on Day 5 to slightly over 4 mg/L on Day 7, after which it was steadily increasing to 11 mg/L on Day 11. Chla concentration of FeO(OH) treatment was firstly on a shallow decline from ca. 5 mg/L on Day 5, which was the highest among all four treatments on the same day, to ca. 4 mg/L on Day 7. Subsequently, it rapidly increased to ca. 12 mg/L on Day 11, having a gap from Control treatment from Day 7 till the conclusion of the experiment.

Chla concentration of Low pH Control treatment was the lowest among those of all four treatments throughout the experiment. It exhibited a decline from ca. 3 mg/L on Day 5 to ca. 1 mg/L on Day 7, then gradually increasing to ca. 3 mg/L on Day 9 and ending at ca. 7 mg/L on Day 11. Chla concentration of Low pH + FeO(OH) treatment was almost the same as that of Low pH Control treatment on Day 5, and then in comparison, continued with a shallower decline to ca. 2 mg/L on Day 7. After that, it experienced a stable increase up to ca. 8 mg/L on Day 11. During the increment, the gap between low pH treatments was larger than that between ambient pH treatments, and the largest gap was located on Day 9, which was ca. 1 mg/L.

Chla concentration of Extra Control treatment was 10 mg/L, in the middle between those of ambient and low pH treatments.

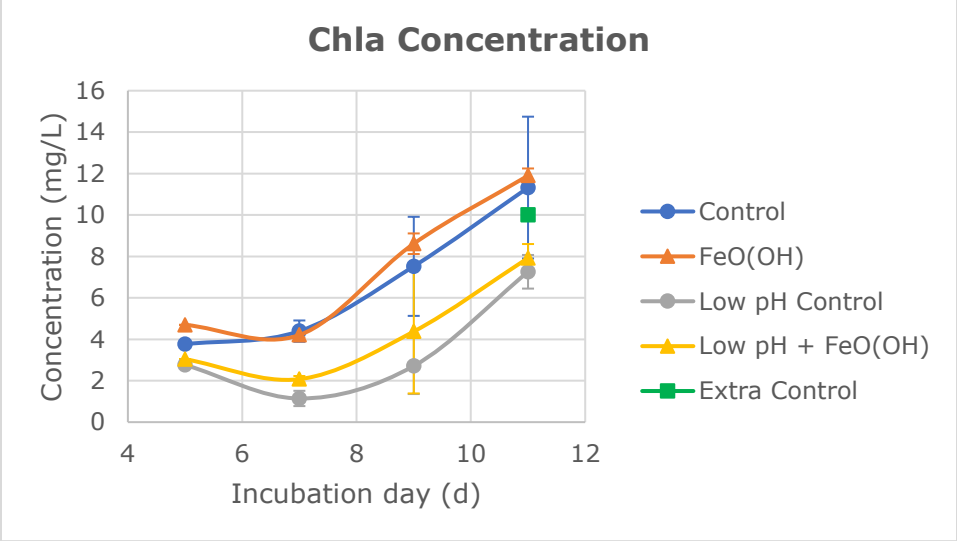

Figure 3.7. Chlorophyll a (Chla) concentration during the incubation.

3.1.4.2 In Vivo Fluorescence

It is depicted in Figure 3.8 that *in vivo* fluorescence has similar trend to Chla concentration. During the incubation ambient pH treatments had considerably higher fluorescence than low pH treatments, especially after Day 7. Moreover, iron enriched treatments also had higher fluorescence than their corresponding control treatments. *In vivo* fluorescence of all four treatments on Day 5 are quite close to each other, varying from 0.38 to 1.15.

In vivo fluorescence of FeO(OH) treatment slowly climbed up from 1.15 on Day 5 to 1.56 on Day 7, drastically increased to 3.44 on Day 9, and then reached 4.18 on Day 11. *In vivo* fluorescence of Control treatment was ca. 0.20 lower than that of FeO(OH) treatment from Day 5 to Day 9 and did not significantly increase before Day 7, after which it rapidly increased to 3.18 on Day 9, and finally ended at 3.69 on Day 11. *In vivo* fluorescence of Low pH + FeO(OH) treatment was on a shallow decline from 0.78 on Day 5 to 0.64 on Day 7. Then it gradually increased to ca. 1.72 on Day 11 at a stable pace. *In vivo* fluorescence of Low pH Control ascended from 0.38 on Day 5 to 0.47 on Day 7, and then increased at a more rapid speed to 1.58 on Day 11.

In vivo fluorescence of Extra Control treatment was ca. 2.70 on Day 11, which is between ambient and low pH treatments.

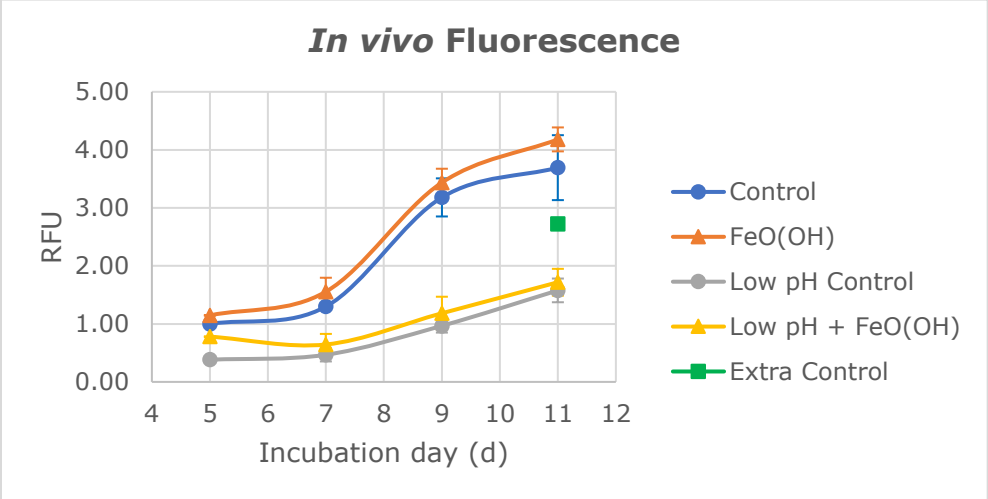

Figure 3.8. *In vivo* fluorescence in relative fluorescence units (RFU) during the incubation.

3.1.4.3 The Correlation between Chla Concentration and In Vivo Fluorescence

Figure 3.9 shows the correlation between Chla concentration and *in vivo* fluorescence: According to the simple linear regression model, *in vivo* fluorescence is proportional to Chla concentration, and coefficient of determination (R^2 = 0.944) approximate to 1 demonstrates that in vivo fluorescence is well correlated to Chla concentration among all treatments during the experiment. This confirms that the sampling and analysis of Chla concentration were properly conducted.

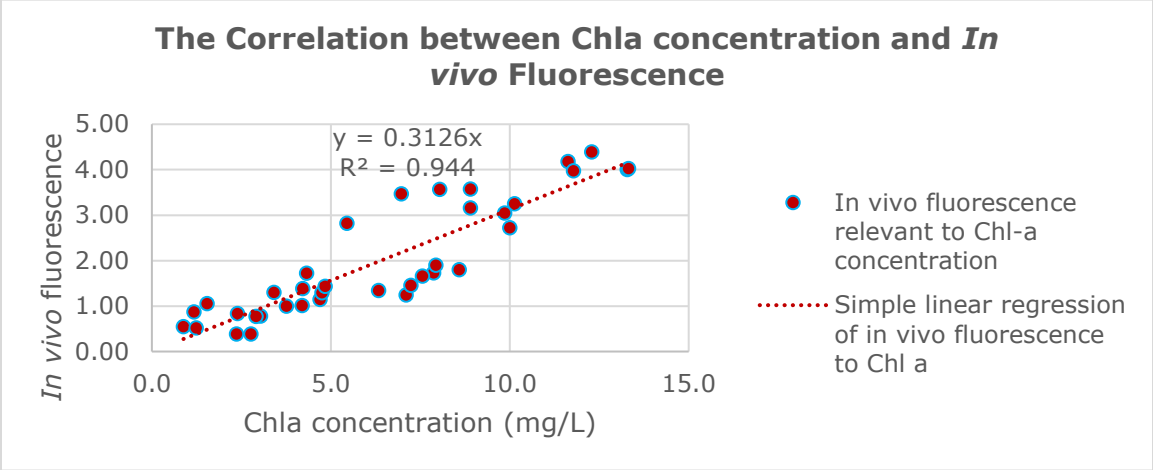

Figure 3.9. The correlation between Chla concentration and *in vivo* fluorescence during the incubation.

3.1.5 Carbonate System

3.1.5.1 Fugacity of CO_2 (fCO_2)

It is described in Figure 3.10 that during the incubation fCO_2 of all treatments was decreasing, and fCO_2 of low pH treatments is 4-6 folds higher than that of ambient pH treatments.

fCO_2 of Low pH Control treatment initialized with 1800 µatm on Day 0, was decreasing at a slower speed till ca. 1200 µatm on Day 9 and then levelled off to the end of the experiment. fCO_2 of Low pH + FeO(OH) treatment was also decreasing with the same initial value on Day 0, and its profile was overlapped with that of fCO_2 of Low pH Control treatment until Day 7. Subsequently, it kept decreasing from ca. 1400 µatm on Day 7 to ca. 1200 µatm on Day 11, which is approximate to that of Low pH Control treatment. During the decrease from Day 7 to Day 10, fCO_2 of Low pH + FeO(OH) treatment was slightly higher than that of Low pH Control treatment.

In comparison to low pH treatments, fCO_2 of ambient pH treatments had a lower initial value of ca. 400 µatm on Day 0, and they were on a shallower decline during the incubation. fCO_2 of Control treatment was on a decline through 300 µatm on Day 7 to ca. 200 µatm on Day 11, and fCO_2 trend of FeO(OH) treatment is overlapped with that of Control treatment during the incubation.

fCO_2 of Extra Control treatment (ca. 270 µatm) on Day 11 was almost the same as that of ambient pH treatments, only very slightly higher.

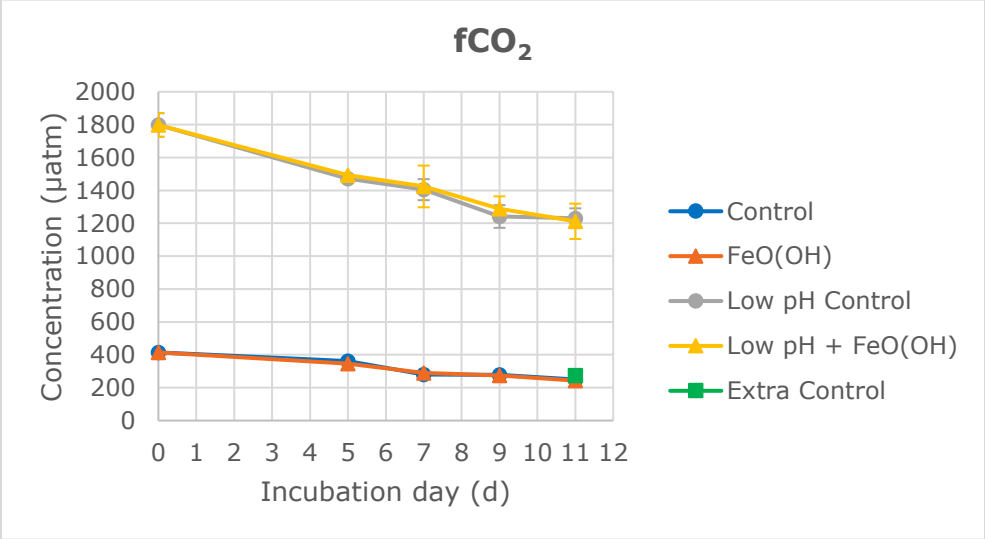

Figure 3.10 Fugacity of CO_2 (fCO_2) during the incubation.

3.1.5.2 CO_2

CO_2 concentration is shown in Figure 3.11, of which the profile is highly similar to that of fCO_2, but there was evident fluctuation between Day 5 and Day 9 in low pH treatments.

Low pH Control treatment firstly decreased from ca. 100 µmol/kg on Day 0 to ca. 73 µmol/kg on Day 5, which was followed by an increment to ca. 87 µmol/kg on Day 7. It later fell to ca. 78 µmol/kg on Day 9 and then stabilized till the end of the experiment. CO_2 concentration of Low pH + FeO(OH) had the same initial value and followed the same fluctuation pattern as Low pH Control treatment: It was decreasing to ca. 77 µmol/kg on Day 5, increasing to ca. 96 µmol/kg on Day 7, and then on Day 9 dropped back to approximately the value as Day 5. Later, it stabilized until the conclusion of the incubation as its control did.

The starting CO_2 concentration of both ambient pH treatments, ca. 25 µmol/kg was approximately four times lower than that of both Low pH treatments. They only decreased by ca. 10 µmol/kg till the end of the experiment, and their profiles were highly similar to each other.

CO_2 concentration of Extra Control treatment (ca. 17 µmol/kg) on Day 11 was almost the same as that of ambient pH treatments.

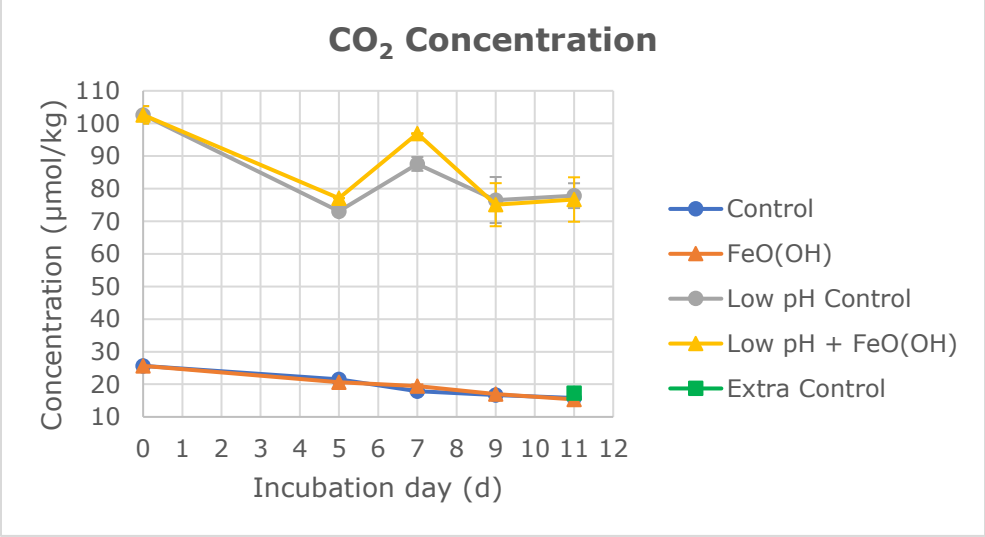

Figure 3.11. Carbon Dioxide (CO_2) concentration during the incubation.

3.1.5.3 Dissolved Inorganic Carbon (DIC)

As is interpreted in Figure 3.12 , DIC concentration of ambient treatments was continuously decreasing throughout the incubation. By contrast, there was fluctuation within low pH treatments during the incubation. What is identical is that DIC of all treatments were at approximately the same concentration on Day 7, which was more or less than 2155 µmol/kg.

DIC concentration of Control treatment was decreasing from nearly 2200 µmol/kg on Day 0 to ca. 2158 µmol/kg on Day 9, passing by ca. 2176 µmol/kg on Day 5. DIC concentration of FeO(OH) treatment was decreasing at a constant speed from Day 0 to Day 7, with a lower value of ca. 2168 µmol/kg on Day 5 compared with that of Control treatment. DIC concentration of both ambient pH treatments were nearly the same from Day 7 to Day 9, ending with ca. 2150 µmol/kg on Day 9.

In comparison with ambient pH treatments, both Low pH treatments had lower DIC concentration of ca. 2163 µmol/kg on Day 0. Then till Day 5, DIC concentration of Low pH + FeO(OH) treatment was decreasing to ca. 2140 µmol/kg, while that of Low pH Control treatment was decreasing to a lower value of ca. 2136 µmol/kg. Subsequently, DIC concentration of both low pH treatments rebounded to the abovementioned identical concentration on Day 7 but collapsed again to ca. 2136 µmol/kg on Day 9.

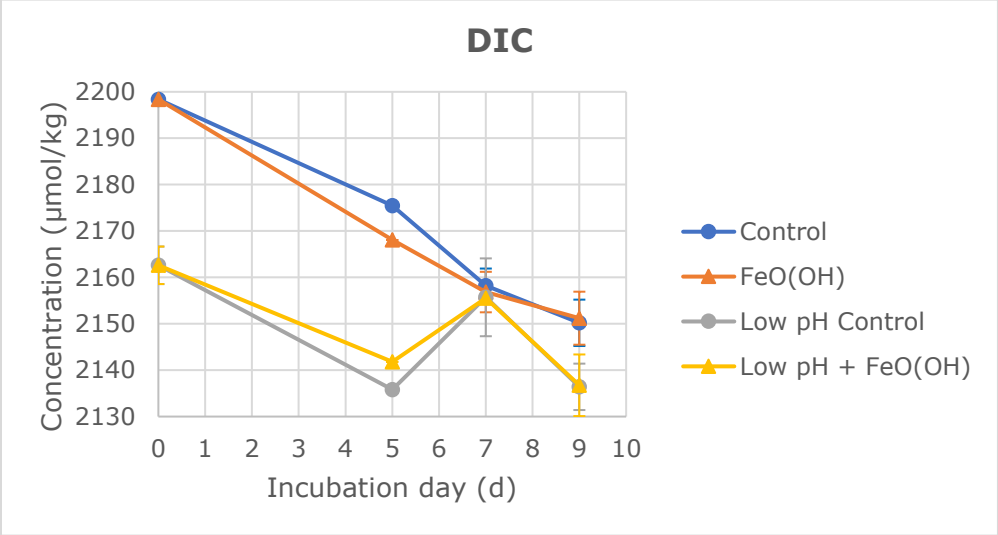

Figure 3.12. Dissolved Inorganic Carbon (DIC) concentration during the incubation.

3.1.5.4 Total pH (pH_T)

It is shown in Figure 3.13 that ambient pH treatments had higher pH_T compared with the low pH treatments, which is expected as a result of the action of artificial acidification. And the alteration of pH also caused the difference of carbon chemistry data between ambient and low pH treatments (Figure 3.10, Figure 3.11 & Figure 3.12). Besides, iron enriched treatments had almost identical pH_T to their corresponding control treatments from Day 0 to Day 11.

pH_T of both ambient pH treatments was ca. 8.02 on Day 0 and then was increasing to ca. 8.20 on Day 11.

In contrast, pH_T of both low pH treatments was drastically lower compared with that of ambient pH treatments on Day 0, only ca. 7.38, and was increasing to ca. 7.55 on Day 11. Nevertheless, it was still ca. 0.65 lower on Day 11 compared with pH_T of ambient treatments.

pH_T of Extra Control treatment on Day 11 (8.18) was slightly lower than that of ambient pH treatments.

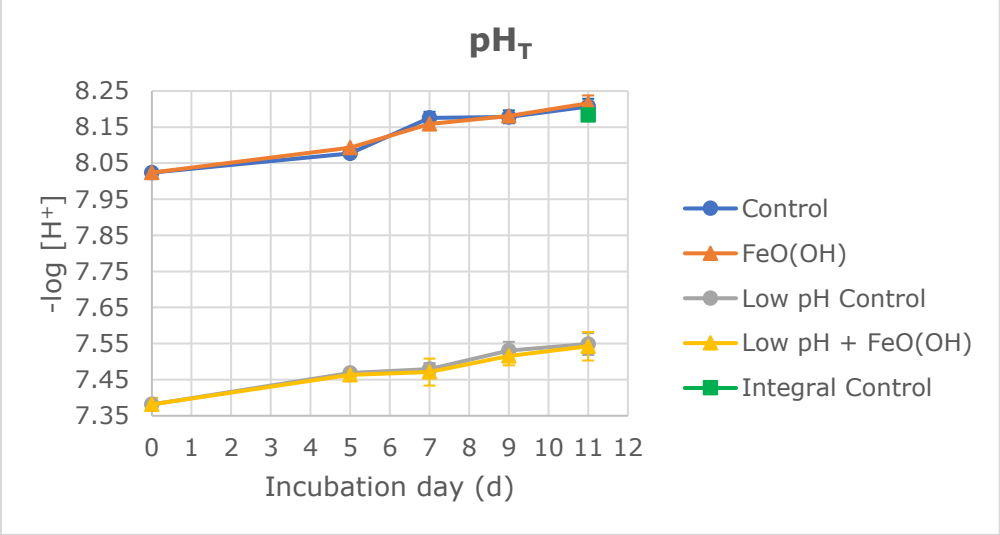

Figure 3.13. Total pH (pH_T) during the incubation.

3.2 Results of Incubation Experiment of Arctic diatom *Nitzschia frigida*

In this subchapter, we only present results from Replicate 1 because samples of Replicate 2 & 3 waited for longer time than Replicate 1 before measurement, even if they were placed in ice bathes. The thawing effect caused high bias of PHYTO-PAM results of Replicate 2 & 3 considering that *Nitzschia frigida* is a polar phytoplankton species.

3.2.1 Photochemical Parameters

3.2.1.1 Fluorescence Yield in Actinic Light (F')

It is shown in Figure 3.14 that the fluorescence yield in actinic light (F') of all four treatments peaked when E_{PAR} was 32 µmol photons m^{-2} s^{-1}, was gradually decreasing when E_{PAR} was approaching 400 µmol photons m^{-2} s^{-1} and stabilized until the measurement was finished. F' of both Goethite treatments reached to the top of 700 at E_{PAR} of 32 µmol photons m^{-2} s^{-1}, decreased to ca. 590 when E_{PAR} went up to 200 µmol photons m^{-2} s^{-1}. But F' of Goethite – 5 µmol EDTA treatment not only had slightly lower initial F' (ca. 570) at E_{PAR} of 0 compared with that of Goethite – 15 µmol EDTA treatment (ca. 590), but also significantly lower F' when E_{PAR} was above 200 µmol photons m^{-2} s^{-1} until the end of the measurement. On the last measurement, F' of Goethite – 15 µmol EDTA treatment was ca. 540, while that of Goethite – 5 µmol EDTA treatment was below 500.

F' of $FeCl_3$ – 5 µmol EDTA treatment had a significantly lower F' at 0 E_{PAR}, only ca. 520, reached to its maximum of ca. 620 when E_{PAR} increased to 32 µmol photons m^{-2} s^{-1}, drastically decreased to 500 at the E_{PAR} of 200 µmol photons m^{-2} s^{-1}, and finally slid to 450 at the end of the measurement while E_{PAR} was reaching 1000 µmol photons m^{-2} s^{-1}. F' of $FeCl_3$ – 15 µmol EDTA treatment was constantly the lowest among all four treatments: It started with ca. 440 at E_{PAR} of 0, had the highest value of ca. 540 at E_{PAR} of 32 µmol photons m^{-2} s^{-1}, decreased to ca. 390 when E_{PAR} was 400 µmol photons m^{-2} s^{-1}, and diminished to ca. 350 till the end of the measurement.

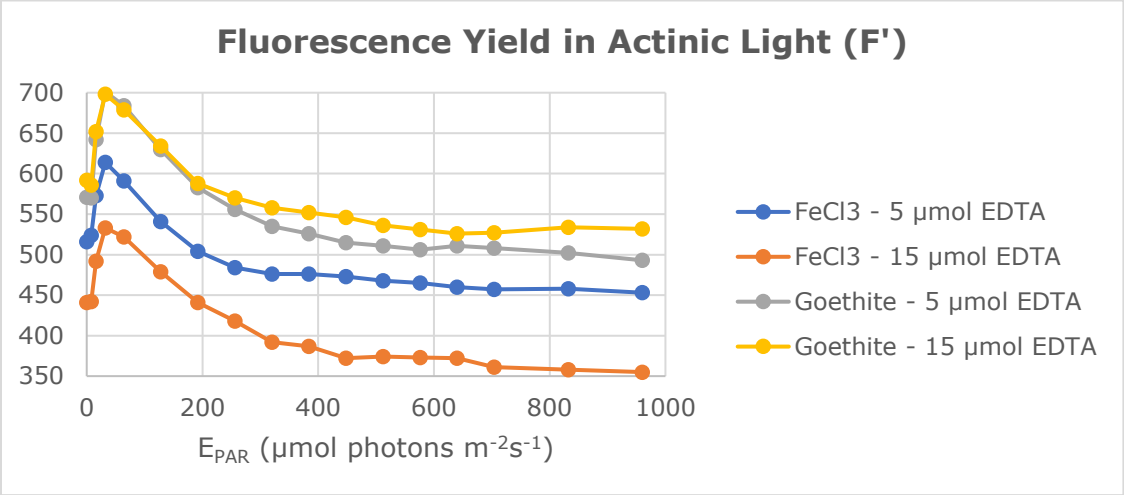

Figure 3.14. Fluorescence yield in actinic light (F') along with E_{PAR}.

3.2.1.2 Maximum Fluorescence Yield in Actinic Light (F_m')

As is interpreted in Figure 3.15, maximum fluorescence yield in actinic light (F_m') of all four treatments decreased from the very beginning until the measurement was finished at E_{PAR} of nearly 1000 µmol photons m^{-2} s^{-1}, especially when E_{PAR} was between 0 and 200 µmol photons m^{-2} s^{-1}.

Goethite treatments had highly similar F_m' on each E_{PAR} measuring intensity. In comparison, Goethite – 15 µmol EDTA treatment had higher initial F_m' than Goethite – 5 µmol EDTA treatment, ca. 1600 and 1550, respectively; both were on a sharp decline to ca. 740, while E_{PAR} was increasing from 0 to 200 µmol photons m^{-2} s^{-1}. They subsequently were slowly decreasing and had become stable since E_{PAR} surpassed 600 µmol photons m^{-2} s^{-1}, during which F_m' of Goethite – 15 µmol EDTA treatment was continuously very slightly higher than that of Goethite – 5 µmol EDTA treatment.

F_m' of $FeCl_3$ – 5 µmol EDTA was constantly lower than the two Goethite treatments, starting with ca. 1350 and ending with ca. 450. F_m' of $FeCl_3$ – 15 µmol EDTA was the lowest among all four treatments, which had an initial value of ca. 1150 and a terminal one of ca. 350.

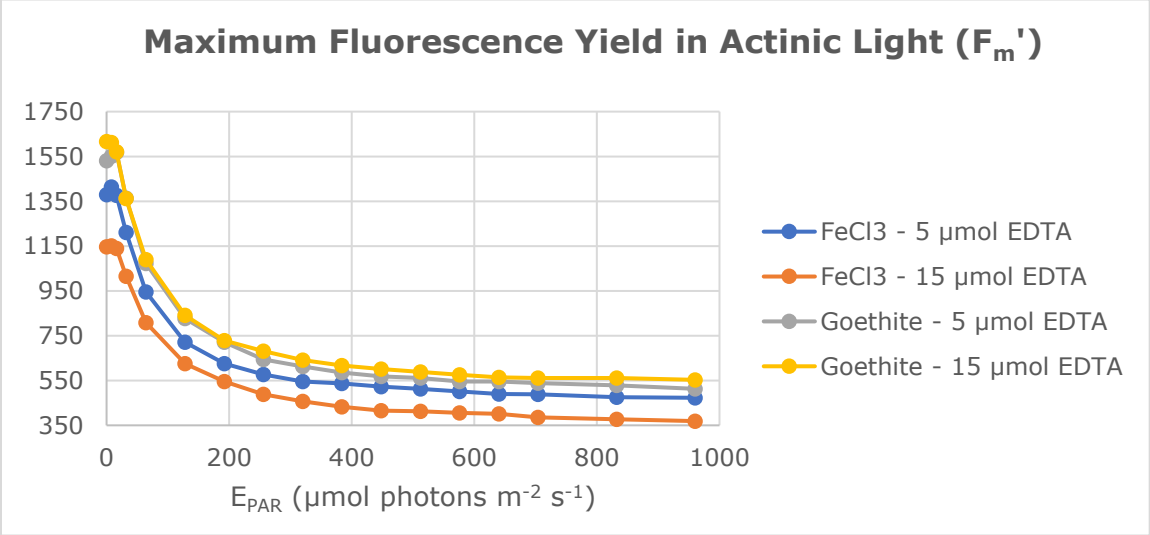

Figure 3.15. Maximum fluorescence yield of in actinic light (F_m') along with E_{PAR}.

3.2.1.3 Effective Quantum Yield (Φ)

It is clearly depicted in Figure 3.16 that there is no significant difference of effective quantum yield (Φ) among all four treatments: Φ of all four treatments initially was ca. 0.65 at E_{PAR} of 0, collapsed to ca. 0.20 while E_{PAR} was increasing to 200 µmol photons m^{-2} s^{-1}, and then slid down to ca. 0.05 at the end of the measurement where E_{PAR} was 960 µmol photons m^{-2} s^{-1}.

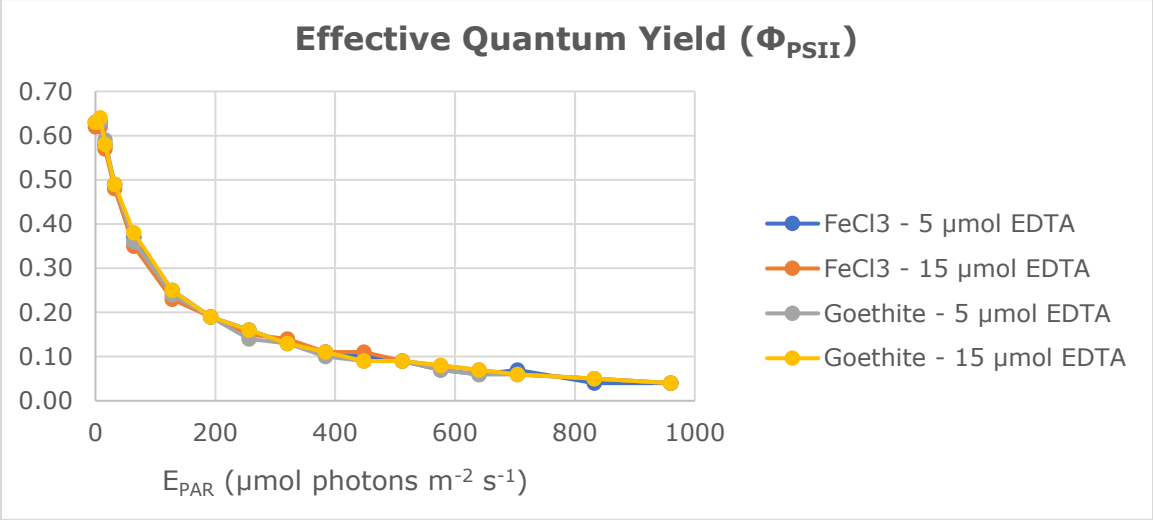

Figure 3.16. Effective quantum yield (Φ) along with E_{PAR}.

3.2.1.4 Non-photochemical Quenching (NPQ)

Figure 3.17 vividly describes the variation of (Stern-Volmer) Non-photochemical quenching (NPQ) along the increasing E_{PAR}. There had been no significant difference of NPQ among the four treatments before E_{PAR} was over ca. 650 µmol photons $m^{-2}s^{-1}$: NPQ of the four treatments rapidly increased from 0 to ca. 1.25 while E_{PAR} was increasing from 0 to 200 µmol photons m^{-2} s^{-1}, and then ascended to ca. 1.8 while E_{PAR} was increasing to 640 µmol photons m^{-2} s^{-1}. Starting from this E_{PAR} intensity, NPQ of $FeCl_3$ – 15 µmol EDTA treatment became outstanding from that of the other three treatments and topped with ca. 2.10 at the end of measurement. In contrast, NPQ of the other three treatments was still highly close with each other. Only Goethite – 5 µmol EDTA was very slightly higher with NPQ of ca. 2.00 than the remaining two treatments with NPQ of ca. 1.90 in the end.

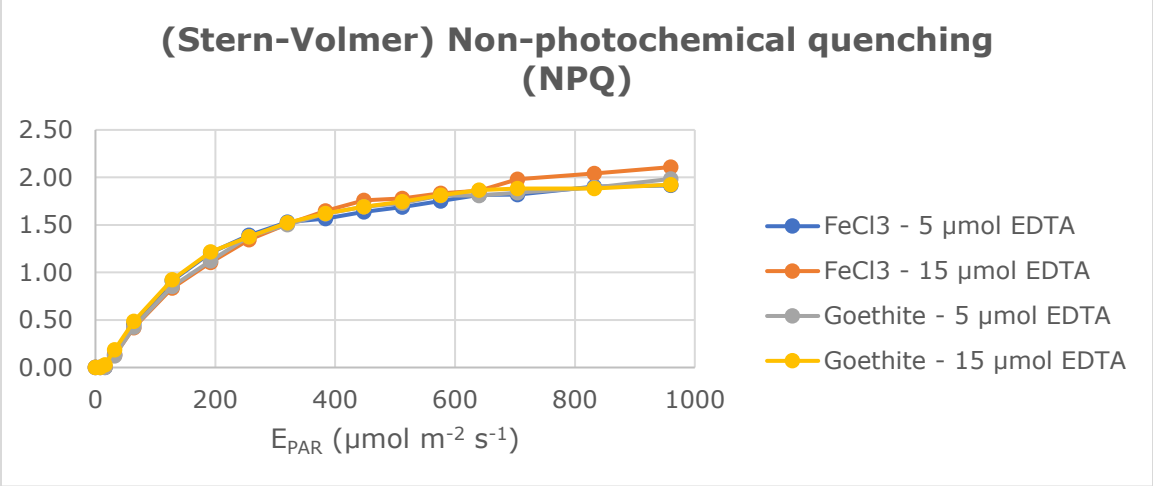

Figure 3.17. Non-photochemical quenching (NPQ) variation along with E_{PAR}.

3.2.2 Rapid Light Curves (RLCs)

3.2.2.1 Relative Electron Transport Rate (rETR)

It can be noticed from Figure 3.18 that rETR of all four treatments firstly increased with increasing E_{PAR} and then plateaued at 40 a.u.: $FeCl_3$ – 5 µmol EDTA, Goethite – 5 µmol EDTA, and Goethite – 15 µmol EDTA treatments all reached their maximum rETR when E_{PAR} increased to 250 µmol photons m^{-2} s^{-1} while $FeCl_3$ – 15 µmol EDTA treatment summitted at a larger E_{PAR} of ca. 320 µmol photons m^{-2} s^{-1}.

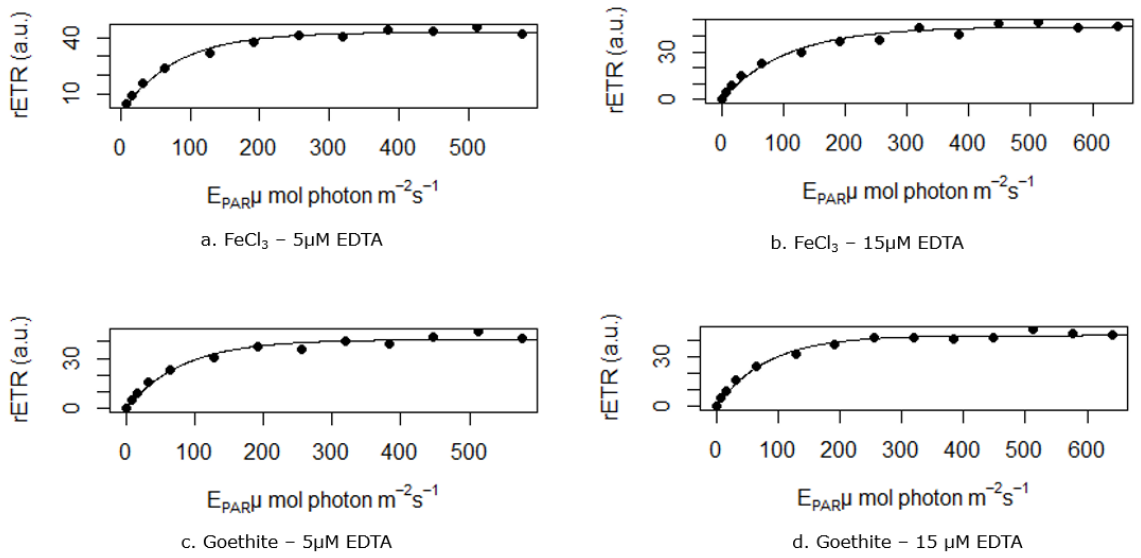

Figure 3.18. Relative electron transport rate (rETR) of along with E_{PAR} (a. $FeCl_3$ – 5 µmol EDTA (top left), b. $FeCl_3$ – 15 µmol EDTA (top right), c. Goethite – 5 µmol EDTA (bottom left), d. Goethite – 15 µmol EDTA (bottom right).)

3.2.2.2 Relevant Parameters of Rapid Light Curves (RLCs)

As is interpreted in Table 3.1, the two $FeCl_3$ treatments had different photosynthetic rate in light-limited region considering their different α values. Among all treatments, $FeCl_3$ - 5 µmol EDTA had the minimum saturating irradiance (E_k) of RLCs whereas $FeCl_3$ -15 µmol EDTA had the maximum E_k. In contrast, E_k of goethite treatments were identical.

Table 3.1: Results of the slope of RLCs (α), minimum saturating irradiance (E_k), and minimum and maximum fluorescence yields of dark-adapted samples (F_0 & F_m).

Sample	α		E_k		F_0	F_m
(Replicate 1)	estimates	Standard deviation	estimates	Standard deviation		
$FeCl_3$ - 5 µmol EDTA	0.54	0.033	79	5.4	577	1441
$FeCl_3$ - 15 µmol EDTA	0.43	0.041	106	11.8	486	1178
Goethite - 5 µmol EDTA	0.50	0.038	98	8.4	622	1594
Goethite - 15 µmol EDTA	0.50	0.038	98	8.4	656	1673

4. Discussion

4.1 The Influence of OA to Particulate Iron (PFe) – Goethite Bioavailability at Queen Maud Land (DML) Region in the Southern Ocean

4.1.1 The Predominant Effect of Ocean Acidification (OA) and No Apparent Iron Limitation

Reflecting upon all figures in subchapter 3.1, the difference between control and iron-enriched treatments on all measured parameters at both ambient and low pH situations seem to be insignificant. More evidently, treatments at the same pH have similar patterns on the measured parameters. These observations suggest that the tested phytoplankton assemblage was more severely influenced by OA than iron bioavailability.

10 nM goethite was added in iron enriched treatments, which is a huge amount of artificial iron enrichment compared with DFe in seawater [130 ,16] and even in coastal water systems [131, 132]. Both DFe and TaLFe of ambient pH treatments display no noticeable difference from each other (Figure 3.1 & Figure 3.2). Therefore, iron was not limited to original phytoplankton assemblage. Besides, DFe & TaLFe concentration of Low pH + FeO(OH) treatment do not show obvious distinctness from those of Low pH Control treatment (Figure 3.1 & Figure 3.2), which is the same to ambient pH treatments. And DFe concentration was generally lower in low pH treatments. These observations implie that goethite, as one type of PFe, is insoluble at the tested low pH and ambient pH (Figure 3.13). Moreover, OA can make goethite less soluble. Shi *et al.* mentioned that unless Fe inputs to surface seawater increase as a result of global change, the net result of seawater acidification should be an increase in the Fe-stress of the phytoplankton in many areas of the oceans [34]. Sugie *et al.* found in 2013 that particulate matter (>1 μm) collected in the nepheloid layer in the Sea of Okhotsk can supply bioavailable Fe that can promote the growth of phytoplankton such as diatoms [86], for which the experiment was not performed with acidified medium. Kanna *et al.* in 2016 discovered that iron stored in sea ice (mainly in particulate form) was bioavailable and can contribute to phytoplankton growth when it was released into surface waters in the spring [87] and published similar results in 2020 that PFe stored in sea ice could be an important source of biologically available Fe to the ice-covered marginal seas [88]. Both corresponding experiments were conducted under non-acidified condition. Interestingly, Garg *et al.* found that compared with organically bound iron, the rate and extent of dissolution of amorphous iron oxyhydroxides ($FeO(OH) \cdot nH_2O$) increased in acidified natural water, because of its strong dependency on pH. Therefore, based on the results of our tested $FeO(OH) \cdot nH_2O$ species, goethite (α-FeO(OH)), it is implied that other $FeO(OH) \cdot nH_2O$ species may be soluble and bioavailable to phytoplankton under certain OA conditions.

4.1.2 The Internal Link of Macronutrients, Redfield Ratio of N/P and Biological Data

Generally, N/P ratio means that the ratio of N: P is 16:1 in the sea. This is controlled by the requirements of phytoplankton, which subsequently release nitrogen and phosphorus to the environment at this ratio as they are broken down (remineralized) [133].

In this experiment, the initial N/P ratio (Figure 3.6) was ca. 13 in both ambient and low pH treatments, which is lower than the well-known N/P ratio of 16 [133]. This observation indicates that the incubation system had sufficient PO_4^{3-}, and if it has abundant iron, which is in fact the limiting nutrient in the Southern Ocean, one of the HNLC regions that have been introduced in 1.5.1, then NO_3^- will be effectively up taken by phytoplankton assemblage. This is confirmed by rapidly decreasing NO_3^- concentration in all treatments in Figure 3.3.

Considering that PO_4^{3-} concentration (Figure 3.4) in both ambient pH and low pH treatments were rebounding in the last few days of incubation and that PO_4^{3-} concentration in all treatments on Day 11 was higher than that of Extra Control treatment, while the constantly increasing Chla (Figure 3.7) and *in vivo* fluorescence (Figure 3.8) demonstrate that there was continuous photosynthesis. Therefore, the rebounded and stable PO_4^{3-} concentration in ambient and low pH treatments (Figure 3.4) can be the result of remineralization of PO_4^{3-}. PO_4^{3-} concentration of ambient pH treatments started increasing after Day 7 because PO_4^{3-} remineralization in ambient pH treatments was earlier than the other two macronutrients (Figure 3.3 & Figure 3.5). In fact, some researchers have found that preferential PO_4^{3-} remineralization from the release of cellular PO_4^{3-} back to the water is possible. Albert S. Colman *et al.* has found that the rapidity of microbiological turnover of the dissolved inorganic phosphate (DIP) pool and that cytolysis is one of the important sources of P remineralization in the euphotic zone [134]. Besides, Claudia R. Benitez-Nelson *et al.* has discovered that DIP turnover times are even less than 10 days in coastal waters in the Gulf of Maine [135].

In contrast to ambient pH treatments, PO_4^{3-} concentration of low pH treatments levelled off after Day 7 possibly because PO_4^{3-} was remineralized and taken up at the same speed. Similar discovery can be dated back to 1965 when EV Grill *et al.* found that the onset of death and autolytic decomposition of the diatom population can happen following nutrient exhaustion [136]. Even earlier, Hoffman demonstrated in 1956 a rapid autolytic release of PO_4^{3-} and dissolved organic phosphorus from killed diatoms [137].

Before discussing the reason why the observed initial N/P ratio of 13 (Figure 3.6) is lower than general N/P ratio of 16, we need to know the reason why 16 is considered a general N/P ratio: the optimization model of Klausmeier *et al.* claims that the Redfield N:P ratio of 16 observed in nature is simply an average value that reflects an ecological balance between the 'survivalists' (cellular N:P > 30) and 'bloomers' (cellular N:P < 10) in a population, and phytoplankton species that have a cellular N:P near N/P ratio is defined as 'generalists' [138].

As is known that the Southern Ocean is one of the HNLC regions, where NO_3^- is redundant. However, along the incubation experiment, N/P ratio was constantly lower than 13, which can be deemed as a normal ratio considering that the zonal mean export ratio of N/P varies between 12.5 and 20 according to Weber and Deutsch [139]. After Day 7, N/P ratios of all treatments were drastically decreasing down to 9.5 and ca.11.8 on Day 11, while PO_4^{3-} concentration started being remenerilized, respectively. This result implies that most of the phytoplankton assemblage were shifting to the so-called "bloomer", which can lead to a low cellular N:P ratio (<10), be adapted to exponential growth and contains a high proportion of growth machinery (ribosomal RNA has a low N:P ratio) [140]. According to Arrigo *et al.*, the low cellular N:P ratio results from that bloom-forming phytoplankton optimally shift their allocation of resource-acquisition machinery, which results in high N:P ratio in enzymes, pigments, and proteins, toward the production of growth machinery, reducing their N:P ratio to ~ 8, far below the general N/P ratio of 16 [133]. Moreover, if surface water in polar regions become more stratified [141], the composition of phytoplankton species could shift towards an increase in the abundance of diatoms, which prefers stratified waters and have a much lower N:P requirement [133]. This could be the reason of drawing-down N:P ratio and NO_3^- depletion in relevance to PO_4^{3-} in this experiment. Donahue *et al.* presented the same result in 2018 that phytoplankton assemblage from subantarctic surface waters (45.83 °S 171.54 °E) had low N:P ratio ranging from 9.5±1.3 to 11.1±0.6 when light intensity was 90 μE and 120 μE [142], which was similar to our experiment: It was possible that the phytoplankton assemblage gradually became dominated by diatoms in Control treatment during the incubation, especially when light intensity was low ((54.15 ± 5.21) μ mol photons m^{-2} *m^{-1}).

The rapid drawdown of silicate of both ambient and low pH treatments from Day 0 to Day 7 also implies the drastic growth of diatoms (Figure 3.5). The drawdown speed of silicate decreasing and even stabilizing for 2 days in FeO(OH) treatment after Day 7 possibly resulted from PO_4^{3-} remineralization, so silicate was concurrently remineralized while being taken up by phytoplankton assemblage. Moreover, comparing to silicate concentration of Extra Control treatment on Day 11, silicate of ambient pH treatments was lower while that of low pH treatments was higher. This observation implies that the massive demand of silicate by phytoplankton assemblage at ambient pH caused by species shift to diatoms.

Unfortunately, silicate concentration of Low pH Control treatment on Day 11 is unavailable (Figure 3.5), but according to the difference of NO_3^- and PO_4^{3-} concentration between Low pH Control and Low pH + FeO(OH) treatments on Day 11 (Figure 3.3 & Figure 3.4), it can be analogically reasoned that silicate concentration of Low pH Control treatment on Day 11 would roughly be equal to that of Low pH + FeO(OH) treatment. In that case, it would be higher than that of Extra Control treatment and thus it was highly possible that there was no species shift in the phytoplankton assemblage toward diatoms of low pH treatment.

In summary, there could be PO_4^{3-} remineralization in all treatments but species shift to diatoms only in ambient pH treatments, which coincides with our judgement that OA impact is predominant in comparison to iron enrichment in this experiment. We should analyze phytoplankton species to test this hypothesis.

4.1.3 Resulting Total pH (pH_T) and Carbonate System

From Figure 3.13 we can see that pH_T of both ambient and low pH treatments was increasing during incubation. Despite this, pH_T of low pH treatments was much lower throughout the experiment, which was expected to be the result of the action of artificial acidification as has been stated in 3.1.5.4.

It has been suggested that the predominantly negative effect caused by OA is due to decline of pH [143, 144]. Usually, metabolic processes such as photosynthesis and respiration can make an influence on H^+ fluxes between cellular compartments, making it necessary to facilitate quick balance of rapidly fluctuating H^+ loads [145]. Under normal oceanic circumstances (pH ~ 8.1), excessively generated intracellular H^+ ions can be moved out of cells by passive diffusion via proton channels [146]. In contrast, abnormal oceanic circumstances (pH < 8.1) can halt this passive removal processes and thus trigger an energy-intensive proton pump that is termed as plasma membrane voltage-gated H^+ (H_v) channel-mediated H^+ efflux mechanism [145]. It is energetically feasible to regulate intracellular pH (pH_i). In this experiment, the initial pH_T of both ambient pH and low pH treatments were below normal oceanic pH circumstances. Therefore theoretically, phytoplankton assemblages in all treatments launched H_v channel-mediated H^+ efflux mechanism to regulate pH_i [145].

Moreover, the action of artificial acidification in low pH treatments possibly resulted in more severe downregulation of carbon concentration mechanisms (CCMs) compared with ambient pH treatments. During photosynthesis, the light-independent process – carbon fixation relies on an enzyme called RuBisCo. Since it has a low affinity to CO_2 and CCMs compensates, which can actively increase intracellular CO_2 [147-150]. Because the H_v channel-mediated H^+ efflux mechanism requires intensive energy [145], CCMs that requires additional energy can be downregulated to lower cellular energy requirement [147], resulting in the decline of carbon fixation rates, i.e., less uptake and utilisation of CO_2 or HCO_3^-, as well as less net H^+ consumption [145]. It could thus offset the impact of H^+ efflux mechanism. As a result, pH_T of all treatments in general did not increase much despite the integral increasing tendency.

The concurrent impact of H_v channel-mediated H^+ efflux mechanism and downregulation of CCMs also exhibit in the concentration of DIC (Figure 3.12) and CO_2 (Figure 3.11) of all treatments. DIC concentration of Low pH treatments was lower than that of ambient pH treatments from the very beginning. This observation may be the result of that the induced less uptake of HCO_3^- or CO_2 and less net consumption H^+ might push the solubility pump of oceanic carbon toward the direction of forming H_2CO_3 and then decomposing as CO_2 and H_2O, potentially leading to CO_2 emitting into the atmosphere. CO_2 concentration was generally decreasing in all treatments despite fluctuation in low pH treatments, which could attribute to PO_4^{3-} remineralization because P remineralization in the deep ocean is a byproduct of microbial carbon and energy requirements [134]. In addition, calcification by calcifiers may contribute to CO_2 because the process of calcification releases CO_2 [151], even though its rate decreases with descending pH.

By the definition of fugacity of a real gas, fugacity of CO_2 (fCO_2) (Figure 3.10) is the effective partial pressure that replaces the mechanical pressure in an accurate

computation of the chemical equilibrium constant [152]. It is equal to the pressure of an ideal gas that has the same temperature and molar Gibbs free energy as CO_2 [152]. Therefore, fCO_2 is physically dependent on pressure and temperature. Despite this, considering that the experiment was conducted onboard in cubitainers of certain volumes with minimum fluctuation of pressure and the temperature only went down by 3 °C during the incubation (see Appendix 1.4), we believe that the decreasing fCO_2 was mostly caused by biological activities. But fCO_2 of Low pH treatments decreased by a larger portion compared with that of ambient treatments. The reason can be as follows: species shift resulted in more tolerant species to thrive and acclimated to low pH and high CO_2 conditions, which led to a more efficient CCM possessed by the phytoplankton assemblage [153].

To summarise, OA can result in that phytoplankton launches H_v channel-mediated H^+ efflux mechanism, CCM down-regulation of some phytoplankton and the thriving of more tolerant species with more efficient CCM.

4.2 The Influence of EDTA on Particulate Iron (PFe) Bioavailability to Arctic Diatom *Nitzschia frigida*

Figure 3.16, Figure 3.17 & Figure 3.18 show that EDTA and different species of iron had no significant difference on Φ, NPQ and rETR among all four treatments, except that NPQ of $FeCl_3$ – 15 µmol EDTA treatment is slightly higher than that of the other three when E_{PAR} is between ca. 600 and 1000 µmol photons/(m^2*s). The following discussion will focus on fluorescence yield parameters and RLC parameters.

4.2.1 Reflection on Fluorescence Yield Parameters

Fluorescence induction curve is a complex phenomenon that can be broken down into two primary phases: a fast phase (up to ~1 s), which is exhibited by RLCs in this experiment and a slow phase (up to several minutes) [154, 155], which are vividly exhibited in Figure 4.1 [101]. As for fast phase, firstly, the samples were dark-acclimated and all RSII centres are open (primary (bound) quinone electron acceptor of PS II (Q_A) in all RCII is oxidised) when incident irradiance with a very weak light intensity (< 0.5 µmol photons/(m^2*s) is applied, which does not induce the reduction of Q_A and closure of any reaction centres, the fluorescence yield is minimum. It is given the terms *dark fluorescence*, *constant fluorescence*, *initial fluorescence*, or *fluorescence minimum* (F_0/F_{min}) [101]. Subsequently, fluorescence emitted from excited Chla molecules in the antennae complex before excitons migrated to the reaction centre [154], resulting in the fluorescence increase during fast phase. Over the course, the increasing can be separated as two phases: photochemical phase [155] and thermal phase [156]: At photochemical phase, fluorescence yield increases proportionally with the reduction of quinone ($Q_A \rightarrow Q_A^-$) [155]. Consequently, the slope and height of this phase is dependent on incident light intensity [156], i.e., E_{PAR} in this experiment. At thermal phase, the increase fluorescence yield is impacted by temperature within the physiological range (slower at lower temperatures) [156] and shaped by the two-step reduction of secondary (mobile) quinone electron acceptor of PS II (Q_B) ($Q_B \rightarrow Q_B^- \rightarrow Q_B^{2-}$) and a heterogeneity in the reduction of the plastoquinone (PQ) pool [157]. In the end, fluorescence reached the peak because the PQ pool became fully reduced and $Q_A^-Q_B^{2-}$ concentration reached a second maximum [158] (the first maximum of $Q_A^-Q_B^{2-}$ concentration is reached halfway during thermal phase at inflection I, also known as I_2 [159, 160]). This happens when a saturating excitation irradiance is applied to a sample to close all RCIIs (reduce all Q_A), a condition is induced where photochemistry is reduced to zero and fluorescence yield is maximal, which is termed maximum fluorescence yield (F_m) [101].

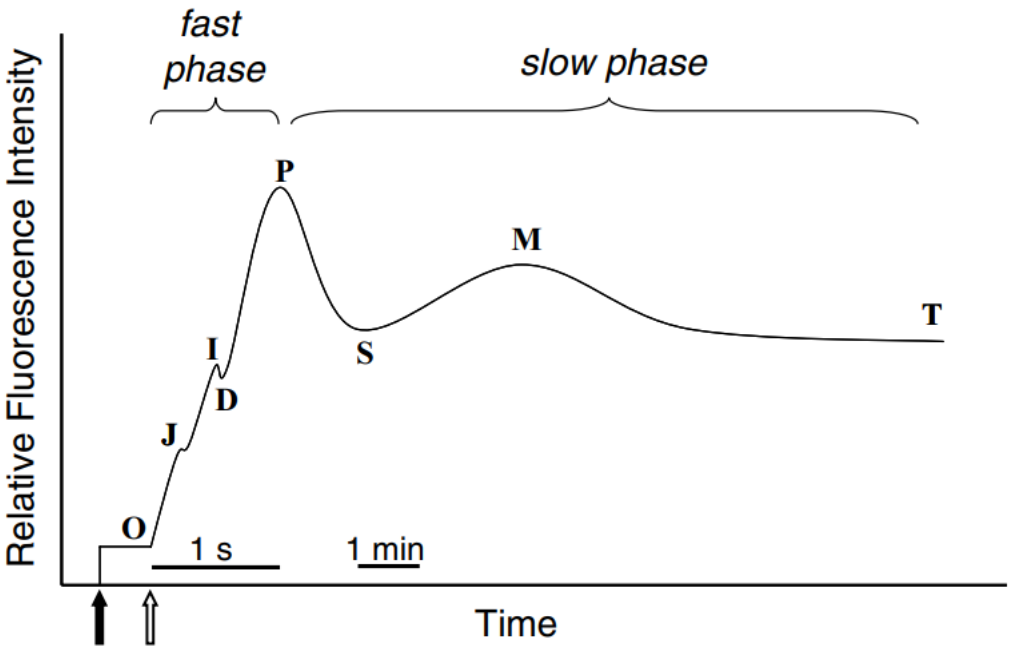

Figure 4.1. Stylised representation of the Chla fluorescence induction curve. Closed arrow represents activation of non-actinic measuring light. On application of strong actinic light (open arrow) fluorescence rises from the origin (O) to a peak (P) via two inflections (J and I). A dip (D) may occur after I. This O-P rise is known as the fast phase and reflects primary photochemistry and redox state of QA. After P fluorescence declines due to formation of a transthylakoid pH gradient and associated ther-mal quenching. The remainder of the transient (S-M-T) is called the slow phase and is the result of induction of Calvin cycle enzyme activity and its subsequent interaction with the electron transport chain (via NADPH) and photochemical and non-pho-tochemical quenching. (Reproduced from [101])

As is shown in Table 3.1 that the four different treatments had different F_0 and F_m. Both parameters of goethite treatments were higher than those of $FeCl_3$ treatments, regardless of the added concentration of EDTA. This observation could result from that there were more RCII in goethite treatments compared with $FeCl_3$ treatments, so that more RCII are open during dark acclimation, and more are closed under saturating light intensity in gothite treatments than $FeCl_3$ treatments. Furthermore, according to the concrete values of F_0 and F_m of all treatments, the ranking of RCII numbers among all 4 treatments should be Goethite – 15 µmol EDTA > Goethite – 5 µmol EDTA > $FeCl_3$ – 5 µmol EDTA > $FeCl_3$ – 15 µmol EDTA.

The increase of F' at the initial stage (E_{PAR} ≥ 32 µmol photons/(m^2*s)) was presumably associated with closure of all PSII reaction centres (RCII) [161]. If RCIIs are closed, they are unable to transfer energy. F' of all treatments was progressively increasing up to actinic light step 4 (32 µmol photons/(m^2*s)), after which they were essentially all closed. When E_{PAR} was over 32 µmol photons/(m^2*s), F' started decreasing, which was probably caused by increasing NPQ (Figure 3.17). It has been discussed that light energy absorbed by a photosystem and its light harvesting complex (LHC) can be used and dissipated through one of the three competing pathways: (1) photochemistry (primary charge separation and photosynthetic electron transport), (2) thermal dissipation (non-radioactive decay) or, (3) fluorescence emission (or radiative decay

(III)) [162-165]. It is assumed that the sum of the quantum yields of each of these processes is unity, and thus changes in fluorescence yield reflect changes in the complementary pathways [101]. Therefore, after photochemistry had saturated at E_{PAR} of 32 µmol photons/(m^2*s), F' started decreasing with increasing E_{PAR} due to increasing NPQ for dissipating excess excitation energy to prevent photodamage [104], which is reflected in decreasing F_m' (Figure 3.14 & Figure 3.17). High excitation pressure can be caused by short-term exposure to high light, but also iron limitation, which comprises the functioning of electron transport current [104]. Considering the same ranking of F_0 and F_m of all four treatments and significantly higher NPQ of $FeCl_3$ – 15 µmol EDTA at E_{PAR} between ca. 600 and 1000 µmol photons/(m^2*s), it is implied that under the same condition of short-term exposure to high light, the ranking of iron limitation among all four treatments should be $FeCl_3$ – 15 µmol EDTA > $FeCl_3$ – 5 µmol EDTA > Goethite – 5 µmol EDTA > Goethite – 15 µmol EDTA, which is in the opposite direction to the ranking of RCII numbers among all 4 treatments.

4.2.2 Reflection on Rapid Light Curves (RLCs)

Since Φ_{PSII} is a characteristic of the photosystems and is not linked with the amount of chlorophyll, rETR gives a relative indication of the photosynthetic electron transport rate. The plots of rETR of all four treatments as a function of irradiance (Figure 3.18) showed the shape of a classic *P/E* curve: rETR displayed a linear rise where irradiance was not strong, and the increase of rETR decelerated at elevating irradiance, which was followed by a plateau. During the variation of rETR, photosynthesis gradually became limited. According to the curve-fitting results of all four treatments from the modFit (Nelder-Mead) model on R studio, their rETR did not decrease after saturation (when E_k was reached), while their NPQ was significantly increasing and F_m' was decreasing. This observation implies that the excessive light energy harvested from elevating irradiance significantly higher than saturation was being dissipated by upregulation of 3 alternative pathways around photosynthetic electron transport chain, especially in iron-limited samples [104]. In addition, there is no significant difference of rETR variation of all 4 treatments, especially on the plateau. This observation indicates that their photosynthetic activity was nearly at the same level.

α is photosynthetic rate in light-limited region of RLC (under saturation), it reflects the efficiency of light capture [166] and E_k is determined by finding the interception of α with the maximum photosynthetic rate [167]. Comparing α values of all treatments (Table 3.1), photosynthetic activities in $FeCl_3$ – 5 µmol EDTA treatment appeared to be the most efficient, followed by two goethite treatments and $FeCl_3$ - 15 µmol EDTA treatments. Besides, the ranking of E_k values of all 4 treatments shows that $FeCl_3$ - 5 µmol EDTA treatment was the most efficient, followed by two goethite treatments and $FeCl_3$ - 15 µmol EDTA treatments. This observation corresponds to the discussion of α and implies that Arctic diatom *Nitzschia frigida* in $FeCl_3$ - 5 µmol EDTA treatment captures light most efficiently in comparison to two goethite treatments and $FeCl_3$ - 15 µmol EDTA treatment. Considering that RLC is a tool normalised to per cell to assess photosynthetic activity and it has been suggested that low-light algae have acclimated to the low light by increasing cellular concentrations of chlorophyll [2], cells of *Nitzschia frigida* in $FeCl_3$ - 5 µmol EDTA treatment could be most abundant in chlorophyll while

those in the two goethite treatments could be less abundant and those in $FeCl_3$ - 15 μmol EDTA treatment was poorest in chlorophyll. Since the only variables in this experiment were the species of iron and the concentration of EDTA, the difference of chlorophyll abundance should result from the difference of iron bioavailability among four treatments. Consequently, goethite is less bioavailable than $FeCl_3$ when they were respectively treated with low concentration of EDTA but more bioavailable than $FeCl_3$ when they were treated with high concentration of EDTA.

However, it has been suggested that α estimates (using P-E curves) were strongly influenced sampling frequency within the light-limiting region of the curve [168], which could influence the estimation of chlorophyll abundance. In addition, since the trace elements, especially iron species, were not removed before the experiment was commenced, EDTA could bind to other iron species or other trace elements and led to bias in the results.

5. Conclusion

According to the results of the experiment at DML, the tested phytoplankton assemblage was more severely influenced by OA than iron bioavailability, especially under severe OA. Goethite, as one type of PFe, is insoluble under the tested OA scenarios. There could be PO_4^{3-} remineralization in all treatments but species shift to diatoms only in ambient pH treatments, which coincides with the judgement that OA impact is predominant in comparison to iron enrichment in this experiment. We should analyze phytoplankton species to test this hypothesis. OA can result in that phytoplankton launches H_v channel-mediated H^+ efflux mechanism, CCM down-regulation of phytoplankton and the thriving of more tolerant species with more efficient CCM. Further research with more proper replicates is needed to determine the pH threshold for phytoplankton assemblage to take up goethite.

According to the results of miniature experiment at TBS, the ranking of iron limitation among all four treatments could be $FeCl_3$ – 15 µmol EDTA > $FeCl_3$ – 5 µmol EDTA > Goethite – 5 µmol EDTA > Goethite – 15 µmol EDTA, which is in the opposite direction to the ranking of RCII numbers among all 4 treatments. Elevating EDTA concentration can thus increase the bioavailability of goethite while decrease that of $FeCl_3$. However, this is inconclusive according to possibly negatively biased α, which results in underestimation of goethite bioavailability under the influence of EDTA.

To summarize, goethite is possibly bioavailable under the impact of EDTA, respectively, but further research is needed for confirmation. And it is interesting to investigate the mutual effect of OA and EDTA on goethite bioavailability to phytoplankton community.

6. Further work

Further experiments are needed because of the following reasons:

In DML experiment, from an experimental point of view, firstly, there could be contamination to Cubitainer 2 from intermittent water freezing problems during experiment setup.

Secondly, all data of DFe, TaLFe, Chla and *in vivo* fluorescence on Day 0 were unavailable, which makes the pertinent discussion and conclusion equivocal. The samples of macronutrients and carbon chemistry on Day 0 were collected before goethite addition, which might result in bias. The results would have been more genuine, if these samples were collected after goethite had been added.

Thirdly, some data missing enough proper replicates, and are suspected biased because of possible human error during analysis. Especially some replicates of Chla and *in vivo* fluorescence data, which are fundamentally pseudo-replicates since they were sampled from the same cubitainers belonging to one treatment.

In addition, some parameters can be measured differently for unequivocal discussion and conclusion, for example, the drawdown rates of macronutrient as are described in Wingert *et al.* [169]. And some parameters like metal quota of Fe:P of natural phytoplankton culture community can be assessed to reflect biochemical demand of iron by tested phytoplankton assemblages in each treatment, because phosphorus is often measured simultaneously with metals, reducing error [170]. Furthermore, we may also be able to extrapolate how this demand is influenced by OA and iron availability according to this quota.

From an ecological point of view, we could not make sure that whether the possible species shift to diatoms in ambient pH treatments results from their largely escaping the grazing pressure of mezozooplankton that consume them and whose replication rate is too slow to keep pace [44].

As for the experiment at TBS, the sampling frequency in PHYTO-PAM needs to be modified in order to make the conclusion more reliable. It will be more persuasive to remove trace element species in collected seawater before composing the culture medium. Additionally, the conclusion would be more solid if we managed to trach cell density at the meanwhile of PHYTO-PAM measurement.

In summary, it will be enlightening to test the mutual effect of mild OA and EDTA to goethite bioavailability to phytoplankton assemblage in polar regions.

References

1. Chisholm S., Falkowski P., Cullen J. Oceans: Dis-crediting ocean fertilization. *Science (American Association for the Advancement of Science)*. 2001;294(5541):309–10.
2. Kaiser MJ, Attrill MJ, Jennings S, Thomas DN, Barnes DK, editors. Marine ecology: processes, systems, and impacts. Second Edition. Oxford: Oxford University Press; 2011.
3. Falkowski PG. The ocean's invisible forest. *Scientific American*. 2002 ;287(2):54-61.
4. Kirk JTO. Light and photosynthesis in aquatic ecosystems. Third edition. Cambridge: Cambridge University Press; 2011.
5. Lindsey R, Scott M, Simmon R. What are phytoplankton [NASA's Earth Observatory]. 2010 Jul 13. Available from http://earthobservatory. nasa. gov/Librar y/phytoplankton.
6. Raven JA, Evans MC, Korb RE. The role of trace metals in photosynthetic electron transport in O 2-evolving organisms*. Photosynthesis research*. 1999;60(2):111-50.
7. Briat JF, Curie C, Gaymard F. Iron utilization and metabolism in plants. *Current opinion in plant biology*. 2007 Jun 1;10(3):276-82.
8. Yruela I. Transition metals in plant photosynthesis. *Metallomics*. 2013;5(9):1090-109.
9. Nealson KH, Saffarini D. Iron and manganese in anaerobic respiration: environmental significance, physiology, and regulation. *Annual review of microbiology*. 1994;48(1):311-43.
10. Kostka JE, Haefele E, Viehweger R, Stucki JW. Respiration and dissolution of iron (III)-containing clay minerals by bacteria. *Environmental Science & Technology*. 1999;33(18):3127-33.
11. Rueter JG. Theoretical Fe limitations of microbial N2 fixation in the oceans. Eos. 1982;63:945.
12. Rueter JG, Hutchins DA, Smith RW, Unsworth NL. Iron nutrition of Trichodesmium in Marine pelagic cyanobacteria: Trichodesmium and other Diazotrophs. 289–306.
13. Petersson L, Gräslund A, Ehrenberg A, Sjöberg BM, Reichard P. The iron center in ribonucleotide reductase from Escherichia coli. *Journal of Biological Chemistry*. 1980;255(14):6706-12.
14. Beal EJ, House CH, Orphan VJ. Manganese-and iron-dependent marine methane oxidation. *Science*. 2009;325(5937):184-7.
15. Vincent JB, Crowder MW, Averill BA. Hydrolysis of phosphate monoesters: a biological problem with multiple chemical solutions. *Trends in biochemical sciences*. 1992;17(3):105-10.
16. Achterberg EP, Holland TW, Bowie AR, Mantoura RF, Worsfold PJ. Determination of iron in seawater. *Analytica Chimica Acta*. 2001;442(1):1-4. Fig. 2. Schematic diagram of biogeochemical iron cycling in the ocean; p. 3.

17. Wells ML, Price NM, Bruland KW. Iron chemistry in seawater and its relationship to phytoplankton: a workshop report. *Marine Chemistry*. 1995;48(2):157-82.

18. Morel FM, Price NM. The biogeochemical cycles of trace metals in the oceans. *Science*. 2003;300(5621):944-7.

19. Breitbarth E, Achterberg EP, Ardelan MV, Baker AR, Bucciarelli E, Chever F, *et al*. Iron biogeochemistry across marine systems–progress from the past decade. *Biogeosciences*. 2010;7(3):1075-97.

20. Edwards R, Sedwick P. Iron in East Antarctic snow: Implications for atmospheric iron deposition and algal production in Antarctic waters. *Geophysical Research Letters*. 2001;28(20):3907-10.

21. Tagliabue A, Arrigo KR. Iron in the Ross Sea: 1. Impact on CO2 fluxes via variation in phytoplankton functional group and non-Redfield stoichiometry. *Journal of Geophysical Research: Oceans*. 2005;110(C3).

22. Tagliabue A, Arrigo KR. Processes governing the supply of iron to phytoplankton in stratified seas. *Journal of Geophysical Research: Oceans*. 2006;111(C6).

23. Von Der Heyden BP, Roychoudhury AN. A review of colloidal iron partitioning and distribution in the open ocean. *Marine Chemistry*. 2015;177:9-19.

24. Bruland KW, Rue EL. Iron: analytical methods for the determination of concentrations and speciation. *The Biogeochemistry of Iron in Seawater*. 2001;255-89.

25. Schoemann V, De Baar HJ, De Jong JT, Lancelot C. Effects of phytoplankton blooms on the cycling of manganese and iron in coastal waters. *Limnology and Oceanography*. 1998;43(7):1427-41.

26. San SA, Rivera-Duarte I, Flegal AR. Distribution of colloidal trace metals in the San Francisco Bay estuary. *Geochimica et Cosmochimica Acta*. 1996;60(24):4933-44.

27. Bruland KW, Orians KJ, Cowen JP. Reactive trace metals in the stratified central North Pacific. *Geochimica et Cosmochimica Acta*. 1994;58(15):3171-82.

28. Gledhill M, van den Berg CM. Determination of complexation of iron (III) with natural organic complexing ligands in seawater using cathodic stripping voltammetry. *Marine Chemistry*. 1994;47(1):41-54.

29. Rue EL, Bruland KW. Complexation of iron (III) by natural organic ligands in the Central North Pacific as determined by a new competitive ligand equilibration/adsorptive cathodic stripping voltammetric method. *Marine chemistry*. 1995;50(1-4):117-38.

30. Nolting RF, Gerringa LJ, Swagerman MJ, Timmermans KR, De Baar HJ. Fe (III) speciation in the high nutrient, low chlorophyll Pacific region of the Southern Ocean. *Marine Chemistry*. 1998;62(3-4):335-52.

31. Rue EL, Bruland KW. The role of organic complexation on ambient iron chemistry in the equatorial Pacific Ocean and the response of a mesoscale iron addition experiment. *Limnology and oceanography*. 1997;42(5):901-10.

32. Granger J, Price NM. The importance of siderophores in iron nutrition of heterotrophic marine bacteria. *Limnology and Oceanography*. 1999;44(3):541-55.

33. Wilhelm SW, Trick CG. Iron-limited growth of cyanobacteria: multiple siderophore production is a common response. *Limnology and Oceanography*. 1994;39(8):1979-84.

34. Wilhelm SW, Trick CG. PHYSIOLOGICAL PROFILES OF SYNECHOCOCCUS (CYANOPHYCEAE) IN IRON-LIMITING CONTINUOUS CULTURES 1. *Journal of Phycology*. 1995;31(1):79-85.

35. Shi D, Xu Y, Hopkinson BM, Morel FM. Effect of ocean acidification on iron availability to marine phytoplankton. *Science*. 2010;327(5966):676-9.

36. Johnson KS, Gordon RM, Coale KH. What controls dissolved iron concentrations in the world ocean?. *Marine chemistry*. 1997;57(3-4):137-61.

37. Fujii M, Dang TC, Rose AL, Omura T, Waite TD. Effect of light on iron uptake by the freshwater cyanobacterium Microcystis aeruginosa. *Environmental Science & Technology*. 2011;45(4):1391-8.

38. Beghoura H, Gorgues T, Aumont O, Planquette HF, Tagliabue A, Auger PA. Impact of inorganic particles of sedimentary origin on global dissolved iron and phytoplankton distribution. *Journal of Geophysical Research: Oceans*. 2019;124(12):8626-46.

39. Schmidt K, Schlosser C, Atkinson A, Fielding S, Venables HJ, Waluda CM, *et al*. Zooplankton gut passage mobilizes lithogenic iron for ocean productivity. *Current Biology*. 2016;26(19):2667-73.

40. Tagliabue A, Bopp L, Dutay JC, Bowie AR, Chever F, Jean-Baptiste P, *et al*. Hydrothermal contribution to the oceanic dissolved iron inventory. *Nature Geoscience*. 2010;3(4):252-6.

41. Tagliabue A, Aumont O, Bopp L. The impact of different external sources of iron on the global carbon cycle. *Geophysical Research Letters*. 2014;41(3):920-6.

42. De Baar HJ. von Liebig's law of the minimum and plankton ecology (1899–1991). *Progress in oceanography*. 1994;33(4):347-86.

43. Redfield AC. On the proportions of organic derivatives in sea water and their relation to the composition of plankton. Liverpool: University Press of Liverpool; 1934.

44. Allsopp M, Santillo D, Johnston P. A scientific critique of oceanic iron fertilization as a climate change mitigation strategy. In: Buesseler K, Doney S, Kite-Powell H, editors (committee). Symposium on Ocean Iron Fertilization. Woods Hole: Greenpeace Research Laboratories; 2007. p. 1-32.

45. Martin JH. Glacial-interglacial CO2 change: The iron hypothesis. *Paleoceanography*. 1990;5(1):1-3.

46. Martin JH, Coale KH, Johnson KS, Fitzwater SE, Gordon RM, Tanner SJ, *et al*. Testing the iron hypothesis in ecosystems of the equatorial Pacific Ocean. *Nature*. 1994;371(6493):123-9.

47. Weiler CS. What controls phytoplankton production in nutrient-rich areas of the open sea?. *Whitman Coll.*, Walla Walla, WA (United States). Dept. of Biology; 1991 Jun 25.

48. Department of Oceanography, University of Hawaiʻi at Mānoa. High Nutrient Low Chlorophyll Ecosystems [Internet]. Hawaii: Department of Oceanography, University of Hawaiʻi at Mānoa; 2008 [cited 2021 Dec 1]. Available from: http://www.soest.hawaii.edu/oceanography/courses/OCN626/2008_OCN%20626/HNLC%20regions%20lecture_2008.pdf

49. Petit JR, Jouzel J, Raynaud D, Barkov NI, Barnola JM, Basile I, *et al*. Climate and atmospheric history of the past 420,000 years from the Vostok ice core, Antarctica. *Nature*. 1999;399(6735):429-36.

50. Kumar N, Anderson RF, Mortlock RA, Froelich PN, Kubik P, Dittrich-Hannen B, *et al*. Increased biological productivity and export production in the glacial Southern Ocean. *Nature*. 1995;378(6558):675-80.

51. Mahowald N, Kohfeld K, Hansson M, Balkanski Y, Harrison SP, Prentice IC, *et al*. Dust sources and deposition during the last glacial maximum and current climate: A comparison of model results with paleodata from ice cores and marine sediments. *Journal of Geophysical Research: Atmospheres*. 1999;104(D13):15895-916.

52. Lefèvre N, Watson AJ. Modeling the geochemical cycle of iron in the oceans and its impact on atmospheric CO2 concentrations. *Global Biogeochemical Cycles*. 1999;13(3):727-36.

53. Watson AJ, Bakker DC, Ridgwell AJ, Boyd PW, Law CS. Effect of iron supply on Southern Ocean CO 2 uptake and implications for glacial atmospheric CO 2. *Nature*. 2000;407(6805):730-3.

54. Assmy P, Henjes J, Klaas C, Smetacek V. Mechanisms determining species dominance in a phytoplankton bloom induced by the iron fertilization experiment EisenEx in the Southern Ocean. *Deep Sea Research Part I: Oceanographic Research Papers*. 2007;54(3):340-62.

55. Buesseler KO, Andrews JE, Pike SM, Charette MA. The effects of iron fertilization on carbon sequestration in the Southern Ocean. *Science*. 2004;304(5669):414-7.

56. Bakker DC. Storage of carbon dioxide by greening the oceans?. SCOPE-SCIENTIFIC COMMITTEE ON PROBLEMS OF THE ENVIRONMENT INTERNATIONAL COUNCIL OF SCIENTIFIC UNIONS. 2004;62:453-68.

57. Yoon JE, Yoo KC, Macdonald AM, Yoon HI, Park KT, Yang EJ, *et al*. Reviews and syntheses: Ocean iron fertilization experiments–past, present, and future looking to a future Korean Iron Fertilization Experiment in the Southern Ocean (KIFES) project. *Biogeosciences*. 2018;15(19):5847-89.

58. Freeland H, Whitney F. Climatic changes: Gulf of Alaska. Global Issues and Processes, III. Pergamon, Amsterdam, Netherlands. 2000. p. 179-86.

59. Barber RT, Hiscock MR. A rising tide lifts all phytoplankton: Growth response of other phytoplankton taxa in diatom-dominated blooms. *Global Biogeochemical Cycles*. 2006;20(4).

60. Gnanadesikan A, Sarmiento JL, Slater RD. Effects of patchy ocean fertilization on atmospheric carbon dioxide and biological production. *Global Biogeochemical Cycles*. 2003;17(2).

61. Sellner KG, Doucette GJ, Kirkpatrick GJ. Harmful algal blooms: causes, impacts and detection. *Journal of Industrial Microbiology and Biotechnology*. 2003;30(7):383-406.

62. Jin X, Gruber N. Offsetting the radiative benefit of ocean iron fertilization by enhancing N2O emissions. *Geophysical research letters*. 2003;30(24).

63. Law CS, Owens NJ. Significant flux of atmospheric nitrous oxide from the northwest Indian Ocean. *Nature*. 1990;346(6287):826-8.

64. Ramaswamy V, Boucher O, Haigh J, Hauglustaine D, Haywood J, Myhre G, *et al*. Radiative Forcing of Climate Change. In: Houghton JT, Ding YD, Griggs DJ, Noguer M, van der Linden PJ, Dai X, Maskell K, *et al.* editors. Climate change 2001: the scientific basis. Cambridge: Cambridge University Press; 2001. p. 349-416.

65. Liss P, Chuck A, Bakker D, Turner S. Ocean fertilization with iron: effects on climate and air quality. *Tellus B: Chemical and Physical Meteorology*. 2005;57(3):269-71.

66. Turner SM, Harvey MJ, Law CS, Nightingale PD, Liss PS. Iron-induced changes in oceanic sulfur biogeochemistry. *Geophysical Research Letters*. 2004;31(14).

67. Gattuso JP, Hansson L. Ocean acidification: background and history. In: Gattuso JP, Hansson L, editors. Ocean acidification. 2011. p. 1-20.

68. Solomon S, Manning M, Marquis M, Qin D. Climate change 2007-the physical science basis: Working group I contribution to the fourth assessment report of the IPCC. Cambridge university press; 2007 Sep 10.

69. National Oceanic and Atmospheric Administration (NOAA). Ocean acidification [Internet]. The United State: National Oceanic and Atmospheric Administration (NOAA). [updated 2020 Apr 1; cited 2021 Nov 30] Available from: https://www.noaa.gov/education/resource-collections/ocean-coasts/ocean-acidification

70. Feely RA, Doney SC, Cooley SR. Ocean acidification: Present conditions and future changes in a high-CO_2 world. *Oceanography*. 2009;22(4):36-47.

71. Doney SC, Fabry VJ, Feely RA, Kleypas JA. Ocean acidification: the other CO2 problem. *Annual review of marine science*. 2009;1:169-92.

72. Milligan AJ, Varela DE, Brzezinski MA, Morel FM. Dynamics of silicon metabolism and silicon isotopic discrimination in a marine diatomas a function of pCO2. Limnology and Oceanography. 2004;49(2):322-9.

73. He YT, Traina SJ. Transformation of magnetite to goethite under alkaline pH conditions. *Clay minerals*. 2007;42(1):13-9.

74. Breitbarth E, Bellerby RJ, Neill CC, Ardelan MV, Meyerhöfer M, Zöllner E, *et al.* Ocean acidification affects iron speciation in seawater. *Biogeosciences Discussions*. 2009;6(4).

75. Rost B, Riebesell U, Burkhardt S, Sültemeyer D. Carbon acquisition of bloom-forming marine phytoplankton. *Limnology and oceanography*. 2003;48(1):55-67.

76. Reinfelder JR, Kraepiel AM, Morel FM. Unicellular C 4 photosynthesis in a marine diatom. Nature. 2000;407(6807):996-9.

77. Meunier V, Geissler L, Bonnet S, Rädecker N, Perna G, Grosso O, *et al*. Microbes support enhanced nitrogen requirements of coral holobionts in a high CO2 environment. *Molecular ecology*. 2021;30(22):5888–99.

78. Kranz SA, Eichner M, Rost B. Interactions between CCM and N 2 fixation in Trichodesmium. *Photosynthesis Research*. 2011;109(1):73-84.

79. Kranz SA, Levitan O, Richter KU, Prái il O, Berman-Frank I, Rost B. Combined effects of CO2 and light on the N2-fixing cyanobacterium Trichodesmium IMS101: physiological responses. *Plant physiology*. 2010;154(1):334-45.

80. Levitan O, Kranz SA, Spungin D, Prái il O, Rost B, Berman-Frank I. Combined effects of CO2 and light on the N2-fixing cyanobacterium Trichodesmium IMS101: a mechanistic view. *Plant physiology*. 2010;154(1):346-56.

81. Chakraborty R, Braun V, Cornelis P, Hantke K. Iron Uptake in Bacteria with Emphasis on E. coli and Pseudomonas. 1. Aufl. Dordrecht: Springer Netherlands; 2013.

82. Hopkinson BM, Morel FM. The role of siderophores in iron acquisition by photosynthetic marine microorganisms. *Biometals*. 2009;22(4):659-69.

83. Boyd PW, Ellwood MJ. The biogeochemical cycle of iron in the ocean. *Nature Geoscience*. 2010;3(10):675-82.

84. Benner R. Loose ligands and available iron in the ocean. *Proceedings of the National Academy of Sciences*. 2011;108(3):893-4.

85. Morel FM, Kustka AB, Shaked Y. The role of unchelated Fe in the iron nutrition of phytoplankton. *Limnology and Oceanography*. 2008;53(1):400-4.

86. Sugie K, Nishioka J, Kuma K, Volkov YN, Nakatsuka T. Availability of particulate Fe to phytoplankton in the Sea of Okhotsk. *Marine Chemistry*. 2013;152:20-31.

87. Kanna N, Nishioka J. Bio-availability of iron derived from subarctic first-year sea ice. *Marine Chemistry*. 2016;186:189-97.

88. Kanna N, Lannuzel D, van der Merwe P, Nishioka J. Size fractionation and bioavailability of iron released from melting sea ice in a subpolar marginal sea. *Marine Chemistry*. 2020;221:103774.

89. Kuma K, Matsunaga K. Availability of colloidal ferric oxides to coastal marine phytoplankton. *Marine Biology*. 1995;122(1):1-1.

90. Chen M, Wang WX. Bioavailability of natural colloid-bound iron to marine plankton: Influences of colloidal size and aging. *Limnology and oceanography*. 2001;46(8):1956-67.

91. Yoshida M, Kuma K, Iwade S, Isoda Y, Takata H, Yamada M. Effect of aging time on the availability of freshly precipitated ferric hydroxide to coastal marine diatoms. *Marine Biology*. 2006;149(2):379-92.

92. Hudson RJ, Morel FM. Distinguishing between extra-and intracellular iron in marine phytoplankton. *Limnology and Oceanography*. 1989;34(6):1113-20.

93. Tovar-Sanchez A, Sañudo-Wilhelmy SA, Garcia-Vargas M, Weaver RS, Popels LC, Hutchins DA. A trace metal clean reagent to remove surface-bound iron from marine phytoplankton. *Marine Chemistry*. 2003;82(1-2):91-9.

94. Taylor RL. Studies in Fe bioavailability: co-limitation of primary productivity by iron, light, and nitrate in the Beaufort Sea, and direct iron-siderophore uptake mechanisms in Fe deficient phytoplankton [Doctoral dissertation] British Columbia: University of British Columbia; 2011.

95. Li J. Particulate trace metals & iron availability to phytoplankton in a changing Arctic Ocean [Doctoral dissertation] British Columbia: University of British Columbia; 2017.

96. Worsfold PJ, Lohan MC, Ussher SJ, Bowie AR. Determination of dissolved iron in seawater: a historical review. *Marine Chemistry*. 2014;166:25-35.

97. Elemental Scientific Incorporated. Elemental Scientific - Improve ICPMS lab results with… [Internet]. Omaha: Elemental Scientific Incorporated; [Cited 2021 Nov 30]. Available from: https://www.icpms.com/pdfv1/seaFAST%20-%20Automated%20Seawater%20Analysis%2014011-4.pdf

98. Wilschefski SC, Baxter MR. Inductively coupled plasma mass spectrometry: introduction to analytical aspects. *The Clinical Biochemist Reviews*. 2019;40(3):115.

99. Thomas R. An Overview of ICP Mass Spectrometry. In: Thomas R. Practical Guide to ICP-MS. Second Edition. Boca Raton: CRC Press; 2008. p. 1-5.

100. Humphrey AM. Chlorophyll. *Food Chemistry*. 1980;5(1):57-67.

101. Cosgrove J, Borowitzka MA. Chlorophyll fluorescence terminology: an introduction. In: Suggett DJ, Prášil O, Borowitzka MA, editors. Chlorophyll a fluorescence in aquatic sciences: methods and applications. Dordrcht: Springer Science & Business Media; 2010. p. 1-17.

102. Bolhàr-Nordenkampf HR, Öquist G. Chlorophyll fluorescence as a tool in photosynthesis research. In: Hall DO, Scurlock JM, Bolhar-Nordenkampf HR, Leegood RC, Long SP, editors. Photosynthesis and production in a changing environment. Dordrcht: Springer Science & Business Media; 1993. p. 193-206.

103. Designs T. Trilogy laboratory fluorometer user's manual. Version. 2006;1:38. Figure 11; p. 38.

104. Schuback N, Schallenberg C, Duckham C, Maldonado MT, Tortell PD. Interacting effects of light and iron availability on the coupling of photosynthetic electron transport and CO2-assimilation in marine phytoplankton. *PLoS One*. 2015;10(7):e0133235.

105. Heinz WG. Phytoplankton Analyzer Phyto-Pam and Phyto-Win Software V 1.45. Effeltrich, Germany. 2003.

106. Rabinowitch EI. Photosynthesis and related processes. LWW; 1951 Dec 1.

107. The 2017 GEOTRACES Standards and Intercalibration Committee. Sampling and sample-handling protocols for GEOTRACES Cruises, Version 3.0 [Internet]. 2017 [Cited 2021 Nov 30]. Available from: https://epic.awi.de/id/eprint/51363/1/Cookbook.pdf

108. Cornell RM, Schwertmann U. Introduction to the iron oxides. In: Cornell RM, Schwertmann U, editors. The iron oxides: structure, properties, reactions, occurrences and uses. Second, completely revised and extended edition. Weinheim: John Wiley & Sons; 2003. p. 1-8.

109. Raiswell R, Benning LG, Tranter M, Tulaczyk S. Bioavailable iron in the Southern Ocean: the significance of the iceberg conveyor belt. *Geochemical transactions*. 2008;9(1):1-9.

110. Pachauri RK, Allen MR, Barros VR, Broome J, Cramer W, Christ R, Church JA, Clarke L, Dahe Q, Dasgupta P, Dubash NK. Climate change 2014: synthesis report. Contribution of Working Groups I, II and III to the fifth assessment report of the Intergovernmental Panel on Climate Change (IPCC) [Internet]. Geneva: IPCC; 2015 [Cited: 2021 Nov 30]. Available from: https://epic.awi.de/id/eprint/37530/1/IPCC_AR5_SYR_Final.pdf

111. Dickson AG, Sabine CL, Christian JR. Guide to best practices for ocean CO2 measurements [Internet]. Sidney: North Pacific Marine Science Organization; 2007 [Cited 2021 Nov 30]. IOCCP REPORT No. 8. Available from: https://www.ncei.noaa.gov/access/ocean-carbon-data-system/oceans/Handbook_2007/Guide_all_in_one.pdf

112. Fransson A, Chierici M, Miller LA, Carnat G, Shadwick E, Thomas H, et al. Impact of sea-ice processes on the carbonate system and ocean acidification at the ice-water interface of the Amundsen Gulf, Arctic Ocean. *Journal of Geophysical Research: Oceans.* 2013;118(12):7001-23.

113. Haraldsson C, Anderson LG, Hassellöv M, Hulth S, Olsson K. Rapid, high-precision potentiometric titration of alkalinity in ocean and sediment pore waters. *Deep Sea Research Part I: Oceanographic Research Papers.* 1997;44(12):2031-44.

114. Johnson KM, King AE, Sieburth JM. Coulometric TCO2 analyses for marine studies; an introduction. *Marine Chemistry.* 1985;16(1):61-82.

115. Johnson KM, Sieburth JM, leB Williams PJ, Brändström L. Coulometric total carbon dioxide analysis for marine studies: automation and calibration. *Marine Chemistry.* 1987;21(2):117-33.

116. Chierici M, Fransson A, Turner DR, Pakhomov EA, Froneman PW. Variability in pH, fCO2, oxygen and flux of CO2 in the surface water along a transect in the Atlantic sector of the Southern Ocean. *Deep Sea Research Part II: Topical Studies in Oceanography.* 2004;51(22-24):2773-87.

117. Bellerby RG, Turner DR, Robertson JE. Surface pH and pC02 distributions in the Bellingshausen Sea, Southern Ocean, during the early Austral summer. *Deep Sea Research Part II: Topical Studies in Oceanography.* 1995;42(4-5):1093-107.

118. Clayton TD, Byrne RH. Spectrophotometric seawater pH measurements: total hydrogen ion concentration scale calibration of m-cresol purple and at-sea results. *Deep Sea Research Part I: Oceanographic Research Papers.* 1993;40(10):2115-29.

119. Lee K, Millero FJ. Thermodynamic studies of the carbonate system in seawater. *Deep Sea Research Part I: Oceanographic Research Papers.* 1995;42(11-12):2035-61.

120. Lewis ER, Wallace DW. Program Developed for CO2 System Calculations. CDIAC, ESS-DIVE repository [Software]. United States; 1998 [Cited 2021 Nov 30]. Available from: https://data.ess-dive.lbl.gov/view/doi:10.15485/1464255

121. Hansson I. A new set of pH-scales and standard buffers for sea water. *Deep Sea Research and Oceanographic Abstracts*. 1973; 20(5):479-491.

122. Arar EJ, Collins GB, editors. Method 445.0: In vitro determination of chlorophyll a and pheophytin a in marine and freshwater algae by fluorescence. Revision 1.2. Cincinnati: Environmental Protection Agency, Office of Research and Development, National Exposure Research Laboratory; 1997.

123. Morel FM, Rueter JG, Anderson DM, Guillard RR. AQUIL: A CHEMICALLY DEFINED PHYTOPLANKTON CULTURE MEDIUM FOR TRACE METAL STUDIES 1 2. *Journal of Phycology*. 1979;15(2):135-41.

124. Price NM, Harrison GI, Hering JG, Hudson RJ, Nirel PM, Palenik B, Morel FM. Preparation and chemistry of the artificial algal culture medium Aquil. *Biological oceanography*. 1989;6(5-6):443-61.

125. Eppley RW, Holmes RW, Paasche E. Periodicity in cell division and physiological behavior of Ditylum brightwellii, a marine planktonic diatom, during growth in light-dark cycles. *Archiv für Mikrobiologie*. 1967;56(4):305-23.

126. Edvardsen B; Moy F; Paasche E. Hemolytic activity in extracts of Chrysochromulina polylepis grown atdifferent levels of selenite and phosphate. In: Smayda TJ, Graneli E, Sundstrom B, Edler L, Anderson DM, editors.Toxic Marine Phytoplankton. New York: Elsevier; 1990. p. 284–89.

127. Bio-Rad Laboratories. Chelex 100 and Chelex 20 chelating ion exchange resin: Instruction manual [Internet]. Hercules: Bio-Rad Laboratories; 2000 [Cited 2021 Nov 30]. Available from: http://www.bio-rad.com/webmaster/pdfs/9184_Chelex.PDF

128. Smith SL, Yamanaka Y. Quantitative comparison of photoacclimation models for marine phytoplankton. *ecological modelling*. 2007;201(3-4):547-52.

129. Fang X, Sommer U. Overwintering effects on the spring bloom dynamics of phytoplankton. *Journal of Plankton Research*. 2017;39(5):772-80.

130. Johnson KS, Elrod V, Fitzwater S, Plant J, Boyle E, Bergquist B, *et al*. Developing standards for dissolved iron in seawater. Eos, Transactions American Geophysical Union. 2007;88(11):131-2.

131. Johnson KS, Chavez FP, Elrod VA, Fitzwater SE, Pennington JT, Buck KR, *et al*. The annual cycle of iron and the biological response in central California coastal waters. *Geophysical Research Letters*. 2001;28(7):1247-50.

132. Lippiatt SM, Lohan MC, Bruland KW. The distribution of reactive iron in northern Gulf of Alaska coastal waters. *Marine Chemistry.* 2010;121(1-4):187-99.

133. Arrigo KR, Robinson DH, Worthen DL, Dunbar RB, DiTullio GR, VanWoert M, *et al*. Phytoplankton community structure and the drawdown of nutrients and CO2 in the Southern Ocean. *Science*. 1999;283(5400):365-7.

134. Colman AS, Blake RE, Karl DM, Fogel ML, Turekian KK. Marine phosphate oxygen isotopes and organic matter remineralization in the oceans. *Proceedings of the National Academy of Sciences*. 2005;102(37):13023-8.

135. Benitez-Nelson CR, Buesseler KO. Variability of inorganic and organic phosphorus turnover rates in the coastal ocean. *Nature*. 1999;398(6727):502-5.

136. Grill EV, Richards FA. Nutrient regeneration from phytoplankton decomposing in seawater. Department of Oceanography, University of Washington; 1965.

137. Hoffmann K. Untersuchungen über die Remineralisation des Phosphors im Plankton. 1956.

138. Klausmeier CA, Litchman E, Daufresne T, Levin SA. Optimal nitrogen-to-phosphorus stoichiometry of phytoplankton. *Nature*. 2004;429(6988):171-4.

139. Weber T, Deutsch C. Oceanic nitrogen reservoir regulated by plankton diversity and ocean circulation. *Nature*. 2012;489(7416):419-22.

140. Arrigo KR. Marine microorganisms and global nutrient cycles. *Nature*. 2005;437(7057):349-55.

141. Sarmiento JL, Hughes TM, Stouffer RJ, Manabe S. Simulated response of the ocean carbon cycle to anthropogenic climate warming. *Nature*. 1998;393(6682):245-9.

142. Donahue K, Klaas C, Dillingham PW, Hoffmann LJ. Combined effects of ocean acidification and increased light intensity on natural phytoplankton communities from two Southern Ocean water masses. Journal of Plankton Research. 2019;41(1):30-45.

143. McMinn A, Müller MN, Martin A, Ryan KG. The response of Antarctic sea ice algae to changes in pH and CO2. *PLoS One*. 2014;9(1):e86984.

144. Coad T, McMinn A, Nomura D, Martin A. Effect of elevated CO2 concentration on microalgal communities in Antarctic pack ice. *Deep Sea Research Part II: Topical Studies in Oceanography*. 2016;131:160-9.

145. Taylor AR, Brownlee C, Wheeler GL. Proton channels in algae: reasons to be excited. *Trends in plant science*. 2012;17(11):675-84.

146. Deppeler S, Petrou K, Schulz KG, Westwood K, Pearce I, McKinlay J, *et al*. Ocean acidification of a coastal Antarctic marine microbial community reveals a critical threshold for CO 2 tolerance in phytoplankton productivity. *Biogeosciences*. 2018;15(1):209-31.

147. Raven JA. Physiology of inorganic C acquisition and implications for resource use efficiency by marine phytoplankton: relation to increased CO2 and temperature. *Plant, Cell & Environment*. 1991;14(8):779-94.

148. Badger MR, Price GD. The role of carbonic anhydrase in photosynthesis. *Annual review of plant biology*. 1994;45(1):369-92.

149. Badger MR, Andrews TJ, Whitney SM, Ludwig M, Yellowlees DC, Leggat W, *et al*. The diversity and coevolution of Rubisco, plastids, pyrenoids, and chloroplast-based CO2-concentrating mechanisms in algae. *Canadian Journal of Botany*. 1998;76(6):1052-71.

150. Hopkinson BM, Dupont CL, Allen AE, Morel FM. Efficiency of the CO2-concentrating mechanism of diatoms. *Proceedings of the National Academy of Sciences*. 2011;108(10):3830-7.

151. Frankignoulle M, Canon C, Gattuso JP. Marine calcification as a source of carbon dioxide: Positive feedback of increasing atmospheric CO2. *Limnology and Oceanography*. 1994;39(2):458-62.

152. Atkins PW, De Paula J. Atkins' physical chemistry. 9th ed. Oxford: Oxford University Press; 2010.

153. Hancock AM, Davidson AT, McKinlay J, McMinn A, Schulz KG, Enden RL. Ocean acidification changes the structure of an Antarctic coastal protistan community. *Biogeosciences*. 2018;15(8):2393-410.

154. Krause GH, Weis E. Chlorophyll fluorescence as a tool in plant physiology. *Photosynthesis research*. 1984;5(2):139-57.

155. Jee G. Sixty-three years since Kautsky: chlorophylla fluorescence. *Aust. J. Plant Physiol*. 1995;22:131-60.

156. Lazár D. The polyphasic chlorophyll a fluorescence rise measured under high intensity of exciting light. *Functional Plant Biology*. 2006;33(1):9-30.

157. Lazár D, Pospíšil P, Nauš J. Decrease of fluorescence intensity after the K step in chlorophyll a fluorescence induction is suppressed by electron acceptors and donors to photosystem 2. *Photosynthetica*. 1999;37(2):255-65.

158. Govindjee G. Chlorophyll a Fluorescence: A Bit of Basics and History. In: Strasser RJ, Tsimilli-Michael M, Srivastava A, Papageorgiou G, editors. Chlorophyll a Fluorescence. Advances in Photosynthesis and Respiration. Dordrecht: Springer; 2004. p. 1-41.

159. Neubauer C, Schreiber U. The polyphasic rise of chlorophyll fluorescence upon onset of strong continuous illumination: I. Saturation characteristics and partial control by the photosystem II acceptor side. *Zeitschrift für Naturforschung C*. 1987;42(11-12):1246-54.

160. Schreiber U, Neubauer C. The polyphasic rise of chlorophyll fluorescence upon onset of strong continuous illumination: II. Partial control by the photosystem II donor side and possible ways of interpretation. *Zeitschrift für Naturforschung C*. 1987;42(11-12):1255-64.

161. White AJ, Critchley C. Rapid light curves: a new fluorescence method to assess the state of the photosynthetic apparatus. *Photosynthesis research*. 1999;59(1):63-72.

162. Falkowski PG, Wyman K, Ley AC, Mauzerall DC. Relationship of steady-state photosynthesis to fluorescence in eucaryotic algae. *Biochimica et Biophysica Acta (BBA)-Bioenergetics*. 1986;849(2):183-92.

163. Seaton GG, Walker DA. Chlorophyll fluorescence as a measure of photosynthetic carbon assimilation. *Proceedings of the Royal Society of London*. Series B: Biological Sciences. 1990;242(1303):29-35.

164. Kolber Z, Falkowski PG. Use of active fluorescence to estimate phytoplankton photosynthesis in situ. *Limnology and Oceanography*. 1993;38(8):1646-65.

165. Nicklisch A, Köhler J. Estimation of primary production with Phyto-PAM fluorometry. *Berichte des IGB*. 2001;13:47-60.

166. Schreiber U. Pulse-amplitude-modulation (PAM) fluorometry and saturation pulse method: an overview. In: Papageorgiou GC, editor. Chlorophyll a fluorescence: a signature of photosynthesis. Dordrecht: Springer; 2004. p. 279-319.

167. Sakshaug E, Bricaud A, Dandonneau Y, Falkowski PG, Kiefer DA, Legendre L, *et al*. Parameters of photosynthesis: definitions, theory and interpretation of results. *Journal of Plankton Research*. 1997;19(11):1637-70.

168. Jassby AD, Platt T. Mathematical formulation of the relationship between photosynthesis and light for phytoplankton. *Limnology and oceanography*. 1976;21(4):540-7.

169. Wingert CJ, Cochlan WP. Effects of ocean acidification on the growth, photosynthetic performance, and domoic acid production of the diatom Pseudo-nitzschia australis from the California Current System. *Harmful Algae*. 2021;107:102030.

170. Twining BS, Baines SB. The trace metal composition of marine phytoplankton. Annual review of marine science. 2013 Jan 3;5:191-215.

Appendices

Appendices 1 DML Experiment

Appendix 1.1 Light measurement before incubation

Unit: µ mol photons m^{-2} *m^{-1}	**Corrected light intensity after cover**	**Light intensity inside the cubitainer**	**light transmission**
	66		
	77	54	70.13%
	77	54	70.13%
	83	58	69.88%
	80	56	70.00%
	80	56	70.00%
	68	48	70.59%
	63	44	69.84%
	82	58	70.73%
	79	55	69.62%
	66	46	69.70%
	87	60	68.97%
	87	61	70.11%
	77	54	70.13%
Average light intensity	76.57	54.15	69.99%
SD	7.84	5.21	0.0044

Appendix 1.2 Dissolved Iron (DFe) Concentration during the Incubation.

The concentration is corrected for blanks and detection limit. Concentration that is highlighted in red is outlier.

seaFAST volume (ml)		Incubation day	Incubation date	Cubitainer number	Treatment	Fe Concentration		Average	SD (%)
Initial volume	Final volume					µg/L	nM	nM	
50	2	5	18.03.2019	6	Control	0.047	0.839	0.84	
50	2	7	20.03.2019	2	Control	0.011	0.201	0.20	
50	2	9	22.03.2019	10	Control	0.027	0.477	0.48	
50	2	11	24.03.2019	2	Control	0.040	0.706	0.46	21.67%
50	2		24.03.2019	6	Control	0.022	0.384		
50	2		24.03.2019	10	Control	0.016	0.294		
50	2	5	18.03.2019	8	FeO(OH)	0.040	0.715	0.72	
50	2	7	20.03.2019	4	FeO(OH)	0.023	0.405	0.40	
50	2	9	22.03.2019	12	FeO(OH)	0.033	0.583	0.58	
50	2	11	24.03.2019	4	FeO(OH)	0.030	0.536	0.47	14.22%
50	2		24.03.2019	8	FeO(OH)	0.017	0.303		
50	2		24.03.2019	12	FeO(OH)	0.031	0.560		
50	2	5	18.03.2019	1	Low pH Control	0.017	0.300	0.30	
50	2	7	20.03.2019	5	Low pH Control	0.078	1.387	1.39	
50	2	9	22.03.2019	9	Low pH Control	0.014	0.244	0.24	
50	2	11	24.03.2019	1	Low pH Control	0.036	0.647	0.59	31.79%
50	2		24.03.2019	5	Low pH Control	0.049	0.881		
50	2		24.03.2019	9	Low pH Control	0.014	0.252		
50	2	5	18.03.2019	11	Low pH + FeO(OH)	0.018	0.322	0.32	
50	2	7	20.03.2019	3	Low pH + FeO(OH)	0.017	0.298	0.30	

50	2	9	22.03.2019	7	Low pH + FeO(OH)	0.012	0.210	0.21	
50	2	11	24.03.2019	3	Low pH + FeO(OH)	0.036	0.650	0.39	23.53%
50	2		24.03.2019	7	Low pH + FeO(OH)	0.018	0.316		
50	2		24.03.2019	11	Low pH + FeO(OH)	0.011	0.196		
50	2	11	24.03.2019	13	Extra Control	0.012	0.212	0.21	

Appendix 1.3 Total Acid Leachable Iron (TaLFe) Concentration during the Incubation.

The concentration is corrected for blanks and detection limit. Concentration that is highlighted in red is outlier.

seaFAST volume (mL)		**Incubation day**	**Incubation date**	**Cubitainer number**	**Treatment**	**Material**	**Preservation with acid**	**Fe Concentration**	
Initial volume	**Final volume**						**Type and strength**	**µg/L**	**nM**
50	2	5	18.03.2019	6	Control	seawater	1 M HNO_3	0.068	1.22
50	2	7	20.03.2019	2	Control	seawater	1 M HNO_3	0.287	5.12
40	2	9	22.03.2019	10	Control	seawater	1 M HNO_3	0.001	0.02
50	2	5	18.03.2019	8	FeO(OH)	seawater	1 M HNO_3	0.061	1.10
50	2	7	20.03.2019	4	FeO(OH)	seawater	1 M HNO_3	0.034	0.62
40	2	9	22.03.2019	12	FeO(OH)	seawater	1 M HNO_3	0.002	0.03
50	2	5	18.03.2019	1	Low pH Control	seawater	1 M HNO_3	0.045	0.80
50	2	7	20.03.2019	5	Low pH Control	seawater	1 M HNO_3	0.040	0.72
40	2	9	22.03.2019	9	Low pH Control	seawater	~ 1 M HNO_3	0.031	0.55
40	2	11	24.03.2019	1	Low pH Control	seawater	1 M HNO_3	0.000	0.00
50	2	5	18.03.2019	11	Low pH + FeO(OH)	seawater	1 M HNO_3	0.083	1.48
50	2	7	20.03.2019	3	Low pH + FeO(OH)	seawater	1 M HNO_3	0.053	0.95
50	2	9	22.03.2019	7	Low pH + FeO(OH)	seawater	1 M HNO_3	0.034	0.61

Appendix 1.4 Data of Salinity, Temperature and Alkalinity.

Sampling Date	**Incubation Day**	**ID**	**Treatment**	**Salinity**	**Temperature (°C)**	**Alkalinity**
		(cubitainer number)				***(µ mol/kg)***
15.03.2019	0	inkub exp2 zero low pH	Low pH Control	34	3	2087
15.03.2019		inkub exp3 d 2110? low pH	Low pH Control	34	3	2098
15.03.2019		inkub exp4 day zero low pH	Low pH Control	34	3	2099
15.03.2019	0	inkub exp1 zero control	Control	34	3	2313
18.03.2019	5	1	Low pH Control	34	3	2111
18.03.2019		6	Control	34	3	2315
18.03.2019		11	Low pH + FeO(OH)	34	3	2111
18.03.2019		8	FeO(OH)	34	3	2314
20.03.2019	7	1	Low pH Control	34	0	2116
20.03.2019		5	Low pH Control	34	0	2100
20.03.2019	7	2	Control	34	0	2324
20.03.2019		6	Control	34	0	2324
20.03.2019	7	3	Low pH + FeO(OH)	34	0	2095
20.03.2019		11	Low pH + FeO(OH)	34	0	2094
20.03.2019	7	4	FeO(OH)	34	0	2308
20.03.2019		8	FeO(OH)	34	0	2307
22.03.2019	9	1	Low pH Control	34	0	2100
22.03.2019		5	Low pH Control	34	0	2117
22.03.2019		9	Low pH Control	34	0	2099
22.03.2019	9	2	Control	34	0	2330
22.03.2019		6	Control	34	0	2327
22.03.2019		10	Control	34	0	2322
22.03.2019	9	3	Low pH + FeO(OH)	34	0	2104
22.03.2019		7	Low pH + FeO(OH)	34	0	2107

22.03.2019		11	Low pH + FeO(OH)	34	0	2113
22.03.2019	9	4	FeO(OH)	34	0	2322
22.03.2019		8	FeO(OH)	34	0	2329
22.03.2019		12	FeO(OH)	34	0	2322
24.03.2019	11	1	Low pH Control	34	0	2116
24.03.2019		5	Low pH Control	34	0	2325
24.03.2019		9	Low pH Control	34	0	2104
24.03.2019	11	2	Control	34	0	2329
24.03.2019		6	Control	34	0	2111
24.03.2019		10	Control	34	0	2329
24.03.2019	11	3	Low pH + FeO(OH)	34	0	2108
24.03.2019		7	Low pH + FeO(OH)	34	0	2105
24.03.2019		11	Low pH + FeO(OH)	34	0	2120
24.03.2019	11	4	FeO(OH)	34	0	2105
24.03.2019		8	FeO(OH)	34	0	2328
24.03.2019		12	FeO(OH)	34	0	2328
24.03.2019	11	13	Control	34	0	2328

Appendix 1.5 Data of Macronutrients

Sampling Date	**Incubation Day**	**ID**	**Treatment**	**NO_3^-**	**Average**	**SD**	**PO_4^{3-}**	**Average**	**SD**	**Silicate**	**Average**	**SD**
		(cubitainer number)		***µmol/L***	***µmol/L***		***µmol/L***	***µmol/L***		***µmol/L***	***µmol/L***	
15.03.2019	0	inkub exp2 zero low pH	Low pH Control	23.6	23.60	0.000	1.8	1.80	0.000	52.2	52.19	0.000
15.03.2019		inkub exp3 d	Low pH Control	23.6			1.8			52.2		

		2110? low pH										
15.03.2019		inkub exp4 day zero low pH	Low pH Control	23.6			1.8			52.2		
15.03.2019	0	inkub exp1 zero control	Control	23.6	23.60	#DIV/0!	1.8	1.80	#DIV/0!	52.2	52.19	#DIV/0!
18.03.2019	5	1	Low pH Control									
18.03.2019		6	Control									
18.03.2019		11	Low pH + FeO(OH)									
18.03.2019		8	FeO(OH)									
20.03.2019	7	1	Low pH Control	21.36	20.89	0.665	1.57	1.63	0.078	45.43	45.44	0.014
20.03.2019		5	Low pH Control	20.42			1.68			45.45		
20.03.2019	7	2	Control	17.87	17.90	0.042	1.41	1.42	0.014	43.28	43.18	0.148
20.03.2019		6	Control	17.93			1.43			43.07		
20.03.2019	7	3	Low pH + FeO(OH)	21.81	20.63	1.669	1.54	1.53	0.014	43.91	44.68	1.082
20.03.2019		11	Low pH + FeO(OH)	19.45			1.52			45.44		
20.03.2019	7	4	FeO(OH)	18.78	18.09	0.983	1.43	1.43	0.000	43.52	43.36	0.233
20.03.2019		8	FeO(OH)	17.39			1.43			43.19		
22.03.2019	9	1	Low pH Control	19.75	19.44	0.534	1.51	1.52	0.026	44.39	44.42	0.421
22.03.2019		5	Low pH Control	18.82			1.5			44.86		

22.03.2019		9	Low pH Control	19.74			1.55			44.02		
22.03.2019	9	2	Control	14.7	15.23	0.932	1.48	1.44	0.055	42.89	42.46	0.396
22.03.2019		6	Control	14.69			1.38			42.11		
22.03.2019		10	Control	16.31			1.47			42.38		
22.03.2019	9	3	Low pH + FeO(OH)	19.83	19.39	0.782	1.55	1.53	0.038	44.62	44.28	0.437
22.03.2019		7	Low pH + FeO(OH)	19.86			1.56			43.79		
22.03.2019		11	Low pH + FeO(OH)	18.49			1.49			44.44		
22.03.2019	9	4	FeO(OH)	15.93	15.18	0.750	1.45	1.44	0.012	44.05	43.42	0.854
22.03.2019		8	FeO(OH)	14.43			1.43			42.45		
22.03.2019		12	FeO(OH)	15.19			1.43			43.77		
24.03.2019	11	1	Low pH Control	18.6	17.96	0.854	1.51	1.52	0.051	43.98	43.78	0.286
24.03.2019		5	Low pH Control	16.99			1.48			43.9		
24.03.2019		9	Low pH Control	18.29			1.58			43.45		
24.03.2019	11	2	Control	13.13	13.83	1.425	1.52	1.48	0.059	42.21	41.00	1.205
24.03.2019		6	Control	12.89			1.41			39.8		
24.03.2019		10	Control	15.47			1.5			41		
24.03.2019	11	3	Low pH + FeO(OH)	18.33	17.84	0.812	1.54	1.53	0.010	44.44	43.61	0.764
24.03.2019		7	Low pH + FeO(OH)	18.28			1.53			42.94		

24.03.2019		11	Low pH + FeO(OH)	16.9			1.52			43.44		
24.03.2019	11	4	FeO(OH)	13.82	13.27	1.023	1.41	1.49	0.106	41.07	41.34	0.766
24.03.2019		8	FeO(OH)	12.09			1.45			42.2		
24.03.2019		12	FeO(OH)	13.9			1.61			40.74		
24.03.2019	11	13	Control	14.75	14.75	#DIV/0!	1.45	1.45	#DIV/0!	42.69	42.69	#DIV/0!

Appendix 1.6 Data of Redfield Ratio of N/P

Sampling Date	Incubation Day	ID (cubitainer number)	Treatment	Redfield ratio of N/P	Average	SD
15.03.2019	0	inkub exp2 zero low pH	Low pH Control	13.111	13.11	0.000
15.03.2019		inkub exp3 d 2110? low pH	Low pH Control	13.111		
15.03.2019		inkub exp4 day zero low pH	Low pH Control	13.111		
15.03.2019	0	inkub exp1 zero control	Control	13.111	13.11	#DIV/0!
18.03.2019	5	1	Low pH Control			
18.03.2019		6	Control			
18.03.2019		11	Low pH + FeO(OH)			
18.03.2019		8	FeO(OH)			
20.03.2019	7	1	Low pH Control	13.605	12.88	1.026
20.03.2019		5	Low pH Control	12.155		
20.03.2019	7	2	Control	12.674	12.61	0.096
20.03.2019		6	Control	12.538		
20.03.2019	7	3	Low pH + FeO(OH)	14.162	13.48	0.966
20.03.2019		11	Low pH + FeO(OH)	12.796		
20.03.2019	7	4	FeO(OH)	13.133	12.65	0.687
20.03.2019		8	FeO(OH)	12.161		

22.03.2019	9	1	Low pH Control	13.079	12.79	0.270
22.03.2019		5	Low pH Control	12.547		
22.03.2019		9	Low pH Control	12.735		
22.03.2019	9	2	Control	9.932	10.56	0.586
22.03.2019		6	Control	10.645		
22.03.2019		10	Control	11.095		
22.03.2019	9	3	Low pH + FeO(OH)	12.794	12.64	0.206
22.03.2019		7	Low pH + FeO(OH)	12.731		
22.03.2019		11	Low pH + FeO(OH)	12.409		
22.03.2019	9	4	FeO(OH)	10.986	10.57	0.450
22.03.2019		8	FeO(OH)	10.091		
22.03.2019		12	FeO(OH)	10.622		
24.03.2019	11	1	Low pH Control	12.318	11.79	0.459
24.03.2019		5	Low pH Control	11.480		
24.03.2019		9	Low pH Control	11.576		
24.03.2019	11	2	Control	8.638	9.36	0.859
24.03.2019		6	Control	9.142		
24.03.2019		10	Control	10.313		
24.03.2019	11	3	Low pH + FeO(OH)	11.903	11.66	0.466
24.03.2019		7	Low pH + FeO(OH)	11.948		
24.03.2019		11	Low pH + FeO(OH)	11.118		
24.03.2019	11	4	FeO(OH)	9.801	8.92	0.774
24.03.2019		8	FeO(OH)	8.338		
24.03.2019		12	FeO(OH)	8.634		
24.03.2019	11	13	Control	10.172	10.17	#DIV/0!

Appendix 1.7 Data of Chlorophyll a

1. Calculation Method

Borosilicate	Value	SD
R_b/R_a=	2.48928582	0.537326565
T_{au}=	5.620568087	12.67720829
F_d=	0.902241632	0.236049418
R_b=fluorometer reading **before** acidification		
R_a=fluorometer reading **after** acidification (addition of two drops of 5% HCl (1.2 M))		
Chla (mg/m^3)= F_d*T_{au}*(R_b*Dilution factor-R_a*Dilution factor)*volume - methanol/volume - filtered		

2. F_d, T_{au}, Volume – methanol & Volume – filtered.

Incubation Date	Incubation Day	Cubitainer No.	Treatment	F_d	T_{au}	Volume filtered (ml)	Volume methanol (ml)
18.03.2019	5	1	Low pH Control	0.902241632	5.620568087	250	5
		1	Low pH Control	0.902241632	5.620568087	250	5
		6	Control	0.902241632	5.620568087	250	5
		6	Control	0.902241632	5.620568087	250	5
		8	FeO(OH)	0.902241632	5.620568087	250	5
		8	FeO(OH)	0.902241632	5.620568087	250	5
		11	Low pH + FeO(OH)	0.902241632	5.620568087	220	5
		11	Low pH + FeO(OH)	0.902241632	5.620568087	225	5
20.03.2019	7	1	Low pH Control	0.902241632	5.620568087	125	5
		1	Low pH Control	0.902241632	5.620568087	125	5
		5	Low pH Control	0.902241632	5.620568087	125	5
		5	Low pH Control	0.902241632	5.620568087	125	5
		2	Control	0.902241632	5.620568087	125	5
		2	Control	0.902241632	5.620568087	125	5
		6	Control	0.902241632	5.620568087	125	5
		6	Control	0.902241632	5.620568087	125	5
		3	Low pH + FeO(OH)	0.902241632	5.620568087	125	5
		3	Low pH + FeO(OH)	0.902241632	5.620568087	125	5
		11	Low pH + FeO(OH)	0.902241632	5.620568087	125	5

		11	Low pH + FeO(OH)	0.902241632	5.620568087	125	5
		4	FeO(OH)	0.902241632	5.620568087	125	5
		4	FeO(OH)	0.902241632	5.620568087	125	5
		8	FeO(OH)	0.902241632	5.620568087	125	5
		8	FeO(OH)	0.902241632	5.620568087	125	5
		12	FeO(OH)	0.902241632	5.620568087	125	5
		12	FeO(OH)	0.902241632	5.620568087	125	5
22.03.2019	9	1	Low pH Control	0.902241632	5.620568087	100	5
		5	Low pH Control	0.902241632	5.620568087	100	5
		5	Low pH Control	0.902241632	5.620568087	100	5
		9	Low pH Control	0.902241632	5.620568087	100	5
		9	Low pH Control	0.902241632	5.620568087	100	5
		2	Control	0.902241632	5.620568087	100	5
		2	Control	0.902241632	5.620568087	100	5
		6	Control	0.902241632	5.620568087	100	5
		10	Control	0.902241632	5.620568087	100	5
		10	Control	0.902241632	5.620568087	100	5
		3	Low pH + FeO(OH)	0.902241632	5.620568087	100	5
		3	Low pH + FeO(OH)	0.902241632	5.620568087	100	5
		7	Low pH + FeO(OH)	0.902241632	5.620568087	100	5
		7	Low pH + FeO(OH)	0.902241632	5.620568087	100	5
		11	Low pH + FeO(OH)	0.902241632	5.620568087	100	5
		4	FeO(OH)	0.902241632	5.620568087	100	5
		4	FeO(OH)	0.902241632	5.620568087	100	5
		8	FeO(OH)	0.902241632	5.620568087	100	5
		8	FeO(OH)	0.902241632	5.620568087	100	5
		12	FeO(OH)	0.902241632	5.620568087	100	5
		12	FeO(OH)	0.902241632	5.620568087	100	5
24.03.2019	11	1	Low pH Control	0.902241632	5.620568087	80	5
		1	Low pH Control	0.902241632	5.620568087	80	5
		1	Low pH Control	0.902241632	5.620568087	80	5
		5	Low pH Control	0.902241632	5.620568087	80	5

		5	Low pH Control	0.902241632	5.620568087	80	5
		9	Low pH Control	0.902241632	5.620568087	80	5
		9	Low pH Control	0.902241632	5.620568087	80	5
		2	Control	0.902241632	5.620568087	80	5
		2	Control	0.902241632	5.620568087	80	5
		6	Control	0.902241632	5.620568087	60	5
		6	Control	0.902241632	5.620568087	80	5
		10	Control	0.902241632	5.620568087	80	5
		10	Control	0.902241632	5.620568087	80	5
		3	Low pH + FeO(OH)	0.902241632	5.620568087	80	5
		3	Low pH + FeO(OH)	0.902241632	5.620568087	80	5
		7	Low pH + FeO(OH)	0.902241632	5.620568087	80	5
		7	Low pH + FeO(OH)	0.902241632	5.620568087	80	5
		11	Low pH + FeO(OH)	0.902241632	5.620568087	80	5
		11	Low pH + FeO(OH)	0.902241632	5.620568087	80	5
		4	FeO(OH)	0.902241632	5.620568087	80	5
		4	FeO(OH)	0.902241632	5.620568087	80	5
		8	FeO(OH)	0.902241632	5.620568087	80	5
		8	FeO(OH)	0.902241632	5.620568087	100	5
		8	FeO(OH)	0.902241632	5.620568087	100	5
		12	FeO(OH)	0.902241632	5.620568087	100	5
		12	FeO(OH)	0.902241632	5.620568087	100	5
		12	FeO(OH)	0.902241632	5.620568087	100	5
		13	Extra Control	0.902241632	5.620568087	80	5
		13	Extra Control	0.902241632	5.620568087	80	5

3. R_b, R_a, Dilution factor and Chla concentration.

Incubation Date	Incubation Day	Cubitainer No.	Treatment	R_b	R_a	Dilution factor	Chla (mg/m^3)
18.03.2019	5	1	Low pH Control	51.5	19.30	1	3.266
		1	Low pH Control	44.6	22.30	1	2.262
		6	Control	71	31.70	1	3.986
		6	Control	68	33.10	1	3.540
		8	FeO(OH)	103.00	56.90	1	4.676
		8	FeO(OH)	102.00	55.50	1	4.716
		11	Low pH + FeO(OH)	58.70	26.50	1	3.711
		11	Low pH + FeO(OH)	39.80	18.80	1	2.367
20.03.2019	7	1	Low pH Control	21.60	9.92	1	2.369
		1	Low pH Control	7.60	5.44	1	0.438
		5	Low pH Control	19.30	15.80	1	0.710
		5	Low pH Control	19.20	14.00	1	1.055
		2	Control	41.00	18.09	1	4.647
		2	Control	38.50	21.70	1	3.408
		6	Control	43.20	21.20	1	4.463
		6	Control	54.90	30.00	1	5.051
		3	Low pH + FeO(OH)	16.10	8.90	1	1.460
		3	Low pH + FeO(OH)	10.50	5.50	1	1.014
		11	Low pH + FeO(OH)	37.00	20.80	1	3.286
		11	Low pH + FeO(OH)	26.80	14.30	1	2.536
		4	FeO(OH)	39.00	20.40	1	3.773
		4	FeO(OH)	44.40	21.40	1	4.665
		8	FeO(OH)	39.00	20.00	1	3.854
		8	FeO(OH)	46.90	23.30	1	4.787
		12	FeO(OH)	37.12	18.23	1	3.832
		12	FeO(OH)	45.34	24.03	1	4.323
22.03.2019	9	1	Low pH Control	18.10	8.68	1	2.388
		5	Low pH Control	27.90	21.60	1	1.597
		5	Low pH Control	27.20	21.30	1	1.496
		9	Low pH Control	21.20	10.60	1	2.688
		9	Low pH Control	43.40	20.90	1	5.705

		2	Control	82.70	40.80	1	10.624
		2	Control	73.60	35.53	1	9.653
		6	Control	57.70	30.20	1	6.973
		10	Control	41.00	19.80	1	5.375
		10	Control	42.80	21.00	1	5.528
		3	Low pH + FeO(OH)	21.10	15.30	1	1.471
		3	Low pH + FeO(OH)	23.90	20.40	1	0.887
		7	Low pH + FeO(OH)	52.40	25.30	1	6.871
		7	Low pH + FeO(OH)	56.00	27.10	1	7.328
		11	Low pH + FeO(OH)	37.10	18.00	1	4.843
		4	FeO(OH)	69.60	34.90	1	8.798
		4	FeO(OH)	75.10	39.60	1	9.001
		8	FeO(OH)	88.00	48.60	1	9.990
		8	FeO(OH)	77.20	46.40	1	7.810
		12	FeO(OH)	81.50	43.40	1	9.660
		12	FeO(OH)	66.43	41.12	1	6.417
24.03.2019	11	1	Low pH Control	39.20	18.00	1	6.719
		1	Low pH Control	34.40	15.50	1	5.990
		1	Low pH Control	39.00	19.10	1	6.307
		5	Low pH Control	46.50	22.30	1	7.670
		5	Low pH Control	47.40	21.90	1	8.082
		9	Low pH Control	35.80	16.40	1	6.149
		9	Low pH Control	52.20	23.90	1	8.970
		2	Control	88.30	44.40	1	*13.914*
		2	Control	82.20	42.30	1	*12.646*
		6	Control	60.80	28.90	1	*13.481*
		6	Control	77.50	36.00	1	*13.153*
		10	Control	28.80	13.40	1	4.881
		10	Control	60.80	29.70	1	9.857
		3	Low pH + FeO(OH)	39.00	18.30	1	6.561

		3	Low pH + FeO(OH)	46.70	21.70	1	7.924
		7	Low pH + FeO(OH)	37.90	17.40	1	6.497
		7	Low pH + FeO(OH)	53.70	24.10	1	9.382
		11	Low pH + FeO(OH)	45.70	21.60	1	7.638
		11	Low pH + FeO(OH)	55.80	25.70	1	9.540
		4	FeO(OH)	78.85	41.00	1	11.996
		4	FeO(OH)	73.90	38.40	1	11.252
		8	FeO(OH)	70.30	33.80	1	11.568
		8	FeO(OH)	106.07	57.20	1	12.391
		8	FeO(OH)	106.00	55.10	1	12.906
		12	FeO(OH)	101.00	55.50	1	11.537
		12	FeO(OH)	84.70	38.30	1	11.765
		12	FeO(OH)	87.30	39.80	1	12.044
		13	Extra Control	56.10	26.70	1	9.318
		13	Extra Control	64.60	30.90	1	10.681

4. Chla concentration and SD of different cubitainers and each treatment.

Incubation Date	**Incubation Day**	**Cubitainer No.**	**Treatment**	**Average Chla conc. & SD of each cubitainer of each treatment**		**Average Chla conc. & SD of each treatment**	
				Average Chla conc. of each cubitianer	**SD of each cubitainer**	**Average Chla conc. of each treatment**	**SD Of each treatment**
18.03.2019	5	1	Low pH Control	2.764	0.710	2.764	0.000
		6	Control	3.763	0.316	3.763	0.000
		8	FeO(OH)	4.696	0.029	4.696	0.000
		11	Low pH + FeO(OH)	3.039	0.951	3.039	0.000
20.03.2019	7	1	Low pH Control	1.404	1.365	1.143	0.369
		5	Low pH Control	0.882	0.244		

		2	Control	4.027	0.876	4.392	0.516
		6	Control	4.757	0.416		
		3	Low pH + FeO(OH)	1.237	0.316	2.074	0.152
		11	Low pH + FeO(OH)	2.911	0.531		
		4	FeO(OH)	4.219	0.631	4.206	0.122
		8	FeO(OH)	4.321	0.660		
		12	FeO(OH)	4.077	0.347		
22.03.2019	9	1	Low pH Control	2.388	0.000	2.711	1.354
		5	Low pH Control	1.547	0.072		
		9	Low pH Control	4.196	2.134		
		2	Control	10.138	0.687	7.521	2.391
		6	Control	6.973	0.000		
		10	Control	5.451	0.108		
		3	Low pH + FeO(OH)	1.179	0.412	4.374	2.988
		7	Low pH + FeO(OH)	7.100	0.323		
		11	Low pH + FeO(OH)	4.843	0.000		
		4	FeO(OH)	8.900	0.143	8.613	0.497
		8	FeO(OH)	8.900	1.542		
		12	FeO(OH)	8.039	2.293		
24.03.2019	11	1	Low pH Control	6.339	0.366	7.258	0.812
		5	Low pH Control	7.876	0.291		
		9	Low pH Control	7.559	1.995		
		2	Control	13.280	0.896	11.322	3.423
		6	Control	13.317	0.232		
		10	Control	7.369	3.519		
		3	Low pH + FeO(OH)	7.242	0.964	7.924	0.674

		7	Low pH + FeO(OH)	7.939	2.039		
		11	Low pH + FeO(OH)	8.589	1.345		
		4	FeO(OH)	11.624	0.527	11.898	0.347
		8	FeO(OH)	12.289	0.675		
		12	FeO(OH)	11.782	0.254		
		13	Extra Control	10.000	0.964	10.000	0.000

Appendix 1.8 Data of In vivo Fluorescence

Incubation Date	**Incubation Day**	**Cubitainer No.**	**Treatment**	**Sample Conc.**	**Average *in vivo* fluorescence and SD of each cubitainer of each treatment**		**Average *in vivo* fluorescence and SD of each treatment**	
					Average *in vivo* fluorescence of each cubitianer	**SD of each cubitainer**	**Average fluorescence of each treatment**	**SD Of each treatment**
18.03.2019	5	6	Control	0.98	1.00	0.02	1.00	#DIV/0!
		6	Control	1.01				
		6	Control	1.02				
		6	Control	0.989				
		8	FeO(OH)	1.01	1.15	0.12	1.15	#DIV/0!
		8	FeO(OH)	1.19				
		8	FeO(OH)	1.24				
		1	Low pH Control	0.357	0.38	0.02	0.38	#DIV/0!
		1	Low pH Control	0.405				
		1	Low pH Control	0.386				
		11	Low pH + FeO(OH)	0.801	0.78	0.02	0.78	#DIV/0!

		11	Low pH + FeO(OH)	0.779				
		11	Low pH + FeO(OH)	0.76				
20.03.2019	7	2	Control	1.29	1.30	0.01	1.30	0.01
		2	Control	1.31				
		2	Control	1.31				
		2	Control	1.3				
		6	Control	1.3	1.30	0.06		
		6	Control	1.21				
		6	Control	1.34				
		6	Control	1.33				
		4	FeO(OH)	1.33	1.39	0.05	1.56	0.24
		4	FeO(OH)	1.36				
		4	FeO(OH)	1.43				
		4	FeO(OH)	1.42				
		8	FeO(OH)	2.04	1.73	0.31		
		8	FeO(OH)	1.94				
		8	FeO(OH)	1.45				
		8	FeO(OH)	1.47				
		1	Low pH Control	0.393	0.39	0.01	0.47	0.11
		1	Low pH Control	0.396				
		1	Low pH Control	0.37				
		5	Low pH Control	0.538	0.55	0.04		
		5	Low pH Control	0.521				
		5	Low pH Control	0.534				
		5	Low pH Control	0.601				

		3	Low pH + FeO(OH)	0.521	0.52	0.01	0.64	0.18
		3	Low pH + FeO(OH)	0.517				
		3	Low pH + FeO(OH)	0.509				
		11	Low pH + FeO(OH)	0.755	0.77	0.02		
		11	Low pH + FeO(OH)	0.768				
		11	Low pH + FeO(OH)	0.799				
22.03.2019	9	2	Control	3.18	3.25	0.20	3.18	0.33
		2	Control	3.09				
		2	Control	3.47				
		6	Control	3.82	3.47	0.35		
		6	Control	3.47				
		6	Control	3.12				
		10	Control	2.96	2.82	0.13		
		10	Control	2.81				
		10	Control	2.7				
		4	FeO(OH)	3.06	3.16	0.19	3.44	0.24
		4	FeO(OH)	3.04				
		4	FeO(OH)	3.38				
		8	FeO(OH)	3.9	3.58	0.44		
		8	FeO(OH)	3.76				
		8	FeO(OH)	3.07				
		12	FeO(OH)	3.42	3.57	0.28		
		12	FeO(OH)	3.89				
		12	FeO(OH)	3.4				
		1	Low pH Control	0.831	0.83	0.02	0.97	0.12
		1	Low pH Control	0.851				

		1	Low pH Control	0.821				
		5	Low pH Control	1.01	1.06	0.06		
		5	Low pH Control	1.13				
		5	Low pH Control	1.03				
		9	Low pH Control	1.01	1.01	0.02		
		9	Low pH Control	0.99				
		9	Low pH Control	1.03				
		3	Low pH + FeO(OH)	0.894	0.87	0.03	1.18	0.29
		3	Low pH + FeO(OH)	0.891				
		3	Low pH + FeO(OH)	0.833				
		7	Low pH + FeO(OH)	1.21	1.24	0.03		
		7	Low pH + FeO(OH)	1.27				
		7	Low pH + FeO(OH)	1.25				
		11	Low pH + FeO(OH)	1.37	1.43	0.06		
		11	Low pH + FeO(OH)	1.48				
		11	Low pH + FeO(OH)	1.45				
24.03.2019	11	2	Control	3.68	4.01	0.22	3.69	0.56
		2	Control	4.08				
		2	Control	4.09				
		2	Control	4.17				
		6	Control	4.06	4.03	0.03		

		6	Control	4.02				
		6	Control	4				
		10	Control	3.05	3.05	0.04		
		10	Control	3.01				
		10	Control	3.08				
		4	FeO(OH)	4.17	4.18	0.17	4.18	0.21
		4	FeO(OH)	4.04				
		4	FeO(OH)	4.08				
		4	FeO(OH)	4.42				
		8	FeO(OH)	4.18	4.39	0.44		
		8	FeO(OH)	4.12				
		8	FeO(OH)	4.21				
		8	FeO(OH)	5.04				
		12	FeO(OH)	3.81	3.98	0.12		
		12	FeO(OH)	3.98				
		12	FeO(OH)	4.08				
		12	FeO(OH)	4.03				
		1	Low pH Control	1.4	1.35	0.08	1.58	0.20
		1	Low pH Control	1.29				
		1	Low pH Control	1.28				
		5	Low pH Control	1.79	1.73	0.09		
		5	Low pH Control	1.81				
		5	Low pH Control	1.71				
		5	Low pH Control	1.61				
		9	Low pH Control	1.68	1.66	0.14		
		9	Low pH Control	1.78				

		9	Low pH Control	1.51				
		3	Low pH + FeO(OH)	1.46	1.46	0.06	1.72	0.23
		3	Low pH + FeO(OH)	1.51				
		3	Low pH + FeO(OH)	1.4				
		7	Low pH + FeO(OH)	1.8	1.90	0.09		
		7	Low pH + FeO(OH)	1.92				
		7	Low pH + FeO(OH)	1.97				
		11	Low pH + FeO(OH)	1.78	1.80	0.17		
		11	Low pH + FeO(OH)	1.64				
		11	Low pH + FeO(OH)	1.98				
		13	Extra Control	3.44	2.72	0.63	2.72	#DIV/0!
		13	Extra Control	2.02				
		13	Extra Control	3.01				
		13	Extra Control	2.42				

Appendix 1.9 Carbon Chemistry Data

1. Total pH (pH_T)

Sampling Date	**Incubation Day**	**ID (cubitainer number)**	**Treatment**	**Tatal pH (pH_T)**		
				Value	**Average**	**SD**
15.03.2019	0	inkub exp2 zero low pH	Low pH Control	7.361	7.381	0.018

15.03.2019		inkub exp3 d 2110? low pH	Low pH Control	7.390		
15.03.2019		inkub exp4 day zero low pH	Low pH Control	7.394		
15.03.2019	0	inkub exp1 zero control	Control	8.024	8.024	#DIV/0!
18.03.2019	5	1	Low pH Control	7.469	7.469	#DIV/0!
18.03.2019		6	Control	8.077	8.077	#DIV/0!
18.03.2019		11	Low pH + FeO(OH)	7.463	7.463	#DIV/0!
18.03.2019		8	FeO(OH)	8.093	8.093	#DIV/0!
20.03.2019	7	1	Low pH Control	7.467	7.479	0.017
20.03.2019		5	Low pH Control	7.491		
20.03.2019	7	2	Control	8.163	8.175	0.017
20.03.2019		6	Control	8.187		
20.03.2019	7	3	Low pH + FeO(OH)	7.445	7.471	0.037
20.03.2019		11	Low pH + FeO(OH)	7.498		
20.03.2019	7	4	FeO(OH)	8.147	8.159	0.016
20.03.2019		8	FeO(OH)	8.170		
22.03.2019	9	1	Low pH Control	7.542	7.531	0.024
22.03.2019		5	Low pH Control	7.547		
22.03.2019		9	Low pH Control	7.503		
22.03.2019	9	2	Control	8.199	8.178	0.018
22.03.2019		6	Control	8.171		
22.03.2019		10	Control	8.166		
22.03.2019	9	3	Low pH + FeO(OH)	7.493	7.516	0.026
22.03.2019		7	Low pH + FeO(OH)	7.509		
22.03.2019		11	Low pH + FeO(OH)	7.544		
22.03.2019	9	4	FeO(OH)	8.178	8.181	0.003
22.03.2019		8	FeO(OH)	8.185		
22.03.2019		12	FeO(OH)	8.179		
24.03.2019	11	1	Low pH Control	7.558	7.549	0.030
24.03.2019		5	Low pH Control	7.573		
24.03.2019		9	Low pH Control	7.515		
24.03.2019	11	2	Control	8.215	8.207	0.022
24.03.2019		6	Control	8.223		

24.03.2019		10	Control	8.182		
24.03.2019	11	3	Low pH + FeO(OH)	7.512	7.543	0.039
24.03.2019		7	Low pH + FeO(OH)	7.529		
24.03.2019		11	Low pH + FeO(OH)	7.587		
24.03.2019	11	4	FeO(OH)	8.207	8.216	0.022
24.03.2019		8	FeO(OH)	8.241		
24.03.2019		12	FeO(OH)	8.201		
24.03.2019	11	13	Control	8.183	8.183	#DIV/0!

2. Fugacity of carbon dioxide (fCO_2)

Sampling Date	**Incubation Day**	**ID (cubitainer number)**	**Treatment**	**fCO_2 *µ atm***	**Average *µ atm***	**SD**
15.03.2019	0	inkub exp2 zero low pH	Low pH Control	1881	1798.13	71.867
15.03.2019		inkub exp3 d 2110? low pH	Low pH Control	1764		
15.03.2019		inkub exp4 day zero low pH	Low pH Control	1750		
15.03.2019	0	inkub exp1 zero control	Control	415	414.63	#DIV/0!
18.03.2019	5	1	Low pH Control	1472	1471.86	#DIV/0!
18.03.2019		6	Control	362	361.94	#DIV/0!
18.03.2019		11	Low pH + FeO(OH)	1492	1492.19	#DIV/0!
18.03.2019		8	FeO(OH)	347	347.21	#DIV/0!
20.03.2019	7	1	Low pH Control	1450	1404.67	63.872
20.03.2019		5	Low pH Control	1360		
20.03.2019	7	2	Control	288	279.25	12.483
20.03.2019		6	Control	270		
20.03.2019	7	3	Low pH + FeO(OH)	1514	1424.38	126.952
20.03.2019		11	Low pH + FeO(OH)	1335		
20.03.2019	7	4	FeO(OH)	298	289.45	11.904
20.03.2019		8	FeO(OH)	281		
22.03.2019	9	1	Low pH Control	1204	1241.64	69.175
22.03.2019		5	Low pH Control	1199		
22.03.2019		9	Low pH Control	1321		

22.03.2019	9	2	Control	263	277.28	12.288
22.03.2019		6	Control	283		
22.03.2019		10	Control	286		
22.03.2019	9	3	Low pH + FeO(OH)	1354	1288.58	75.502
22.03.2019		7	Low pH + FeO(OH)	1306		
22.03.2019		11	Low pH + FeO(OH)	1206		
22.03.2019	9	4	FeO(OH)	277	275.12	1.964
22.03.2019		8	FeO(OH)	273		
22.03.2019		12	FeO(OH)	276		
24.03.2019	11	1	Low pH Control	1167	1230.80	60.132
24.03.2019		5	Low pH Control	1239		
24.03.2019		9	Low pH Control	1287		
24.03.2019	11	2	Control	252	249.79	25.911
24.03.2019		6	Control	223		
24.03.2019		10	Control	275		
24.03.2019	11	3	Low pH + FeO(OH)	1299	1212.13	107.730
24.03.2019		7	Low pH + FeO(OH)	1246		
24.03.2019		11	Low pH + FeO(OH)	1092		
24.03.2019	11	4	FeO(OH)	232	243.09	16.154
24.03.2019		8	FeO(OH)	235		
24.03.2019		12	FeO(OH)	262		
24.03.2019	11	13	Control	274	273.99	#DIV/0!

3. CO_2 concentration

Sampling Date	Incubation Day	ID (cubitainer number)	Treatment	CO_2 *µmol/kg*	Average *µmol/kg*	SD
15.03.2019	0	inkub exp2 zero low pH	Low pH Control	105.2	102.62	2.675
15.03.2019		inkub exp3 d 2110? low pH	Low pH Control	99.9		
15.03.2019		inkub exp4 day zero low pH	Low pH Control	102.7		
15.03.2019	0	inkub exp1 zero control	Control	25.7	25.65	#DIV/0!
18.03.2019	5	1	Low pH Control	73.1	73.08	#DIV/0!
18.03.2019		6	Control	21.5	21.51	#DIV/0!
18.03.2019		11	Low pH + FeO(OH)	77.1	77.08	#DIV/0!
18.03.2019		8	FeO(OH)	20.6	20.62	#DIV/0!
20.03.2019	7	1	Low pH Control	86.1	87.57	2.119
20.03.2019		5	Low pH Control	89.1		
20.03.2019	7	2	Control	17.5	17.84	0.407
20.03.2019		6	Control	18.1		
20.03.2019	7	3	Low pH + FeO(OH)	96.9	96.89	0.045
20.03.2019		11	Low pH + FeO(OH)	96.9		
20.03.2019	7	4	FeO(OH)	19.8	19.46	0.523
20.03.2019		8	FeO(OH)	19.1		
22.03.2019	9	1	Low pH Control	83.3	76.51	7.060
22.03.2019		5	Low pH Control	69.2		
22.03.2019		9	Low pH Control	77.1		
22.03.2019	9	2	Control	16.1	16.75	0.896
22.03.2019		6	Control	16.4		
22.03.2019		10	Control	17.8		
22.03.2019	9	3	Low pH + FeO(OH)	82.6	75.08	6.607
22.03.2019		7	Low pH + FeO(OH)	72.2		
22.03.2019		11	Low pH + FeO(OH)	70.4		
22.03.2019	9	4	FeO(OH)	18.0	17.05	0.815
22.03.2019		8	FeO(OH)	16.4		
22.03.2019		12	FeO(OH)	16.8		
24.03.2019	11	1	Low pH Control	73.8	77.85	3.803

24.03.2019		5	Low pH Control	78.3		
24.03.2019		9	Low pH Control	81.4		
24.03.2019	11	2	Control	15.9	15.80	1.639
24.03.2019		6	Control	14.1		
24.03.2019		10	Control	17.4		
24.03.2019	11	3	Low pH + FeO(OH)	82.2	76.67	6.814
24.03.2019		7	Low pH + FeO(OH)	78.8		
24.03.2019		11	Low pH + FeO(OH)	69.0		
24.03.2019	11	4	FeO(OH)	14.7	15.37	1.022
24.03.2019		8	FeO(OH)	14.9		
24.03.2019		12	FeO(OH)	16.5		
24.03.2019	11	13	Control	17.3	17.33	#DIV/0!

4. DIC concentration

Sampling Date	**Incubation Day**	**ID**	**Treatment**	**DIC**	**Average**	**SD**
		(cubitainer number)		***µ mol/kg***		
15.03.2019	0	inkub exp2 zero low pH	Low pH Control	2159	2162.61	4.045
15.03.2019		inkub exp3 d 2110? low pH	Low pH Control	2162		
15.03.2019		inkub exp4 day zero low pH	Low pH Control	2167		
15.03.2019	0	inkub exp1 zero control	Control	2198	2198.38	#DIV/0!
18.03.2019	5	1	Low pH Control	2136	2135.82	#DIV/0!
18.03.2019		6	Control	2175	2175.45	#DIV/0!
18.03.2019		11	Low pH + FeO(OH)	2142	2141.79	#DIV/0!
18.03.2019		8	FeO(OH)	2168	2168.05	#DIV/0!
20.03.2019	7	1	Low pH Control	2162	2155.71	8.389
20.03.2019		5	Low pH Control	2150		
20.03.2019	7	2	Control	2156	2158.23	3.680
20.03.2019		6	Control	2161		
20.03.2019	7	3	Low pH + FeO(OH)	2156	2155.55	0.810

20.03.2019		11	Low pH + FeO(OH)	2155		
20.03.2019	7	4	FeO(OH)	2160	2156.84	4.364
20.03.2019		8	FeO(OH)	2154		
22.03.2019	9	1	Low pH Control	2142	2136.41	5.001
22.03.2019		5	Low pH Control	2136		
22.03.2019		9	Low pH Control	2132		
22.03.2019	9	2	Control	2147	2150.21	4.998
22.03.2019		6	Control	2148		
22.03.2019		10	Control	2156		
22.03.2019	9	3	Low pH + FeO(OH)	2144	2136.75	6.639
22.03.2019		7	Low pH + FeO(OH)	2132		
22.03.2019		11	Low pH + FeO(OH)	2134		
22.03.2019	9	4	FeO(OH)	2158	2151.21	5.715
22.03.2019		8	FeO(OH)	2149		
22.03.2019		12	FeO(OH)	2147		

Appendix 2 Supplement materials of *Nitzschia frigida* Incubation Experiment

Appendix 2.1 Relevant data of PHYTO-PAM Analysis

$FeCl_3$ - 5 µmol EDTA				Zoff:	1	7	2	9	
No	**Time**	**Gain**	**E_{PAR}**	**F2(F')**	**F_m2 (F_m')**	**Y2 (Φ_{PSII}) = (F_m'-F')/F_m'**	**rETR**	**Calculated NPQ**	**True NPQ**
1	12:58:25	10	16	577	1441	0.6			
2	12:58:56	10	0	516	1379	0.63	0.00	0.000	0.000
3	12:59:26	10	8	524	1414	0.63	5.04	-0.025	0.000
4	12:59:56	10	16	573	1377	0.58	9.28	0.001	0.001
5	13:00:27	10	32	614	1211	0.49	15.68	0.139	0.139
6	13:00:57	10	64	591	945	0.37	23.68	0.459	0.459
7	13:01:27	10	128	541	721	0.25	32.00	0.913	0.913
8	13:01:57	10	192	504	625	0.19	36.48	1.206	1.206

9	13:02:27	10	256	484	577	0.16	40.96	1.390	1.390
10	13:02:57	10	320	476	545	0.13	41.60	1.530	1.530
11	13:03:27	10	384	476	537	0.11	42.24	1.568	1.568
12	13:03:57	10	448	473	523	0.1	44.80	1.637	1.637
13	13:04:27	10	512	468	513	0.09	46.08	1.688	1.688
14	13:04:57	10	576	465	501	0.07	40.32	1.752	1.752
15	13:05:27	10	640	460	490	0.06	38.40	1.814	1.814
16	13:05:58	10	704	457	489	0.07	49.28	1.820	1.820
17	13:06:28	10	832	458	475	0.04	33.28	1.903	1.903
18	13:06:58	10	960	453	473	0.04	38.40	1.989	1.915
$FeCl_3$ - 15 µmol EDTA				Zoff:	1	7	2	9	
No	**Time**	**G**	**E_{PAR}**	**F2(F')**	**F_m2 (F_m')**	**Y2 (Φ_{PSII}) = (F_m'-F')/F_m'**	**rETR**	**Calculated NPQ**	**True NPQ**
1	13:35:38	10	16	486	1178	0.59			
2	13:36:10	10	0	441	1147	0.62	0.00	0.000	0.000
3	13:36:40	10	8	442	1151	0.62	4.96	-0.003	0.000
4	13:37:10	10	16	492	1139	0.57	9.12	0.007	0.007
5	13:37:40	10	32	533	1016	0.48	15.36	0.129	0.129
6	13:38:10	10	64	522	809	0.35	22.40	0.418	0.418
7	13:38:40	10	128	479	625	0.23	29.44	0.835	0.835
8	13:39:10	10	192	441	545	0.19	36.48	1.105	1.105
9	13:39:40	10	256	418	489	0.15	38.40	1.346	1.346
10	13:40:10	10	320	392	457	0.14	44.80	1.510	1.510
11	13:40:40	10	384	387	433	0.11	42.24	1.649	1.649
12	13:41:11	10	448	372	416	0.11	49.28	1.757	1.757
13	13:41:41	10	512	374	413	0.09	46.08	1.777	1.777
14	13:42:11	10	576	373	405	0.08	46.08	1.832	1.832
15	13:42:41	10	640	372	401	0.07	44.80	1.860	1.860
16	13:43:11	10	704	361	385	0.06	42.24	1.979	1.979
17	13:43:41	10	832	358	377	0.05	41.60	2.042	2.042
18	13:44:11	10	960	355	369	0.04	38.40	2.108	2.108
Goethite - 5 µmol EDTA				Zoff:	1	7	2	9	
No	**Time**	**G**	**E_{PAR}**	**F2(F')**	**F_m2 (F_m')**	**Y2 (Φ_{PSII}) = (F_m'-F')/F_m'**	**rETR**	**Calculated NPQ**	**True NPQ**

1	14:10:42	10	16	622	1594	0.61			
2	14:11:14	10	0	571	1531	0.63	0.00	0.000	0.0000
3	14:11:44	10	8	570	1551	0.63	5.04	-0.013	0.0000
4	14:12:14	10	16	642	1568	0.59	9.44	-0.024	0.0000
5	14:12:44	10	32	701	1364	0.49	15.68	0.122	0.1224
6	14:13:14	10	64	684	1073	0.36	23.04	0.427	0.4268
7	14:13:44	10	128	630	827	0.24	30.72	0.851	0.8513
8	14:14:14	10	192	583	721	0.19	36.48	1.123	1.1234
9	14:14:44	10	256	556	644	0.14	35.84	1.377	1.3773
10	14:15:14	10	320	535	612	0.13	41.60	1.502	1.5016
11	14:15:45	10	384	526	585	0.1	38.40	1.617	1.6171
12	14:16:15	10	448	515	569	0.09	40.32	1.691	1.6907
13	14:16:45	10	512	511	561	0.09	46.08	1.729	1.7291
14	14:17:15	10	576	506	545	0.07	40.32	1.809	1.8092
15	14:17:45	10	640	511	545	0.06	38.40	1.809	1.8092
16	14:18:15	10	704	508	539	0.06	42.24	1.840	1.8404
17	14:18:45	10	832	502	529	0.05	41.60	1.894	1.8941
18	14:19:15	10	960	493	513	0.04	38.40	1.984	1.9844
Goethite - 15 µmol EDTA				Zoff:	1	7	2	9	
No	**Time**	**G**	**E_{PAR}**	**F2(F')**	**F_m2 (F_m')**	**Y2 (Φ_{PSII}) = (F_m'-F')/F_m'**	**rETR**	**Calculated NPQ**	**True NPQ**
1	14:47:10	10	16	656	1673	0.61			
2	14:47:41	10	0	592	1617	0.63	0.00	0.000	0.000
3	14:48:11	10	8	586	1613	0.64	5.12	0.002	0.002
4	14:48:41	10	16	652	1571	0.58	9.28	0.029	0.029
5	14:49:11	10	32	698	1363	0.49	15.68	0.186	0.186
6	14:49:41	10	64	679	1089	0.38	24.32	0.485	0.485
7	14:50:11	10	128	634	841	0.25	32.00	0.923	0.923
8	14:50:41	10	192	588	729	0.19	36.48	1.218	1.218
9	14:51:12	10	256	570	681	0.16	40.96	1.374	1.374
10	14:51:42	10	320	558	641	0.13	41.60	1.523	1.523
11	14:52:12	10	384	552	617	0.11	42.24	1.621	1.621
12	14:52:42	10	448	546	601	0.09	40.32	1.691	1.691

13	14:53:12	10	512	536	589	0.09	46.08	1.745	1.745
14	14:53:42	10	576	531	575	0.08	46.08	1.812	1.812
15	14:54:12	10	640	526	564	0.07	44.80	1.867	1.867
16	14:54:42	10	704	527	561	0.06	42.24	1.882	1.882
17	14:55:12	10	832	534	561	0.05	41.60	1.882	1.882
18	14:55:43	10	960	532	553	0.04	38.40	1.924	1.924

Appendix 2.2 Instruction of PHOTO-PAM

The main procedure using PHYTO-PAM analyser is presented as follows:

1) Turn on PHYTO-PAM analyzer,
2) Turn on temperature control unit and set it equal to that of culture room (4 °C),
3) Fill 3 ml culture sitting in ice bath into the cuvette,
4) Observe the temperature panel until set temperature is reached,
5) Start PhytoWin software and select the US-version when the user is asked during start-up,
6) Set measuring frequency (MF) and damping (D) (Suggested MF=32 and D=3), and save the settings (visible on the report),
7) Make sure Zoff is unchecked in channels tab,
8) Press "Gain" button to adjust the signal to the concentration of the sample
9) Take sample out, keep in dark and if possible, at in suite temperature,
10) Filter 3 ml of the *in-situ* water into a new cuvette using a syringe with a 0.2 µm sterile filter. This will be the blank,
11) Put the blank into the optical unit with the Peltier. Wait for the temperature to settle,
12) Once the signal is stable, check Zoff in channels tab in channel tab, and make sure Ft is close to 0,
13) Place the sample back into the optical unit with the Peltier and wait for the temperature to reach in-situ temperature,
14) Wait a couple of minutes for sample to be dark-acclimated,
15) Press "start" in light curve mode (Irradiance settings can be changed by pressing "Edit" in light curve),
16) Save report as RPT file,
17) To extract report, open the save PRT file stored by default in "PhytoPam\Data_US" in view mode or in notepad, go to "File" → "Export report",
18) Process data and plot in R studio with the packages "dplyr", "phytotools", "ggplot2" and "reshape2",
19) In this experiment, since the cultured phytoplankton species is an Arctic diatom, only data from the wavelength of green light is recommended to focus, which correspond to F2, Fm2 and Y2 in the report.